X-RAY BINARY SYSTEMS - ARIEL V SSI OBSERVATIONS

Thesis submitted by

MICHAEL GEOFFREY WATSON

to the University of Leicester for the degree of
Doctor of Philosophy

January 1979

X-ray Astronomy Group
Department of Physics
University of Leicester

ProQuest LLC
789 East Eisenhower Parkway
P.O. Box 1346
Ann Arbor, MI 48106-1346

Declaration

I hereby declare that no part of this thesis has been previously submitted to this or any other University as part of the requirements for a higher degree. The work described here was conducted by the undersigned except for the contributions from colleagues as indicated in the Acknowledgments, in the text and in the following Note on Publications.

M.G. Watson

Michael Watson

January 1979

Note on Publications

Much of the work reported here has been published (in full or in part) elsewhere, as follows:

Chapter 1: Watson, M.G., 1978. Proc. Roy. Soc. Lond. A, in press.

Chapter 3: Watson, M.G., and Griffiths, R.E., 1977. M.N.R.A.S., 178, 513.

Davison, P.J.N., Watson, M.G., and Pye, J.P., 1977. M.N.R.A.S. 181, 73P.

Chapter 4: Kaluzienski, L.J., Holt, S.S., Boldt, E.A., Serlemitsos, P.J., Eadie, G., Pounds, K.A., Ricketts, M.J., and Watson, M.G., 1975. Ap.J.(Lett.), 201, L121.

Murdin, P., Griffiths, R.E., Pounds, K.A., Watson, M.G., and Longmore, A.J., 1976. M.N.R.A.S., 178, 27P.

Watson, M.G., Ricketts, M.J., and Griffiths, R.E., 1978. Ap.J.(Lett.), 221, L69.

Watson, M.G., and Ricketts, M.J., 1978. M.N.R.A.S., 183, 35P.

Watson, M.G., 1976. M.N.R.A.S., 176, 19P.

Chapter 5: Watson, M.G., Eadie, G.R., and Rolf, D.P., 1978. M.N.R.A.S., submitted.

Watson, M.G., Shervington, M.R., and Jameson, R.F., 1978. M.N.R.A.S., 184, 79P.

CONTENTS

X-ray Binary Systems - Ariel V SSI Observations

M.G.Watson

ABSTRACT

The basis of our current theoretical understanding of galactic x-ray sources is reviewed. Models are outlined involving close binary systems containing a compact object accreting mass which has been lost from the nondegenerate star by a variety of mechanisms. The present status of galactic x-ray astronomy is discussed, with emphasis on the links between established observational categories and the characteristics of the proposed models.

Observational results, consisting primarily of extended x-ray light curves derived from analysis of Ariel V SSI data are presented for two main classes of galactic x-ray source: (i) high-mass x-ray binaries containing an early-type giant or supergiant star; (ii) low-mass x-ray binaries in which the nondegenerate star is a late-type dwarf. For the high-mass binaries emphasis is placed on the determination and improvement of the orbital parameters; for the low-mass binaries, where a less complete picture is available, the discussion centres on the type of system involved, taking into account the optical observations of the source.

Finally, the properties of two further categories - the sources in the galactic bulge and those associated with dwarf novae - are discussed as examples of rather different types of galactic x-ray emitter. In the case of the galactic bulge sources current observations have not lead so far to a clear picture of the nature of the systems involved, indeed their binary membership is not established. X-ray emission from dwarf novae and related objects is a relatively recent discovery and represents the opening up of a new field of galactic x-ray astronomy.

Abbreviations and Units

A: designation of a number of new sources detected by any of the Ariel V experiments (e.g. A0620-00).

2A: designation of sources listed in the "2A" catalogue (Cooke et al. 1978) based on SSI observations.

2S: designation of sources accurately positioned by the SAS-3 RMC (see compilation in Bradt 1978).

3U/4U: designation of sources listed in the third/fourth Uhuru catalogues (Giacconi et al. 1974; Forman et al. 1978).

ASM: the Ariel V All Sky Monitor,

MJD: Modified Julian Date. MJD = JD (Julian Day) - 2 400 000.5

RMC: Rotation Modulation Collimator (Ariel V or SAS-3).

SSI: the Ariel V Sky Survey Instrument.

U.F.U.: Uhuru Flux Unit = 1 Uhuru count s^{-1} (see Units).

Units A number of different intensity units are used in x-ray astronomy; they are inter-related as follows:

1 SSI count s^{-1} = 2.5 μJy (averaged over 2 - 11 keV)
1 Uhuru count s^{-1} = 1.1 μJy (" " " ")
I_{Crab} = 1060 μJy (" " " ")

where 1 μJy = 2.42×10^{-12} erg $cm^{-2} s^{-1}$ KeV^{-1}.

Each conversion assumes an incident Crab-like spectrum. Note that the actual energy ranges of the SSI, and Uhuru, differ from the nominal band used here for the conversion factors.

Preface

For a new discipline, x-ray astronomy has reached maturity remarkably quickly, It is already clear that the study of x-ray astronomy plays an essential part in our understanding of the fate of ordinary stars at the endpoint of stellar evolution where almost unrestrained gravitational contraction leads to the formation of exotic superdense forms of matter: white dwarfs and neutron stars, or the final collapse of the star to the black hole state.

On a more mundane level, the discoveries concerning the binary nature of some, if not all, compact galactic x-ray sources have revitalised interest in the structure and evolution of close binary systems of all kinds. Whereas it is true that many of the more exciting of these discoveries have already emerged (particularly from the observations made by the Uhuru satellite in the first three years of this decade) it is only now, with the accumulation of ever increasing amounts of information about galactic sources, that a pattern of sorts is beginning to emerge.

In a way this stage of consolidation is more interesting, and certainly more demanding on those actively involved in the field. Throughout this thesis the relationships between apparently disparate behaviour in a variety of sources is stressed with emphasis on the "standard" binary model, without, hopefully, ignoring the possibility of the existence of totally new classes of object.

Chapter 1

GALACTIC X-RAY SOURCES: THEORY AND OBSERVATION

1.1 Introduction

This thesis is concerned with the analysis and interpretation of observations of galactic x-ray sources. This chapter outlines the theoretical work on which our current understanding of such sources is based, and reviews the present status of galactic x-ray sources from the point of view of the observational data available. Since much of the data later presented is analysed in terms of temporal variability, this topic is discussed in the last section.

1.2 Theoretical Considerations

1.2.1 Basic Ingredients

The basic features of compact* galactic x-ray sources which any successful theory must explain are:

(i) luminosities $10^{35} - 10^{38}$ erg s^{-1};

(ii) variability on timescales $\sim$ 0.1 s (down to 1 ms);

(iii) temperatures (inferred from x-ray spectra) of $10^{7} - 10^{8}$K.

Most current theories explain this picture in terms of accretion of material onto a compact object*. As was first noted by Ginzburg (1967), the energetics of such a system are dominated by the gravitational energy available to the accreting material as it falls down the potential well of the compact object. The first papers dealing with accretion onto a compact object were by Zel'dovich and Novikov (1966) and Shlovsky (1968). Since then the basic idea has been developed by many authors (see § 1.2.2).

---

* Throughout this thesis the term "compact x-ray source" will be used to imply an unresolved, i.e. stellar object, and the term "compact object" to mean a gravitationally collapsed star i.e. white dwarf, neutron star or black hole. In practice many compact sources contain compact objects, but this is not necessarily the case.

The success of the model depends critically on the inclusion of the compact object. With the benefit of hindsight it is easy to see why this must be the case. Consider the infall of particles of mass m_o from infinity to the bottom of the gravitational well of an object of mass M, radius R. In the Newtonian approximation (which suffices for order of magnitude calculations) the energy gained by each test particle is:

$$\Delta E = m_o \left(\frac{GM}{R}\right) \tag{1.1}$$

For a steady flow of matter $\frac{dm}{dt}$ into the potential well the average rate of energy release will be:

$$\frac{dE}{dt} = \left(\frac{GM}{R}\right) \frac{dm}{dt} \tag{1.2}$$

If a fraction ϵ of this energy appears as x-ray radiation, the x-ray luminosity will be:

$$L_x = \epsilon \left(\frac{GM}{R}\right) \frac{dm}{dt} \tag{1.3}$$

Without detailed knowledge of the accretion and radiation processes involved, we can only set limits on the temperature of the emergent radiation. Assuming cooling is efficient (e.g. Lamb 1975) we have for the radiation temperature T:

$$T_{bb} \leqslant T \ll T_{ff} \tag{1.4}$$

where T_{bb} is the black body temperature given by:

$$T_{bb} = \left[\frac{L}{4\pi R^2 \sigma}\right]^{\frac{1}{4}} \tag{1.5}$$

and T_{ff} is the free-fall temperature given by:

$$kT_{ff} = \left(\frac{GM}{R}\right) m_N \tag{1.6}$$

where σ and k are Stefan's and Boltzmann's constants and m_N is the nucleon mass, and we have assumed the emitting region to have dimension R equal to the radius of the object.

In order to make some quantitative estimates of the likely luminosities and temperatures of the radiation resulting from accretion, we shall assume an accretion rate $\frac{dm}{dt} = 10^{-8} M_\odot y^{-1}$ ($\approx 7 \times 10^{17}$ g s^{-1}) and an efficiency $\epsilon = 0.1$ (the justification of these values will be apparent later). The resultant luminosities and temperatures for accretion onto a normal star, white dwarf, neutron star and black hole, all with mass $M = 1 M_\odot$, are given in Table 1.1.

It is clear that, in general terms, the luminosity and temperature characteristics of galactic x-ray sources can only be obtained by accretion onto a neutron star or black hole. Accretion onto an ordinary star produces negligible luminosity especially as the true efficiency factor in this case will be several orders of magnitude less than the value assumed. In the case of a white dwarf the radiation would be primarily optical and UV. A more detailed study of accretion processes reveals a less clear cut situation - accretion onto a white dwarf can give x-ray emission in certain circumstances, especially if the accreting gas is shocked up to free fall temperatures ($T_{ff} \sim 2 \times 10^9$K!). In any system it is also essential that the radiation be able to escape without serious absorption or degradation by surrounding matter. In general terms, however, a fuller analysis leads to essentially the same conclusions.

The values assumed for the efficiency and accretion rate are those typical for a close neutron star binary. The efficiency can be estimated theoretically; for white dwarfs it is probably ~ 0.001, for neutron stars ~ 0.1 and for black holes $\sim 0.1 - 0.4$, the precise magnitude depending on the details of the accretion process (e.g. Novikov and Thorne 1973, Rees 1976).

Any model which will explain the gross features of the luminous galactic x-ray sources will most probably involve accretion onto a neutron star or black hole. This conclusion is reinforced by the timescales of variability observed in many galactic sources which are just those expected from an emitting region close to a compact object (see § 1.4).

T A B L E 1.1

Results of Accretion

Object	Radius $(\frac{R}{R_\odot})$	Luminosity (erg s^{-1})	T_{bb}(K)	T_{ff}(K)
Main-sequence star	~ 1	10^{32}	2×10^3	2×10^7
White dwarf	$\sim 10^{-2}$	10^{34}	5×10^4	2×10^9
Neutron star	$\sim 10^{-5}$	10^{37}	10^7	2×10^{12}
Black hole	$\sim 10^{-6}$	10^{38}	5×10^7	2×10^{13}

T A B L E 1.2

Current Status of Galactic X-ray Sources

Category	Number known
Supernova remnants and associated pulsars (e.g. Crab, Vela, Pup A, IC443, etc.)	6 (>2 keV) (~ 13 in total)
X-ray bursters	>30
X-ray bursters associated with steady sources	~ 10
Globular cluster sources	7
Binary systems	12 + 7 possible
Pulsating systems	14 + 2 possible
Transients and transient-like variables	~ 30
Galactic centre sources	~ 10
Cataclysmic variables	~ 4 (>2 keV)
Total number of galactic sources ($\lvert b \rvert < 10^\circ$ or known to be galactic)	~ 150

1.2.2 The "Standard" Binary Model

The idea of powering the x-ray emission in compact x-ray sources from the gravitational energy released by accretion onto a compact object has been developed to a stage where a reasonably well defined "standard" model now exists (e.g. Gursky and Schreier 1975). The basic hypotheses on which this model is based are (e.g. Lamb 1975):

(i) the compact object is a member of a close binary system ($P \sim$ days) with an "ordinary" non-degenerate star;

(ii) mass transfer from the ordinary star to the compact object is taking place;

(iii) the mass flow is accreted onto the compact object resulting in x-ray emission.

This model has been outstandingly successful in explaining specific source behaviour, and its plausibility has led to speculation that all compact x-ray sources might be explained in these terms (e.g. Gursky and Schreier 1975). At present I am not aware of any specific observation which cannot be explained in terms of this model, although this is not surprising considering the large number of free parameters available. Most of this chapter assumes that the "standard" model is indeed applicable. In the remainder of this section some aspects of this model are discussed in more detail.

1.2.3 Mass-loss Mechanisms

The possibility of mass-loss and mass transfer within normal close binary systems has played an important part in investigations of the evolution of close binaries. In the specific context of x-ray binaries attention has focussed on a small number of mass-loss mechanisms. Although these are discussed individually below, the possibility of intermediate modes of mass transfer should be borne in mind.

(i) Stellar Wind

All stars probably possess a stellar wind at some level - the sun itself has a stellar wind amounting to $\sim 10^{-14}\ M_\odot y^{-1}$. Strong stellar

winds, however, are only found in early-type stars, mainly giants and supergiants with spectral types earlier than B1 (Lamers et al. 1976). In such stars stellar winds ranging between 10^{-5} and 10^{-9} $M_{\odot}y^{-1}$ are established on the basis of optical and UV studies (Lamers et al. 1976) and also of course from x-ray observations. The actual mechanism for the production of such strong stellar winds may involve the effects of radiation pressure on the outer atmosphere of the star, probably enhanced by the low surface gravity* of these stars (Castor et al. 1975).

The importance of stellar winds in explaining the behaviour of the high-mass binary x-ray sources (see Fig. 1.1 for typical system) was first emphasised by Davidson and Ostriker (1973) with particular reference to Cen X-3. It is important to note that not all of the stellar wind will be accreted by the compact object (see Fig.1.1). Only material which passes within the Bondi-Hoyle accretion radius r_A is captured, where r_A is given by:

$$r_A \approx \frac{2GM_x}{(V_k^2+V_w^2)} \tag{1.7}$$

where V_k and V_w are the orbital and wind velocities respectively. In the spherically symmetric case the accretion rate onto the compact object is:

$$\dot{m}_x = \frac{\dot{m}_p}{4\pi a^2} \pi r_A^2 \tag{1.8}$$

where a is the orbital separation, $\dot{m}_x$ is the mass-transfer rate onto the compact object and $\dot{m}_p$ the mass-loss rate from the primary star. For typical values of M_x, V_k, V_w and a, $r_A \lesssim 0.1a$, resulting in accretion rates onto the compact object $\sim 10^{-2} - 10^{-3}$ times smaller than the mass-loss by stellar wind from the primary.

---

* In close binary systems the effective surface gravity will be even further lowered if the star is close to filling its Roche lobe.

(a)

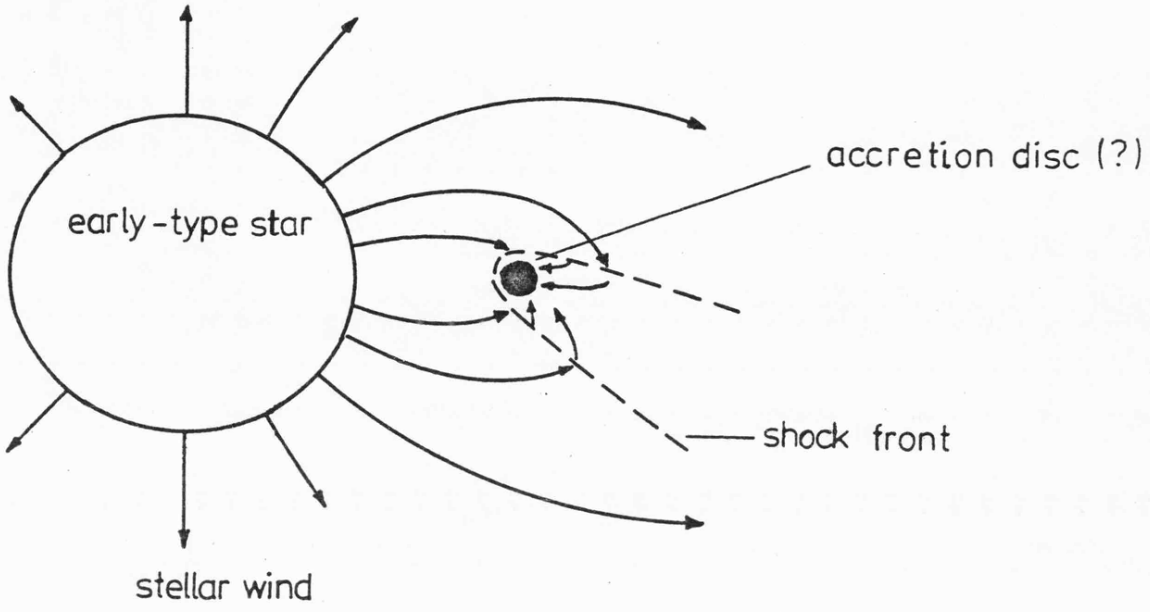

(b)

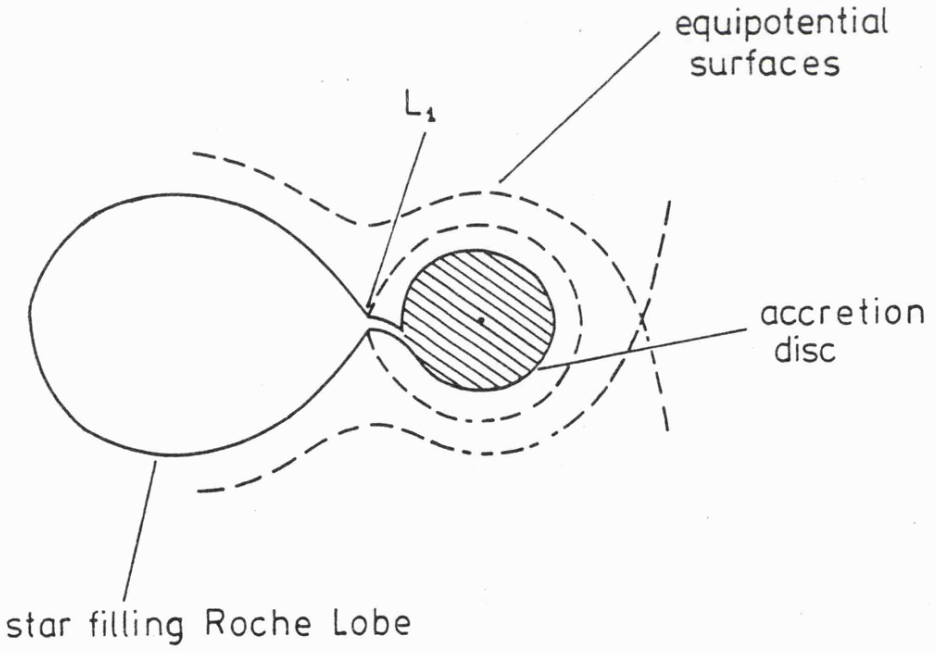

Fig. 1.1 (a) Accretion via stellar wind mass-loss
(b) Accretion via Roche-lobe overflow

Because the mass-loss by stellar wind is approximately isotropic, the angular momentum of the wind relative to the compact object is small and the formation of an accretion disc, the central feature of many models of binary x-ray sources, is somewhat marginal. The outer radius of the accretion disc for accretion from a stellar wind can be estimated as (McCray 1976):

$$r_D \approx \tfrac{1}{4}\left(\frac{r_A^4}{a^3}\right) \approx 3 \times 10^5 \left(\frac{M_x}{M_\odot}\right)^4 V_w^{-8} \left(\frac{M_P}{M_\odot}\right)^{-1} P^{-2} \text{ cm} \qquad (1.9)$$

where V_w is the wind velocity in units of 1000 Km s^{-1}, and P is the binary period in days. As can be readily seen, the dimensions of the disc are of the same order as the radius of the compact object. The existence of a disc around a magnetised neutron star where the influence of the magnetic field may influence the gas motions out to $\sim 10^8$ cm is in particular doubtful, although there is indirect evidence for discs in systems of this type from spin-up timing measurements on x-ray pulsars (Rappaport and Joss 1977).

(ii) Roche-lobe Overflow

The second major possibility which has been considered is accretion from material flowing through the inner Lagrangian point (L_1) of a system where the ordinary star is overfilling its Roche equipotential surface (Roche Lobe). Strictly speaking the precise description of the mass-loss depends on the rotational state of the star in relation to the binary system ~~(see Appendix A)~~, but the discussion here will apply equally well if the star does not corotate. Roche-lobe overflow occurs as the result of expansion of the star in response to nuclear exhaustion and thus is expected to be particularly important in stars which have just started their evolution off the main sequence*. Mass-loss from a star filling its Roche-lobe will

---

* Another possibility is Roche-lobe overflow caused by a decrease in the Roche-lobe size due to decay of the binary orbit, as may occur in very close binaries as a result of tidal interaction and gravitational radiation losses (Faulkner 1976).

occur on a timescale similar to the evolutionary timescale for the expansion. Thus for early-type stars Roche-lobe overflow will result in mass-loss rates of $\sim 10^{-3} - 10^{-5}\ M_\odot\ y^{-1}$, a rate high enough to totally obscure the x-ray source. For late-type main sequence stars (later than F0) Roche-lobe overflow rates $\sim 10^{-8} - 10^{-10}\ M_\odot\ y^{-1}$ are expected - exactly the rates needed to power a typical galactic source. In constrast with the stellar wind mass-loss, Roche-lobe overflow involves a narrow stream of material which will have significant angular momentum with respect to the compact object. In this situation we naturally get the formation of an accretion disc (see Fig. 1.1). The dimensions of the disc are typically of the same order as the Roche-lobe surrounding the compact object (i.e. comparable with the orbital separation)and thus it is likely to be very much larger than either the radius of the compact object, or the magnetospheric radius if a magnetic field is present.

Observational evidence for Roche-lobe overflow is mainly indirect, often based on the determination of the orbital elements of the system revealing that the primary is semi-detached, and that the Roche-lobe overflow is therefore a likely mode of mass-loss. This is certainly the case with dwarf nova systems (e.g. Bath 1976). The best studied case of mass-loss by Roche-lobe overflow in an x-ray binary is Her X-1 where both x-ray (Jones and Forman 1976) and optical studies (Middleditch and Nelson 1976) indicate the presence of a large accretion disc, very plausibly resulting from the Roche-lobe overflow of HZ Her.

(iii) Other Possibilities

Although the terms stellar wind and Roche-lobe overflow probably describe the main modes of mass-loss likely to occur within close binary systems, there is a greater variety of underlying mechanisms driving the mass-loss than discussed above. In particular, mass-loss by stellar

wind may be enhanced by the heating effects of the x-ray flux impinging on the atmosphere, producing a "self-excited" wind (e.g. Basko et al. 1977). The magnitude of the wind produced in this manner has been the subject of some debate and at present the results are not conclusive (Basko et al. 1977; McCray 1976). A second possibility has been studied by Alme and Wilson (1976) who considered a wind powered by density waves (driven by radiation pressure) in a star nearly filling its Roche-lobe. This mechanism comes close to being intermediate between the stellar wind and Roche-lobe overflow cases.

Low-mass stars in very close binary orbits may, as mentioned in the footnote (p.6), overflow their Roche-lobes as a result of orbital decay. This has been considered in the specific case of 4U1626-67 where x-ray pulse timing implies a very short binary period for the system (Rappaport et al. 1977b).

1.2.4 Accretion Discs

Accretion taking place as a result of Roche-lobe overflow, and possibly in the case of stellar wind mass-loss, is likely to lead to the formation of an accretion disc. Accretion onto the compact object via an accretion disc is very efficient, principally because the radial inflow timescale is long enough to allow adequate thermalisation of the gravitational energy, and thus the study of discs, for example as performed by Pringle and Rees (1972) and Shakura and Sunyaev (1973), is of great importance to the understanding of x-ray binaries. Comprehensive reviews of this subject are found in Lightman et al. (1977) and Shu (1976). Here the basic disc structure and characteristics are outlined following Rees (1976).

Material lost from the primary star moves in towards the compact object under the influence of Coriolis forces until it encounters the outer edge of the disc (see Fig 1.1). The material in the disc then

follows approximately Keplerian orbits, but spirals inwards due to the effects of viscosity at a rate determined by the efficiency with which viscous drag transports angular momentum outwards. The disc is heated mainly by viscous friction, and not directly by the release of gravitational energy; this thermal energy is then radiated. This is rather important since the gas has time to radiate before it moves into tightly-bound orbits and is accreted onto the compact object. For radiation from a thin disc (scale height $\ll$ disc radius r_D) we have for the luminosity per unit area at radius r from the compact object:

$$L(r) = \frac{3}{8\pi}\left(\frac{GM_x}{r^3}\right)\left[1-\beta\left(\frac{r_b}{r}\right)^{\frac{1}{2}}\right]\dot{m}_x \qquad (1.10)$$

where $\dot{m}_x = \frac{dm}{dt}$ as before, β is a numerical factor ($\beta \leq 1$) which depends on the inner boundary conditions, and r_b is the radius of this boundary.

The spectrum of the disc radiation depends principally on the disc density which is determined by the accretion rate and viscosity. An estimate of the disc temperature can be made however (cf. equations 1.3 - 1.6):

$$T(r) \geqslant T_{bb}(r) \approx (7 \times 10^6\, \dot{m}_{10}^{\frac{1}{4}}\, r_b^{-\frac{3}{4}}\, M_x^{\frac{1}{4}})\ K \qquad (1.11)$$

where $\dot{m}_{10}$ is in units of $10^{-10}\ M_\odot\ y^{-1}$, r_b is in units of 10^6 cm and M_x is expressed in solar masses. This relationship ensures emission at x-ray wavelengths from the region near a black hole or neutron star ($r \sim r_b$)*, provided the disc extends this far in, and provided the accretion rate $\dot{m} \geqslant \dot{m}_{10}$, equivalent to luminosities $L_x \geqslant 10^{35}$ erg s^{-1}.

1.2.5 Accretion Processes

The behaviour of a binary system as an x-ray source is dominated by the accretion processes taking place close to the compact object. Here we consider the likely results of accretion, both radial and disc-like, onto a black hole, neutron star and white dwarf.

---

* Note that the bulk of the luminosity comes from small radii - eqn. (1.10)

(i) Accretion onto a Black Hole

For disc accretion onto a black hole the inner boundary of the disc r_b is conventionally taken as the radius of the innermost stable circular orbit. For a Schwarzschild hole $r_b = 3r_g = \frac{6GM_x}{c^2}$ (where r_g is the "gravitational radius" of the black hole $r_g = \frac{2GM}{c^2}$), for a "maximal Kerr" hole $r_b = r_g$. Accretion onto a black hole from an accretion disc can be very efficient, estimates of the efficiency range from ~6% for a Schwarzschild hole to ~ 42% for a "maximal Kerr" hole. In the absence of an accretion disc, i.e. if the accretion flow is radial, the x-ray luminosity of the black hole system may be very low, since the matter may fall directly into the hole without having time to radiate significantly. If, however, turbulent viscosity is important radiative cooling may still occur (Meszaros 1975). Note that a detailed analysis of the processes taking place near the black hole demands a full general relativistic treatment.

(ii) Accretion onto a Neutron Star

For disc accretion onto an unmagnetised neutron star, the inner boundary of the disc will be just the neutron star radius. Significant x-ray emission can be expected from the neutron star surface, this is true whether or not accretion is from a disc. If the neutron star has a substantial magnetic field, the accretion flow near the neutron star will be dominated by the effects of the magnetic field. The inner boundary of the accretion disc will be the Alfven surface (or loosely the magnetosphere) at a radius r_m from the neutron star. This radius can be estimated by considering the balance between the gas and magnetic pressure, giving (McCray 1976):

$$r_m \approx 3 \times 10^8 \mu_{30}^{4/7} \left(\frac{M_x}{M_\odot}\right)^{1/7} L_{37}^{-2/7} \quad \text{cm} \qquad (1.12)$$

where μ_{30} is the magnetic moment of the neutron star in units of 10^{30} gauss cm^3 (corresponding to surface field $B \approx 10^{12}$ gauss) and L_{37} is the x-ray luminosity in units of 10^{37} erg s^{-1}. Rotation of the neutron star can have significant effects on the Alfven surface, however, and stability of the magnetosphere is not always ensured (Lamb 1975).

Inside the magnetosphere the accretion flow follows the field lines leading to accretion onto the magnetic pole caps of the neutron star. Providing most of the luminosity comes from these small regions, high radiation temperatures ($T > 10^8$K) can be expected. This mode of accretion also provides a natural explanation for the behaviour of x-ray pulsars, since any misalignment of the magnetic and rotation axes of the neutron star will result in anisotropic radiation, i.e. a "beaming" effect.

(iii) Accretion onto a White Dwarf

The possibilities for x-ray emission from a white dwarf have been relatively little studied until recently, simply because of the difficulty of achieving the high luminosity and temperature required for the "standard" galactic x-ray source. Straightforward application of eqn.(1.11) for disc accretion onto a white dwarf (remembering that $\epsilon \sim 0.001$) implies that extraordinarily high accretion rates ($\dot{m}_x \gtrsim 10^{-2}\ M_\odot\ y^{-1}$) are required to produce x-ray temperatures ($T \gtrsim 10^7$K). However, in the spherical accretion case a stand-off shock may be formed above the white dwarf surface in which the gas is shock heated to $\sim 10^8$K (e.g. Katz 1977). A similar model invoking the presence of a magnetic field which effectively yields radial accretion onto the magnetic pole caps even in the presence of an accretion disc has been discussed by Fabian et al. (1976). Ricketts et al. (1978), following Fabian et al., have successfully applied this model to the hard x-ray observations of SS Cyg, a dwarf nova which is almost certainly an accreting white dwarf. It now seems that accreting white dwarfs can be "hard" ($> 10^7$K) x-ray emitters but it is unlikely that any will have luminosities $L_x > 10^{36}$ erg s^{-1}, since higher luminosities

demand such an accretion flow that the x-rays have little chance of escaping from the emission region.

1.2.6 Radiation Spectrum

The dominant radiation mechanism for a hot plasma with $T \geqslant 10^7 K$ is thermal bremsstrahlung (or free-free) emission leading to a differential spectrum of the form:

$$\frac{dP_T}{dE} = gA\, n_e^2\, T^{-\frac{1}{2}} \exp(-E/kT) \qquad (1.13)$$

for a unit volume of plasma at temperature T with electron density n_e (g is the Gaunt factor which depends on both T and E, and A is a constant) (cf. Blumenthal and Tucker 1975). In a realistic situation the emitting region will have a range of electron temperatures, thus the emitted spectrum will be the sum of the contributions at each T, giving a spectrum which may be closer to a power law than the original exponential form.

At x-ray energies the emitting region in a typical galactic source will be optically thin to free-free absorption. Electron scattering opacity may be important, however, and will tend to change the shape of the spectrum, and the total luminosity. The high energy end of the spectrum tends to a Wien form with photons at this end being degraded by electron scattering to lower energies.

Outside the emitting region the passage of the x-rays through "cold" matter, both locally (e.g. in the accretion disc) and in the interstellar medium, will lead to photoelectric absorption. Since photoelectric absorption can only take place if $E \geqslant I$, where I is the ionisation potential of the atomic species in question, each element will make a separate contribution to the overall absorption with an edge at $E_o = I$. The overall absorption opacity has the form:

$$\left.\begin{aligned} K(E) &\propto E^{-8/3} \quad \text{for } E \approx I \\ K(E) &\propto E^{-3} \quad \text{for } E \gtrsim I \\ K(E) &\propto E^{-7/2} \quad \text{for } E \gg I \end{aligned}\right\} \qquad (1.14)$$

Since the absorption coefficient depends on Z^4, photoelectric absorption is dominated by the effects of the heavier elements even though their cosmic abundance is low. For convenience the photoelectric absorption is often parameterised in terms of a "cut-off" energy E_a where $I_{observed} = I_{emitted} \cdot \exp\left[-\left(\frac{E_a}{E}\right)^{8/3}\right]$. Note that the strong energy dependence of the absorption means that only the low energy x-rays below ~ 3 keV are significantly affected.

The spectral resolution of "typical" x-ray detectors, such as those used on the SSI (see Chapter 2), is often of the order 50% which severely limits the precision with which source spectra can be measured. Indeed most spectral fits are made to simple spectral forms characterised by only three or four parameters. Thus at the moment the observations are making few demands on the theory.

1.2.7 The Evolutionary History of X-ray Binaries

The formation of close binary systems of the type thought to be responsible for the bright galactic x-ray sources has been the subject of much investigation. Indeed if a plausible evolutionary scenario were not forthcoming, the existence of such systems, as inferred from a wealth of observational data, would be rather problematic. Most of the work to date has focussed on the evolutionary history of high-mass x-ray binaries, although low-mass systems have recently received a little more attention.

Firstly we trace the evolution of a massive binary system, closely following the work of van den Heuvel (1976), in which it is assumed that the orbit is circular, mass and angular momentum is conserved, and that both stars corotate (note that these assumptions are not totally self-consistent). The initial system (see Fig.1.2) consists of a 4.7 day binary system with stars of masses 20 $M_\odot$ and 8 $M_\odot$. Star 1 (the more massive star) evolves first and will fill its Roche-lobe after 6.2×10^6 yr.* Subsequent mass-transfer from star 1 to star 2 occurs via Roche-lobe

* This is case B mass-exchange since the more massive star leaves the main-sequence before filling its Roche-lobe.

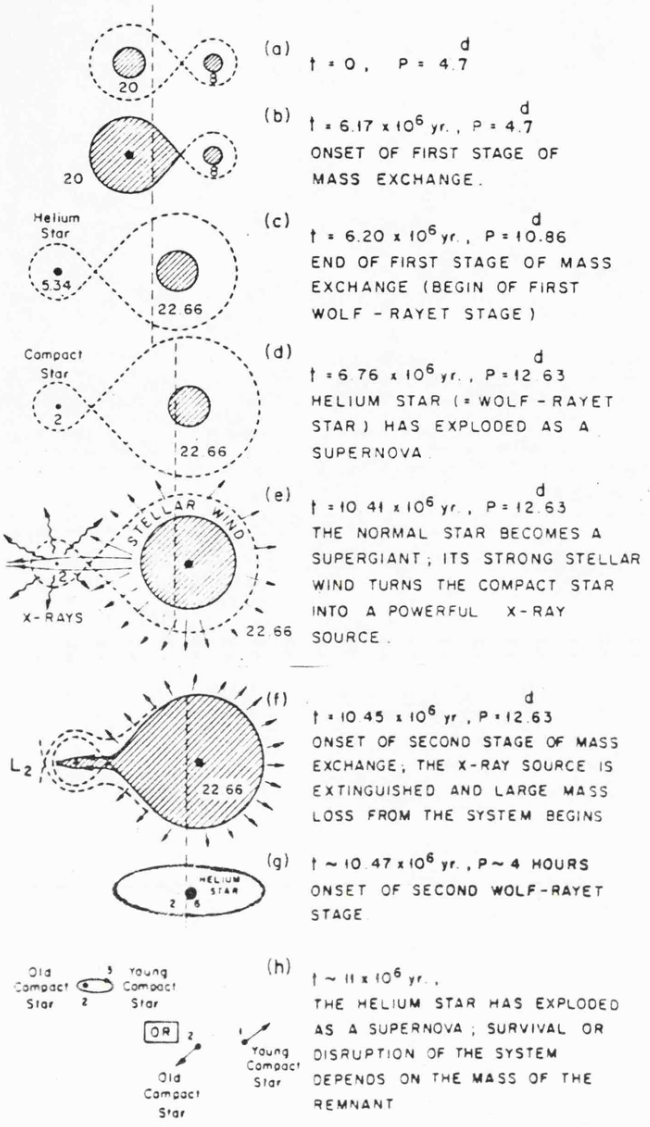

Fig. 1.2 Possible evolutionary history for a high-mass x-ray binary (from van den Heuvel 1976)

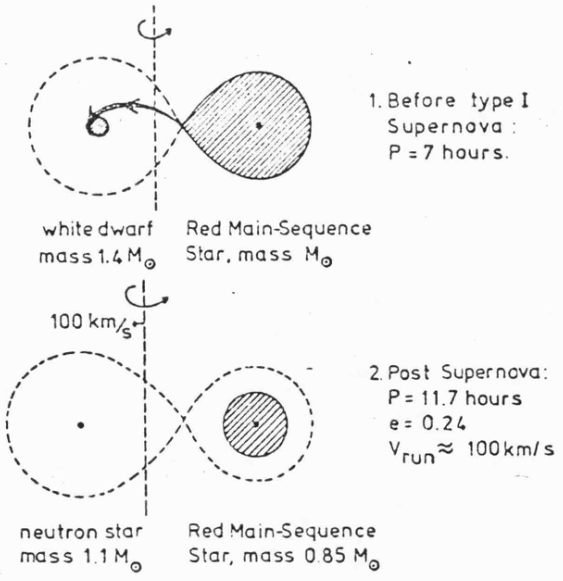

Fig. 1.3 Possible scenario for the origin of a low-mass x-ray binary from a cataclysmic variable system (from van den Heuvel 1977)

overflow on a thermal timescale. After $\sim 3 \times 10^4$ yr mass-transfer ceases when star 1 initiates core helium burning. Star 2 is now the more massive with $M_2 \approx 22\ M_\odot$. Within 6×10^5 yr the helium star will explode as a supernova, leaving behind a neutron star. The results of supernova explosions in binary systems have been extensively studied; in this specific case the system is very unlikely to be disrupted since the explosion occurs in the least massive star. The condition for disruption in a symmetric explosion is $M_1 > 2\ M_{NS} + M_2$, where M_{NS} is the mass of the neutron star left as the remnant of the supernova explosion. Since $M_2 > M_1$, this condition is not satisfied. Assymetrical effects (recoil and "rocket" processes) may cause disruption but only increase the disruption probability by a small amount (principally because the assymetric kick has to be in the right direction in order to significantly affect the system) (De Cuyper et al. 1976).

After the SN explosion the evolution of star 2 continues until, after $\sim 4 \times 10^6$ yr, it will become a supergiant with a strong stellar wind and the system now resembles the "standard model" discussed above. The lifetime of the x-ray source is determined by the evolution of the supergiant. After $\sim 4 \times 10^4$ yr the supergiant will overflow its Roche-lobe and the copious mass-loss is expected to extinguish the x-ray emission. In the subsequent evolution of this system the second phase of mass-transfer will eventually end with the SN explosion of the core of star 2, leading most probably to disruption of the system. If the system remains bound it might then resemble the binary pulsar PSR1913+16.

A number of objections can be made to this scenario, particularly in respect of the conservative assumptions concerning mass and angular momentum. In particular, if the evolution progresses via a contact stage, significant mass-loss from the system will occur (Flannery and Ulrich 1977). Van den Heuvel's scenario does however give reasonable

estimates for the total number of high-mass x-ray binaries in the galaxy at any time. For example, assuming progenitor binaries number $\sim$ 20,000, of which 1/5 evolve via case B mass exchange, the expected lifetime in the x-ray phase ($\sim 2 - 5 \times 10^4$ yr) yields an estimate of $\sim 0.6 - 1.6$ sources within 3 Kpc of the sun. The number actually observed is 3 (Cyg X-1, Vel X-1 and 4U1700-37).

Secondly we consider the evolutionary possibilities for the formation of low-mass x-ray binaries, following van den Heuvel (1977). One of the more plausible scenarios involves evolution of the low-mass binary from a cataclysmic variable, implying that the neutron star originates from a white dwarf driven over the Chandrasekhar limit by mass accretion during the semi-detached stage of evolution. The formation of the neutron star may involve a supernova explosion, or it may be possible for the collapse to take place "quietly", in which case there is no problem of disruption. Fig.1.3 illustrates this scenario for a specific system, chosen to be initially similar to Z Cam. In this case a supernova does occur, leading to mass-loss, widening of the binary system and the production of an eccentric orbit.

A number of uncertainties in this scenario preclude any sensible estimate of the number of progenitor systems which will produce x-ray binaries of this sort. Since cataclysmic variables are reasonably common objects, such a scenario may be sufficient to explain the number of low-mass x-ray binaries observed, provided the probabilities involved are not too low. Note that the x-ray phase of the system shown in Fig.1.3 will only commence when the evolution of the "red main-sequence star" fills its Roche-lobe unless some other form of mass transfer takes place. Such a system will therefore be very old ($\sim 10^{10}$ yr) before significant x-ray emission occurs and, as pointed out by van den Heuvel, will be very long-lived since Roche-lobe overflow from the <u>least massive</u> component is stable and will occur on a nuclear timescale.

Other evolutionary scenarios have been considered, particularly in connection with Her X-1. For example, Suntantyo (1974) has considered the origin of Her X-1 from a progenitor massive system with an extreme initial mass ratio. Although his scenario reproduces the present features of the Her X-1 system, it involves a supernova explosion of the more massive component, which implies a high disruption probability, and thus that systems of this type will be rather rare.

1.3 Galactic X-ray Sky

1.3.1 Introduction

Observations in the "hard" x-ray band ($\gtrsim 2$ keV) by a series of x-ray astronomy instruments on board earth-orbiting satellites have revealed the existence of ~ 400 discrete sources of cosmic x-ray emission. The positions of many of these sources* are shown in galactic coordinates in Fig. 1.4. Something like 50% of these sources are concentrated at low galactic latitudes ($|b| \lesssim 15^{\circ}$). This concentration of sources in the plane of the galaxy has long been interpreted as implying that the majority of low latitude sources are galactic in nature, and conversely that the high latitude sources are primarily extragalactic (e.g. Matilsky et al. 1973).

General confirmation of this view is provided by the differing log N - log S distributions for high and low latitude sources. For sources with $|b| < 20^{\circ}$ a distribution consistent with $N(>S) \propto S^{-0.4}$ is found, whereas sources with $|b| > 20^{\circ}$ have $N(>S) \propto S^{-1.5}$ (Forman et al. 1978; Warwick and Pye 1978). The high latitude distribution is consistent with source isotropy i.e. an extragalactic (or nearby galactic) population; the low latitude distribution indicates a "line" distribution which has been taken as indicative of spiral arm population, although it is more likely that the distribution seen arises from the convolution of the source luminosity function with a complex spatial distribution (cf. Johnson 1978)

---

* Sources plotted are mainly those in the 3U and 2A Catalogues together with a variety of other Ariel V, SAS-3 and HEAO-A sources.

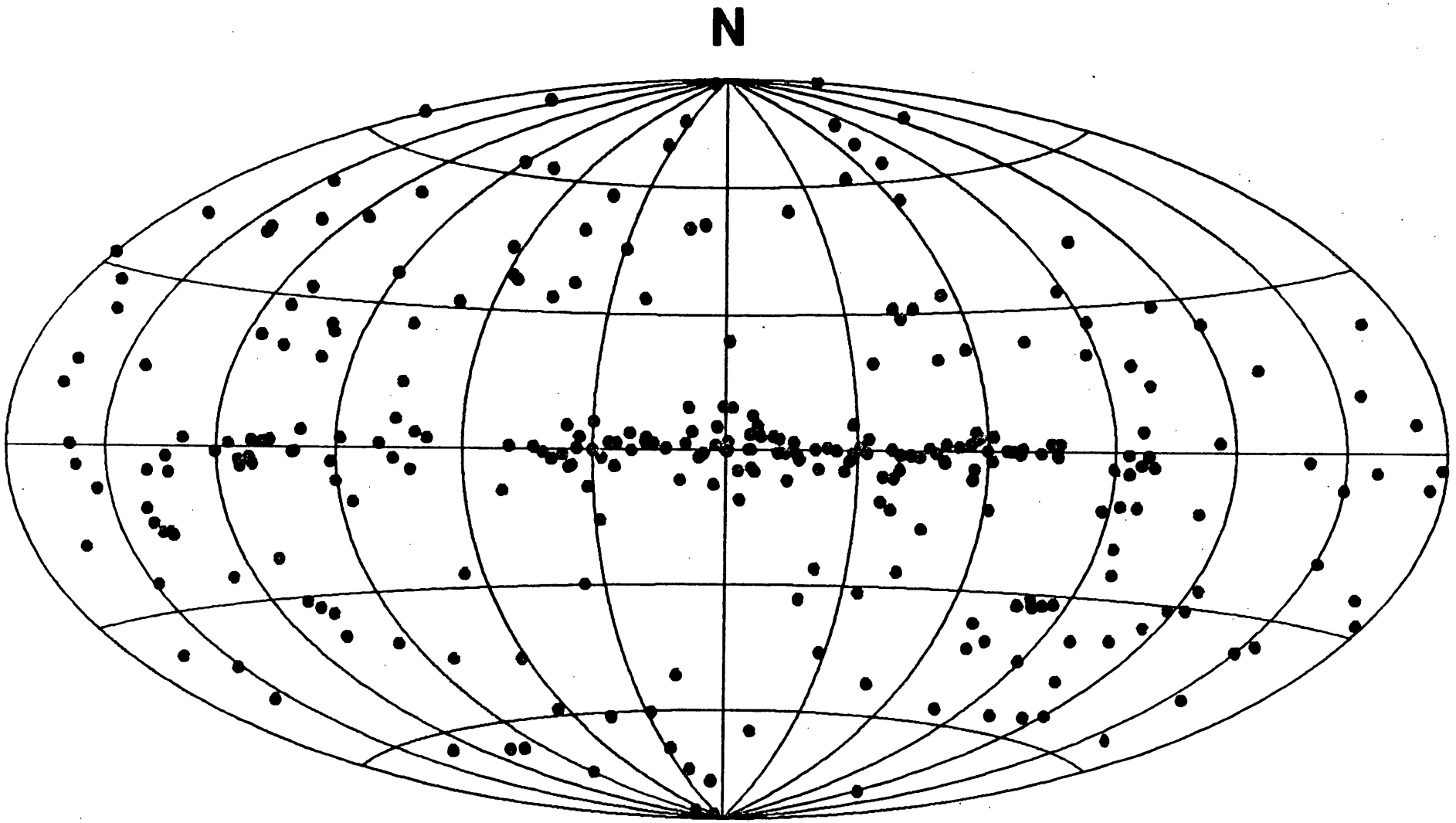

Fig. 1.4 The x-ray sky in galactic coordinates showing approximately 300 catalogued sources. Galactic centre is at the centre of the map. (Aitoff projection).

Detailed support for this picture comes from the individual identifications of low latitude sources. At the time of writing (1978 September), some 30% of all low latitude sources have been identified, almost entirely with galactic objects: supernova remnants, globular clusters, binary star systems, etc. (Bradt 1978; Margon 1978). A small number of sources identified with galactic objects have of course been found at high galactic latitudes; these sources are mainly nearby ($\lesssim$ 1 Kpc distant) or are galactic halo objects with large scale heights above the galactic disc.

Apart from a small number of supernova remnants, all galactic sources are unresolved, i.e. point-like with the highest resolution currently available. All sources which have been studied with sufficiently high time resolution show variability on timescales of seconds, if not shorter (Forman et al. 1976). This is evidence that the majority of galactic sources are compact, "stellar" objects. Detailed observations of a small number of sources have shown that they are members of close binary systems with a general similarity to the "standard" model outlined in §1.3.

As well as showing strong concentration in the galactic plane, galactic sources are also on average brighter than the high latitude population. Individual observations indicate that the brighter galactic sources have luminosities in the range $L_x = 10^{35} - 10^{38}$ erg s^{-1}. This conclusion is also reached if an approximately uniform distribution of sources across the galactic disc is assumed with the observed source count distribution. (Note that several lower luminosity sources are known - see §1.3.2). The limiting sensitivity of the current generation of x-ray instruments ($I_{min} \approx$ 1 U.F.U. for 4U Catalogue; $I_{min} \approx$ 0.5 SSI counts $s^{-1} \approx$ 1.3 U.F.U. for 2A Catalogue) indicates that a source with $L_x \gtrsim 10^{36}$ erg s^{-1} should be detectable, and hence known anywhere within the galaxy ($d \lesssim$ 25 Kpc). In practice source confusion severely limits

the effective sensitivity to weak sources in crowded regions of the galactic place, so that a more conservative value $L_x \gtrsim 10^{37}$ erg s^{-1} probably represents the lower limit to which all galactic sources are known. For transient sources with a small duty cycle of x-ray emission the situation is even worse - for example only sources with $L_x \gtrsim 10^{38}$ erg s^{-1} would have definitely been detected by the Ariel V ASM (Kaluzienski 1977).

1.3.2 Classes of Galactic X-ray Source

On an observational basis galactic x-ray sources can be subdivided into different categories according to a variety of criteria, e.g. spectra, time variability, type of object associated with, galactic position. Such categorisation can be useful in sorting out the wealth of observational data, but unless it reflects the fundamental nature of the sources discussed, such a procedure is unlikely to promote further understanding. Arguably the most powerful method for classifying galactic x-ray sources (and indeed extragalactic sources also) has been by the nature of the optical counterpart. The classification scheme then is based on the firm foundation of optical astronomy rather than the sometimes rather tentative interpretation of x-ray observations.

The current status of galactic x-ray sources is summarised in Table 1.2 in the form of observational categories. Note that the categories overlap and some sources are members of two or more categories. Only three of these categories rely on optical identifications but in fact the majority of both binary and pulsating, and a number of transients and bursters, have optical counterparts. (Indeed the binary nature of some systems is only established by optical studies).

1.3.3 Optical Identification

Most optical identifications are initially suggested on the grounds of positional coincidence alone. The positional accuracy of scanning

experiments such as Uhuru* or the Ariel V SSI is typically of the order 10 arcminutes for a weak source, but can be $\lesssim 1$ arcminute for a modulation collimator experiments (e.g. The Ariel V RMC or SAS-3 RMC). In the galactic plane ($|b| < 10^{\circ}$) the stellar density is on average ~ 14 stars per square arcminute for stars brighter than 20^{m} (Allen 1973), thus stellar identifications are only feasible if arcminute RMC positions are available for the x-ray source. Identifications with objects other than individual stars is much easier, provided these objects are rare (e.g. globular clusters, supernova remnants) and can be accomplished with the larger errorboxes available from scanning experiments.

Positional coincidence is rarely enough to establish an identification; various other properties have been used to confirm the association with the optical object. These include:

(i) unusual colours. Many x-ray counterparts are noticeably blue. In retrospect this is somewhat fortuitous since the reasons for this are rather complex (see § 1.3.7 and 1.3.8);

(ii) unusual spectral lines. He II λ 4686 emission lines, for example, are often present in x-ray binary systems (McClintock et al. 1975).

(iii) correlated x-ray/optical activity. Photometric or radial velocity variations at the known x-ray period establish the identification without doubt. Other correlated variability, such as transient flaring, has also established identifications (e.g. Murdin et al. 1977).

The criteria used for establishing optical identifications are of course based to a large extent on observations of other optically identified x-ray sources, so that the process is both iterative and subject to some

---

* The Uhuru positions for the strongest sources are $\lesssim 1$ arcminute in size however.

uncertainty. Once established however, observations of the optical counterpart can yield a wealth of information including a range of orbital parameters for binary systems and estimates of the distance and age of the object.

1.3.4 Globular Cluster X-ray Sources

At present seven* x-ray sources are known to be associated with globular clusters. Their properties are outlined in Table 1.3, based on a recent review by Grindlay (1977a). Except for the transient source in NGC 6440, all of the x-ray sources have been positioned accurately enough by the SAS-3 satellite (Bradt 1978) to establish that the emission emanates from within the cluster core, although this need not necessarily be a central object. On the basis of the small sample available there may be some correlation of x-ray emission with concentration class although, as noted by Grindlay (1978), there is some evidence that NGC 6712, Liller I and the two new candidates are tidally disrupted clusters.

The x-ray spectra of globular cluster sources generally show low bremsstrahlung temperatures $kT \sim 5 - 8$ keV, similar to those found for the galactic centre sources. Their luminosities are generally lower: - $L_x \approx 10^{36} - 10^{37}$ erg s^{-1}. All the sources are known to be variable on a range of timescales, but none so far has shown periodic modulation. Three, possibly five, globular cluster sources are associated with x-ray bursters. The association of bursters with globular clusters has been the subject of much debate. It is probably safe to say that a high proportion of globular cluster sources are bursters, but that the majority of bursters are not in globular clusters (Lewin and Joss 1977).

The nature of the globular cluster sources is still unresolved. Most models involve either a nuclear, massive ($\sim 10^3 M_\odot$) black hole or a low-mass short period binary system (Grindlay 1977a), although direct evidence for either model is not forthcoming.

---

* Kron 3 and Terzan 2 have also been suggested very recently (Grindlay 1978)

T A B L E 1.3

Globular Cluster X-ray Sources
(after Grindlay 1977a)

X-ray Source	Globular Cluster	ℓ^{II}	b^{II}	θ_o +	d(Kpc)	$L_x(10^{36}$erg $s^{-1})$	Notes
MX0513-40 2S0512-400	NGC 1851	244.5	-35.0	20"	11	<0.6 - 5	Burster, see Table 1.4
MX1746-20	NGC 6440	7.7	3.8	15'	10?	<0.5 - 36	Transient, see Table 1.7
4U1746-37 2S1746-370	NGC 6441	353.5	-5.0	30"	9.3	5.3 - 17	Possible burster (Lewin 1978)
4U1820-30 2S1820-303	NGC 6624	2.8	-7.9	20"	6	3.7 - 20	Burster, see Table 1.4
A1850-08 2S1850-087	NGC 6712	25.4	-4.3	30"	6.8	<0.7 - 4	Possible burster (Lewin 1978)
4U2129+12 2S2127+119	NGC 7078	65.0	-27.3	20"	10	0.8 - 3.3	
MXB1730-335 1S1730-333	Liller I	354.8	-0.1	120"	10	<3	Rapid burster, see Table 1.4

+ Approximate uncertainty in x-ray source location (taken from Bradt (1978)) corresponding to maximum possible offset of source from cluster core.

1.3.5 X-ray Bursters

The first x-ray burster was discovered in late 1975, since then over 30 burst sources have been detected - most of them in the galactic plane with a marked concentration towards the galactic centre. The overall properties of bursters are summarised by Lewin and Joss (1977) and in a recent review by Lewin (1978).

Bursters are characterised by impulsive x-ray flares with rise-times 0.1 - 1 sec and decay times $\sim$10 - 100 seconds, with luminosity at peak of $L_x \approx 10^{38}$ erg s^{-1}. Recent observations have lead to the classification of bursts into Types I and II (Lewin 1978). Type I bursts have been seen from more than 25 of the known bursters. They show spectral softening during the evolution of the burst and recur on timescales of hours to days. Type II bursts have been seen from the Rapid Burster (MXB1730-335) and possibly from several ordinary x-ray binaries and pulsars. They show no spectral changes during the burst and recur on timescales of seconds to minutes. Type II bursts may also have been seen from Cyg X-1, LMC X-4, 4U1258-61 and 4U1223-62, although there is no certainty that the flare-like events detected are caused by the same mechanism as in the Rapid Burster.

Four burst sources have been tentatively identified with faint blue stars ($m_B \sim 18^m$). The identification of MXB1735-44 is certain, since optical bursts have recently been detected from the counterpart star (Grindlay et al. 1978). At least three, and probably five, burst sources are located in globular clusters; as remarked earlier this association seems to be well established. Ten burst sources have associated "steady" x-ray emission. Indeed several were known as steady sources before burst activity was noted, and these sources are listed in Table 1.4 (taken from Lewin 1978). The x-ray spectra of these associated sources are generally"soft", having typical bremsstrahlung temperatures similar

T A B L E 1.4

"Steady" sources associated with bursters*
(after Lewin 1978)

Burst Source	Optical Identification	ℓ^{II}	b^{II}	Notes
MXB0512-40	NGC 1851	244.5	-35.0	See Table 1.3
MXB1636-53	blue star, 18^m	332.9	- 4.8	See Table 1.6
MXB1659-29 (H1658-298)	blue star, 18^m ++	353.9	7.3	See Table 1.7
MXB1728-34	-	354.3	-0.2	
MXB1730-335	Liller I	354.8	-0.1	See Table 1.3. "Steady" emission from type II bursts**.
MXB1735-44	blue star, $17^m.5$	346.1	-7.0	See Table 1.6 Optical bursts recently discovered.+
MXB1820-30	NGC 6624	2.8	-7.9	See Table 1.3
MXB1837+05	blue star, 19^m	36.1	4.8	See Table 1.6
MXB1906+00	-	35.0	-3.7	
MXB1916-05	-	31.4	-8.5	

Type I bursts may also have been detected from 8 other steady sources.

* Type I bursts only. + Grindlay et al (1978) ++ Grindlay (1978) ** See comment in Lewin (1978)

to both the globular cluster and galactic centre sources. There are no reported periodicites (eclipsing or otherwise) in any burst source despite extensive searches (Lewin et al. 1976; Buff et al. 1977).

Some progress has been made in constructing models for bursters. These centre on either accretion instabilities onto a compact object, or thermonuclear flashes in matter accreted onto the surface of a neutron star. The current view favours thermonuclear flashes for Type I bursts; Type II bursts are almost certainly due to accretion flow instabilities (hence their occurrence in "ordinary" sources).

1.3.6 Galactic Centre Sources

The third group of sources which may have links with both globular clusters and x-ray bursters are those bright sources located near the galactic centre, variously termed "galactic centre" or "galactic bulge" sources. These sources are discussed in more detail in Chapter 5.

It is difficult to give a precise definition of the galactic centre sources, but it is clear if we examine the longitude distribution for the brightest galactic sources (see Chapter 5) that there is a remarkable concentration towards longitude zero, with over 80% of the sources with $I \geqslant 100$ UFU being within 30° of the galactic centre. If these sources, or a subset of them, are physically similar then their longitude distribution must imply that they are all close to the galactic centre, certainly within the galactic bulge region. As is argued in Chapter 5, there are certain observational similarities in terms of x-ray spectra and time variability which probably imply physical similarities. If these sources are all at ~ 10 Kpc in the galactic bulge then they are the most luminous galactic x-ray emitters with $L_x \sim 10^{38}$ erg s^{-1} (close to the Eddington limit for a 1 $M_{\odot}$ compact object).

The nature of the galactic centre sources remains problematic - this is in part due to the lack of optical identifications. A low-mass binary model for these sources can certainly be constructed (Jones and Raine, 1978; Milgrom 1978) but other possibilities exist, e.g. for isolated

black holes accreting from the interstellar medium. One important approach to this problem may be to clarify the obvious links of these sources with those in globular clusters and with x-ray bursters.

1.3.7 High-mass Binary Systems

To be able to classify a source as being a high-mass binary implies a more detailed knowledge of the system than for the three previous categories discussed, thus the list given in Table 1.5 is subject to greater uncertainty. The sources listed were selected by the criterion that their optical counterpart be a high-mass star ($M > 3\ M_\odot$, in many cases $M > 5\ M_\odot$). Thus, provided the identification is correct, and the systems are all binaries, the description "high-mass binary" will be appropriate. Note that this list includes the five "Uhuru" binaries often referred to as "Supergiant binaries" and is, in a sense, an extension to this class of source.

Of the 20 sources listed all but one (GX2+5) are associated with a star of spectral type earlier than A0. Where the information is available, main sequence stars, giants and supergiants are more or less equally represented. Such early-type stars all have masses in excess of $5\ M_\odot$ with the exception of late B main-sequence stars for which $M \sim 3 - 4\ M_\odot$ (Allen 1973). (The optical counterpart of the unusual system GX2+5 is classified as M6 III and will thus have $M \approx 8\ M_\odot$).

A variety of regular periodicities are seen in the sources in this list at x-ray and optical wavelengths. Twelve sources have long periods ($P > 10^4$ s) which are almost certainly orbital, mainly in the range 1 - 20 days. Seven of these sources (i.e. $\sim 30\%$ of the total) show x-ray eclipses, which is about the number expected by chance if all 20 sources are high-mass binaries with a random distribution of inclination angles and binary periods similar to those already established. Thus the prospects

TABLE 1.5

High-mass binary x-ray sources

	(1)	(2)	(3)	(4)	(5)		(6)	(7)	(8)	(9)
	X-ray Source	Optical ID	Sp.T/LC	m_v	ℓ^{II}	b^{II}	XS	P_s(sec)	P_L(day)	Notes
	2S0050-725 SMC X-3	Star? [1]	OB:	15^m	302.9	-44.7	H [1]	-	-	In SMC. [1]
	2S0052-739 SMC X-2	Star? [1] see also [43]	OB:	15^m	302.6	-43.4	H [1]	-	-	In SMC. [1]
	4U0054+60 2S0053+604	γ Cas [2]	B0.5e II-V	2^m	123.6	-2.1	-	-	0.7(0)? [2]	$L_x \approx 2\times10^{33}$ erg s^{-1} [2]
	2S0114+650	Star? [3]	OB: [4]	11^m	125.7	2.6	-	-	-	
*	4U0115-73 SMC X-1	Sk160	B0 Ia	13^m	300.5	-43.6	H	0.72(X) [5]	3.9(EXO)	In SMC, extended lows
	4U0115+63	Star? [6]	B: [39]	16^m	125.9	1.0	H	3.6(X) [7]	24 (Xrv) [40]	Recurrent transient
	4U0352+30 1S0352+308	X Per [2]	0.9.5e III-V	6^m	163.1	-17.1	M	835(XO) [8]	0.9(X)? 580:(O) [8,9,10]	$L_x \approx 5\times10^{33}$ erg $^{-1}$ [2]
	4U0532-66 2A0532-664 LMC X-4	Star [11]	OB:	14^m	276.6	-32.6	H [32]	-	1.4(EXO) [11,12]	In LMC

Continued...

	(1)	(2)	(3)	(4)	(5)		(6)	(7)	(8)	(9)
	X-ray Source	Optical ID	Sp.T/LC	m_v	ℓ^{II}	b^{II}	XS	P_s(sec)	P_L(day)	Notes
	A0535+26 1S0535+26	HDE245770 [13,38]	BO pe	9^m	181.4	-2.6	M	104(X) [14]	-	Recurrent transient
*	4U0900-40 Vel X-1	HD77581	BO.5 Ib	7^m	263.1	3.9	H	283(XO) [15,16]	9.0(EXO)	
	A1118-61	Star? [17]	Be:	12^m	292.5	-0.8	M	405(X) [18]	-	Transient [18]
*	4U1118-60 Cen X-3	Krzeminski's Star	06.5 III-V [19]	13^m	292.1	0.4	H	4.8(X)	2.1(EXO)	Extended lows
	4U1145-61 2S1145-619	Hen 715? [2]	B1neV	9^m	295.6	-0.2	M	297(X) [20]	-	
	4U1223-62 2S1223-624	Wray 977 [2]	B1.5 Ia	11^m	300.1	-0.0	H	696(XO) [21,22]	23(XO)?? [23,24]	
	4U1258-61 2S1258-613	'MMV'Star? [2]	B2-AO:	15^m	304.1	1.2	M	272(X) [25]	-	
	4U1516-56 Cir X-1	Star [26]	Early?:	22^m	322.1	0.0	HS	-	16.6(XR(E)) [26,27]	Extended lows, ms time variability, radio source.

Continued.....

	(1)	(2)	(3)	(4)	(5)		(6)	(7)	(8)	(9)
	X-ray Source	Optical ID	Sp.T/LC	m_v	ℓ^{II}	b^{II}	XS	P_s(sec)	P_L(day)	Notes
	4U1538-52 2S1538-522	Star '12' [28,29,41]	-	15^m	327.4	2.2	H [33]	529(X) [30]	3.7(EX) [30]	See Chapter 3.
*	4U1700-37	HD153919	O7f	6^m	347.8	2.2	H	5808(X) [42]	3.4(EXO)	
	4U1728-24 2S1728-247 GX2+5	Star [31]	M6III	19^m	1.9	4.8	H	122(X) [21]	-	
	4U1956+35 Cyg X-1	HDE226868	O9.7 Iab	9^m	71.3	3.1	HS	-	5.6(O(X))	High-low states, ms time variability

Notes to Table 1.5

Column (1) X-ray source name. 4U and 2S designations are given when possible. (Refs. [36] and [37]).

(2) Optical identification. Question marks indicate uncertain identifications. Figure in square brackets is reference to identification, and to columns (3) and (4) if not given there.

(3) Spectral type and luminosity class of optical ID. Colon indicates uncertain or incomplete classification.

(4) Approximate V magnitude.

(5) Galactic coordinates of x-ray source. (Degrees, 1950.0)

(6) X-ray spectrum of source, taken from Jones (1977) (ref. [34]) unless given. Code letter indicates approximate bremsstrahlung spectrum:

H : $kT \gtrsim 10$ keV

M : $10 \gtrsim kT \gtrsim 7$ keV

S : $kT \lesssim 5$ keV

HS : spectrum with 'H' and 'S' components

(7) Known periods $\lesssim 10^4$s. Letters in brackets have the following meaning:

X : seen in x-ray band

O : seen at optical wavelengths

R : seen at radio wavelengths

I : seen at infra-red wavelengths

rv : seen in radial velocities only

E : eclipsing (in x-ray band)

Extra brackets indicate doubt about that category; question marks doubt about the reality of the period.

(8) Known periods $\gtrsim 10^4$s. Details as for (7).

(9) Extra information about source.

Figures in square brackets refer to references. No attempt has been made to find the original reference in every case. Those sources marked with an asterisk are the well-studied "Uhuru" binaries. For these, unless references are given, data has been taken from one of the standard sources, such as ref. [35] .

References to Table 1.5

1 Clark et al. (1978)

2 Bradt et al. (1977)

3 Margon and Bradt (1977)

4 Bidelman and Sanduleak (1977)

5 Lucke et al. (1976)

6 Cominsky et al. (1978b)

7 Johnson et al. (1978)

8 White et al. (1976a)

9 White et al. (1977)

10 Hutchings et al. (1974)

11 Chevalier and Ilovaisky (1977)

12 White (1978)

13 Stier and Liller (1976)

14 Rosenberg et al. (1975)

15 McClintock et al. (1976)

16 Steiner (1977)

17 Chevalier and Ilovaisky (1975)

18 Ives et al. (1975)

19 Osmer et al. (1975)

20 White (1977)

21 White et al. (1976b)

22 Mauder (1976)

23 Hammerschlag-Hensberge et al. (1976)

24 Unpublished Ariel V SSI data

25 McClintock et al. (1977a)

26 Whelan et al. (1977b)

27 Kaluzienski et al. (1976)

28 Cowley et al.(1977)

29 Schwarz et al. (1978)

30 Davison et al. (1977)

31 Davidsen et al. (1977)

32 Epstein et al. (1977)

33 Davison (1977a)

34 Jones (1977)

35 Giacconi and Gursky (1974)

36 Forman et al. (1978)

37 Bradt (1978)

38 Bartolini et al. (1978)

39 Johns and Koski (1978)

40 Rappaport et al. (1978)

41 Parkes et al. (1978)

42 Matilsky and Jessen (1978)

43 Morton and Murdin (1978)

for finding further eclipsing binaries in this list are rather poor. Thirteen of the sources listed have short periods (pulsation periods*) ($P < 10^4$S) ranging from $\sim$1 - 6000 seconds. These periods are thought to arise from the spin modulation of the x-ray emission from a rotating neutron star (or possibly white dwarf, although this can be discounted in several well studied cases - see Rappaport and Joss 1977). Two sources, Cyg X-1 and Cir X-1, almost certainly do not have pulsation periods. Their short timescales ($\lesssim$ 10 ms) behaviour is characterised by irregular flaring (Rothschild et al. 1977; Toor 1977) which has often been interpreted as supporting evidence for the presence of a black hole in these systems. Regular modulation of the x-ray emission from a black hole is probably impossible, since the magnetic and spin axes of the hole must be aligned (Ruffini 1975).

The clearest similarity between sources in this Table exists in their x-ray spectra which are all "hard" in the sense of having bremsstrahlung temperatures in excess of 7 keV ($\sim 8 \times 10^7$K). In fact the majority have temperatures > 10 keV. This feature has often been noted previously (e.g. Ostriker 1977).

These high-mass binary sources show a variety of non-periodic variability on longer timescales than the typical binary periods. In particular A1118-61 is an x-ray transient which flared up briefly in 1974-5 and has not been detected at any other time; A0535+26 and 4U0115+63 have recently been established to be "recurrent" transients (possible recurrence period for A0535+26 $\sim$ 200 days). Cen X-3 and SMC X-1 have periods of low intensity occurring on a timescale of months, Cir X-1 shows a similar pattern with a timescale of years. Cyg X-1 displays

---

* Note that the term "pulsation period" refers to a pulsed modulation and not to a period of pulsation (i.e. radial oscillation) of the object.

two quite distinct intensity states with correlated changes in x-ray spectrum and radio activity, again on a timescale of years.

It is important to note however that some important differences exist between sources in this list. Most striking must be the inclusion of two nearby x-ray sources: X Per and γ Cas which have x-ray luminosities 2 - 3 orders of magnitude smaller than the others. In addition the specific properties of Be stars may dominate the behaviour of the 5 sources which are identified with them.

To summarise the observational features of high-mass x-ray binaries, these systems are characterised by:

(i) short binary periods ($\sim$ 1 - 30 days?);

(ii) hard x-ray spectra;

(iii) presence of x-ray pulse periods ($\sim$ 1 - 6000 seconds);

(iv) irregular variability on timescales from months to years.

The study of these systems indicates that a very likely accretion mechanism is mass-loss from the primary star by a dense stellar wind (as discussed in § 1.2.3). The possibility of Roche-lobe overflow, and mass-loss enhanced by large rotational velocities in Be stars must also be considered (see e.g. Maraschi et al. 1977). The presence of pulsation periods is most easily interpreted in terms of the compact secondary being a rotating, magnetised neutron star and this also provides a natural explanation for the high x-ray temperatures observed (cf. Davidson and Ostriker 1973).

1.3.8 Low-mass Binary Systems

Remarkably few galactic x-ray sources are known to be in low-mass binary systems with any certainty. There is however very strong indirect evidence that many systems of this type are x-ray emitters.

The 20 sources listed in Table 1.6 have been selected on the criterion that their optical counterpart has $M < 3\ M_{\odot}$, and in most cases $< 2\ M_{\odot}$. The status of both the identifications and the spectral types assigned to the optical counterparts is far more uncertain than for the objects listed.

TABLE 1.6

Low-mass binary x-ray sources

	(1)	(2)	(3)	(4)	(5)		(6)	(7)	(8)	(9)
	X-ray source	Optical ID	Sp.T/LC	m_v	ℓ^{II}	b^{II}	XS	P_s(sec)	P_L(day)	Notes
	2A0042+323 4U0042+32 2S0042+327	Star? [1]	GO-8 V	19^m	121.3	-29.8	H [2]	-	11.6(X)? [3]	Flaring behaviour [3]
	4U0142+61 2S0142+614	Star? [4]	n.s.	20^m:	129.4	-0.4	-	-	-	
	4U0619+09 2S0614+091	Star? [5,6]	n.s.	20^m	200.9	-3.4	M	-	-	
	A0620-00 1S0620-003	V616 Mon [7]	K5V: [8]	11^m-22^m	210.0	-6.5	S+ [9]	-	7.8(XO)? [10]	Transient [11] Previous optical outburst [12]
	A1524-61 2S1524-617	Star [13]	Late V:	17^m- 23^m	320.3	-4.4	S+ [14]	-	-	Transient [14]
	4U1608-52 2S1608-523	Star [15]	?	21^m:	330.9	-0.9	S	-	-	Recurrent transient, burst source? [15]
*	4U1617-15 Sco X-1	V818 Sco	n.s.	12^m-13^m	359.1	23.8	M	-	0.8(Orv) [16,17]	
	4U1626-67 2S1627-673	Star? [18]	blue	19^m	321.8	-13.1	H	7.7(X) [19]	-	
	4U1630-47	Star? [20]	G-K V**	16^m:	336.9	0.3	S	-	-	Recurrent transient [21]

Continued ...

	(1)	(2)	(3)	(4)	(5)		(6)	'7)	(8)	(9)
	X-ray source	Optical ID	Sp.T/LC	m_v	ℓ^{II}	b^{II}	XS	P_s(sec)	P_L(day)	Notes
	4U1636-53 2S1636-536	Star? [18]	blue	18^m	332.9	-4.8	S	-	-	X-ray burster [22]
*	4U1656+35 Her X-1	HZ Her	A-F V:	13^m-15^m	58.1	37.5	H	1.2(XO) [23]	1.7(EXO)	35d cycle
	H1705-25	Nova Oph 77 [24]	late V:	16^m-22^m	358.6	9.1	S [24]	-	-	Transient [25]
	4U1728-16 2S1728-169 GX9+9	Star'DMB'? [26]	n.s.	17^m	8.5	9.0	S	-	-	
	4U1735-44 2S1735-444	Star? [18]	blue	18^m	346.1	-7.0	S	-	-	X-ray burster [27]
	4U1813-14 2S1813-140 GX17+2	Star?? [28]	G V:	18^m	16.4	1.3	S	1914?? [30]	-	Coincident variable radio source [29]
	4U1837+04 2S1837+049 Ser X-1	Star? [31]	blue	19^m	36.1	4.8	S	-	-	X-ray burster [32]
	4U1908+00 2S1908+005 Aql X-1	Star [33]	KO V:	17^m-20^m	35.7	-4.1	S	-	1.3(X)? [34]	Recurrent transient [35]

Continued ....

	(1)	(2)	(3)	(4)	(5)		(6)	(7)	(8)	(9)
	X-ray source	Optical ID	Sp.T/LC	m_v	ℓ^{II}	b^{II}	XS	P_s(sec)	P_L(day)	Notes
	4U1956+11 2S1957+115	Star ? [36]	n.s.	19^m	51.3	-9.3	S	-	-	
*	4U2030+40 Cyg X-3	IR object	-	-	79.8	0.7	M	-	0.2(XI) 17.0(X)? [42]	Radio source, low mass system [37,38]
*	4U2142+38 Cyg X-2	Star [39]	F2 IV:	14^m	87.3	-11.3	S	-	0.9(rv)? 11.2(X)? [39,40]	

Notes to Table 1.6

Columns as in Table 1.5, except for:

Column (3): n.s.: indicates non-stellar spectrum similar to that of Sco X-1

blue: star shows UV excess and is inconsistent with being reddened early-type star (see text).

(6): Sources marked with (+) show strong spectral changes. Typical spectrum is quoted.

Figures in square brackets refer to references. No attempt has been made to find the original reference in every case. These sources marked with an asterisk are the well-studied "Uhuru" binaries. For these references are given, data has been taken from one of the standard sources such as [41].

** spectral type for 1630-47 counterpart estimated from U, B, V, I colours given in ref. [20].

References to Table 1.6

1 Charles et al. (1978)

2 Rappaport et al. (1977a)

3 Watson and Ricketts (1978)

4 Dower et al. (1978)

5 Murdin et al. (1974)

6 Davidsen et al.(1974)

7 Whelan et al. (1977a)

8 Wu et al. (1976)

9 Ricketts et al. (1975)

10 Matilsky et al. (1976)

11 Elvis et al. (1975)

12 Eachus et al. (1976)

13 Murdin et al. (1977)

14 Kaluzienski et al. (1975)

15 Grindlay and Liller (1978)

16 Gottlieb et al. (1975)

17 Cowley and Crampton (1975)

18 McClintock et al. (1977b)

19 Rappaport et al. (1977b)

20 Grindlay (1977b)

21 Jones et al. (1976)

22 Hoffman et al. (1977)

23 Middleditch and Nelson (1976)

24 Griffiths et al. (1978)

25 Watson et al. (1978)

26 Davidsen et al. (1976)

27 Lewin et al. (1977)

28 Tarenghi and Reina (1972)

29 Hjellming and Wade (1971)

30 White et al. (1976b)

31 Davidsen (1975)

32 Li et al. (1977)

33 Thorstensen et al. (1977)

34 Watson (1976)

35 Kaluzienski et al. (1977)

36 Margon et al. (1978)

37 Hjellming (1976)

38 Basko et al. (1974)

39 Crampton and Cowley (1976)

40 Holt et al. (1976a)

41 Giacconi and Gursky (1974)

42 Holt et al. (1976b)

in Table 1.5, principally because the majority are faint stars with $m_v > 15^m$. For those stars whose spectral type is available, G and K dwarfs predominate. The other counterparts in this list have been judged to be low-mass, either by their similarity to Sco X-1 (5 sources) or, more certainly, if they exhibit a non-stellar blue continuum (4 sources). For the latter category one can argue that, if the source is a binary, the optical star must be low luminosity and hence low-mass for the spectrum to be dominated by the blue continuum, assuming this to arise from either the accretion disc or x-ray heating of the optical star (e.g. Joss and Rappaport 1978).

Remarkably few of the sources listed show evidence for binary periods (3 definite and 4 possible) and only two have pulsation periods. The x-ray spectra are predominately "soft" with bremsstrahlung temperatures < 7 keV, although several "harder" sources appear in this list (N.B. both pulsating sources are "hard"). These sources display a remarkable range of time variability. The list includes three x-ray transients, three "recurrent transients" and four of the steady sources associated with bursters.

These low-mass binaries, if indeed they are all of this type, do not form as homogenous a group as the high-mass class. Nevertheless, we note the predominance of low x-ray temperatures and paucity of pulsation and binary periods. These features are arguably also properties of two other categories of galactic source - those in globular clusters and the galactic centre sources (see § 1.3.4 and 1.3.5) and this is the principal evidence for low-mass binary models for these sources.

The differences in the x-ray properties of the high-mass and low-mass binaries must reflect some basic feature of these systems. One possibility is that differences arise from the stellar population types of the systems. The high-mass systems are mainly pop I, young objects, whereas the low-mass systems are expected to be predominantly pop II, i.e. older. If the magnetic field of neutron stars decays with time, as has been suggested(Gunn and Ostriker 1970; Ewart et al. 1975), the low-mass, older binary systems

may contain neutron stars with insignificant surface fields. This would certainly explain the lack of x-ray pulsations and also the lower x-ray temperatures, since for a similar accretion mechanism, "harder" x-ray emission is expected from a neutron star with a strong magnetic field (since the size of the emitting region r_e will be that of the polar caps rather than the neutron star radius, cf. eqn.1.11).

It is also interesting to note that, on the basis of the identifications made to date, low-mass binaries must be much more numerous than high-mass binaries as x-ray sources. This follows simply from the strong selection effect towards identification with early-type stars due to both their rarity and intrinsic brightness.

1.3.9 Transients

Although the existence of transient x-ray sources has been recognised for over 10 years, their nature remains obscure, with the exception of a small number of sources which have been observed extensively, particularly with the Ariel V satellite (see Chapter 4). The sources listed in Table 1.7 have all been designated "transients" although the precise definition has never been established. A working definition has been suggested by Kaluzienski (1977). His definition (which would exclude a number of those sources listed) requires:

(i) large variability ($I_{max}/I_{min} \geqslant 10^3$);

(ii) mean interval between possible recurrent outbursts $T_{rec} \gtrsim 2$ yr (note that this is similar to the condition suggested by Cominsky et al. 1978 that the sources have a small duty-cycle relative to the total observation time);

(iii) for sources which are well observed, the light curve should show the typical rapid rise ($\sim$ days) and slow decline ($\sim$ weeks - months) characteristic of optical novae.

TABLE 1.7

Transients and transient-like variables
(after Cominsky et al. 1978a and Kaluzienski 1977)

	X-ray Source	ℓ^{II}	b^{II}	I_{max}/I_{Crab}	I_{max}/I_{min}	τ_{e^+}(days)	kT**	Notes
	A0025+59	120.1	-3.2	$\lesssim 0.1$				
r	4U0115+63	125.9	1.0	0.07	>14	14	H	See Table 1.5 . Optical ID
r	A0535+26	181.5	-2.7	2	>800	19	H	See Table 1.5 . Optical ID
*	A0620-00	210.0	-6.5	50	$>10^4$	25	S	See Table 1.6 and Ch.4 . Optical ID radio source.
	MX0656-07	220.2	-1.7	0.08	>40		S	
	MX0836-42	261.9	-1.0	0.06	>27		S	
*	A1118-61	292.5	-0.8	0.08	>15	7	H	See Table 1.5 . Optical ID?
	A1246-58	302.0	3.5	0.2		30		
	Cen X-2	305.3	0.5	6.5	>1300	20	S	Pre-Uhuru transient
	Cen X-4	331	23	25		40	S	Pre-Uhuru transient
*	A1524-61	320.2	-4.5	0.9	>450	60	S	See Table 1.6 and Ch.4 . Optical ID
	4U1543-47	330.9	5.4	2	>200	10	S	

* "classical" x-ray transient ** Approximate spectral temperature + Approximate e-folding timescale of decay

r has shown repetitive outbursts (recurrent transient) S: $\lesssim 7$ keV; H: $\gtrsim 10$ keV See Table 1.5 notes

Continued....

X-ray Source	ℓ^{II}	b^{II}	I_{max}/I_{Crab}	I_{max}/I_{min}	e^{+}(days)	kT**	Notes
r 4U1608-52	330.9	-0.8	1.1	>370		var.	Burster? See also Table 1.6 Optical ID?
r 4U1630-47	336.9	0.3	0.22	>22		S	See Table 1.6 Optical ID??
4U1658-48	338.9	-4.3	0.3	>60		S	Optical ID??
H1658-29	353.9	7.3	0.1				Burster? See Table 1.4 Optical ID?
* H1705-25	358.6	9.1	3.5		32	S	See Table 1.6 and Ch.4 Optical ID
* 4U1730-22	4.5	5.9	0.13	>31	30	S	
4U1735-28	359.6	1.6	0.57	>14	-	S	
A1742-28	359.9	-0.0	2.3	>57	12;90	S	
A1743-29	359.6	-0.4	0.15	>3	-		
H1743-32	357.2	-1.7	0.7		long	H	
A1745-36	354.1	-4.2	0.25	>25	-		
MX1746-20	7.7	3.8	0.15	>20		S	See Table 1.3
MX1803-24	6.1	-1.9	1	>500	-		
4U1901+03	37.2	-1.4	0.09	>43	-	H	
r 4U1908+00	35.7	-4.0	1	>40		S	See Table 1.6 and Ch.4 Optical ID
Cep X-4	99.0	3.4	0.2	>25		H	

Since many "steady" galactic x-ray sources show variability by factors > 10, the relaxation of condition (i) above will almost certainly mean that some of the sources listed are not true transients, and that their apparent transient characteristics are due only to the limited sensitivity of current x-ray instruments.

Only a few transients have been reliably identified with optical objects (these are included in Tables 1.3, 1.5 and 1.6), and there is direct evidence of binary membership for only one transient source (4U0115+63, Rappaport et al. 1978 - note that this is a recurrent transient). Nevertheless most transient models involve binary systems containing a compact object, essentially similar to the models for steady sources discussed in § 1.2. In these models the large variability shown by transients is usually interpreted as being due to drastic variations in the accretion rate onto the compact object. Transient source models are discussed in more detail in Chapter 4.

A classification of transients into two classes showing different spectral temperatures, timescales and luminosities has been suggested by Kaluzienski (1977). The bimodal temperature distribution is confirmed by the work of Cominsky et al. (1978), the other differences are perhaps less compelling. The temperature distribution found is precisely the same as that seen in "steady" binary sources - the "hard" sources being associated with the high-mass, pulsating sources, the "soft" sources with low-mass systems (cf. § 1.3.7 and 1.3.8).

1.3.10 Low Luminosity Sources

It is only fair to conclude this section on the observational aspects of galactic x-ray sources by mentioning the existence of a class of object which is rather outside the terms of reference of this thesis. A recent review by Garmire (1978) lists 30 x-ray sources which have been identified with nearby stars ($d \lesssim 100$ pc) and have very low x-ray luminosities ($L_x \ll 10^{35}$ erg s^{-1}). Such sources can only be detected at present out to a few hundred

parsecs and thus have a very broad latitude distribution, making them difficult to distinguish from extragalactic objects unless very precise positions are available. In addition to their low luminosity, many of these sources are characteristically very soft ($kT < 1$ keV). The softest sources will never be detected at large distances from the sun due to the large interstellar absorption at these low photon energies.

Garmire divides these low luminosity sources into five main categories: cooling white dwarfs (e.g. HZ43), coronal emission sources (e.g. α Cen), flare stars (emission from magnetically active regions? e.g. RS CVn binaries, UV Cet), interacting stellar wind sources (e.g. Algol?) and cataclysmic variables (e.g. AM Her, U Gem). The emission mechanisms responsible for the x-ray flux observed are thus probably rather different from those discussed above with the exception of the cataclysmic variables where accretion onto a white dwarf is thought to be responsible for the x-ray activity (see § 1.2.5).

In addition to the low luminosity sources discussed by Garmire, we expect to find a number of ordinary accreting neutron star sources of the type discussed earlier at low luminosities. X Per, with a luminosity $L_x \approx 10^{33}$ erg s^{-1}, is almost certainly a system of this sort, since pulsar timing measurements strongly suggest that the compact object in this system is a neutron star (Rappaport and Joss 1977). The lower luminosity of such systems is presumably just the result of much lower accretion rates, and their apparent rarity probably only reflects the limited sensitivity of current surveys (although the luminosity function of galactic x-ray sources has yet to be adequately determined).

With the advent of a new generation of vastly more sensitive x-ray observatories (starting with HEAO-B) we can expect the study of lower luminosity sources of all types to become of prime importance in the understanding of the phenomenology of galactic x-ray emitters.

1.4 Time Variability

1.4.1 Observational Considerations

In contrast with most astronomical objects (with a few notable exceptions) galactic x-ray sources show a remarkable degree of variability on a vast range of timescales from 10^{-3} sec to > 10 yr. On the shortest timescales (< 100 ms) the variability seen is unique to galactic x-ray sources (and the Crab and Vela pulsars!).

From an observational point of view the timescales on which variability can be observed are set by a variety of constraints. At the shortest timescales photon statistics, even for the brightest source, limit the time resolution to ~ 1 ms, and a time resolution of 10 ms - 100 ms is typical of the current generation of x-ray astronomy satellites. Observations on timescales from seconds to days are usually possible with even modest instruments, although timescales of the order a few hours are often problematic since the earth orbital period of most x-ray astronomy satellites is in this range, and the observations are almost always interrupted at least once per orbit. Observations longer than a few days are often difficult to make, either because of demands on observing time or because of a variety of constraints on keeping the satellite attitude steady for extensive periods. The Ariel V satellite is unusual in this respect in that continuous observations of up to 30 days have been possible. On even longer timescales the only continuous monitoring possible is with instruments such as the Ariel V ASM (see Chapter 2) which have large fields of view, but suffer from rather low sensitivity.

Figure 1.5 illustrates the variability, both chaotic and periodic, seen in several typical galactic sources on both short and long timescales. Figure 1.6 summarises the observational picture for x-ray variability in galactic sources, together with a few examples for ordinary stellar systems.

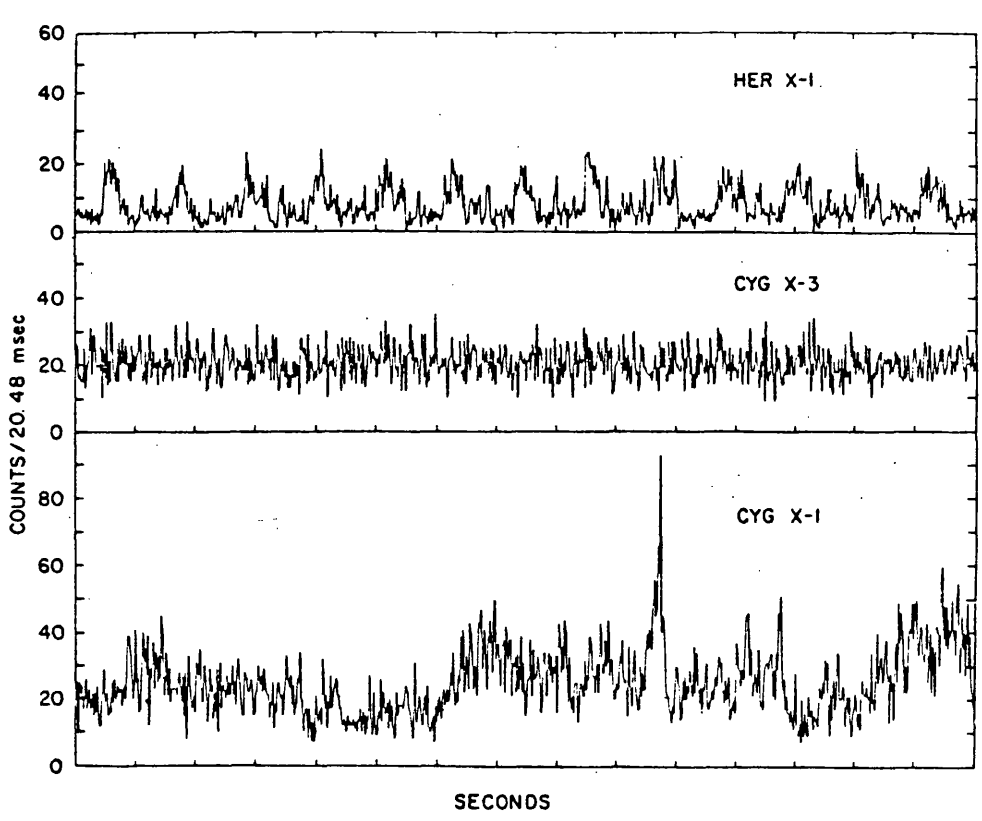

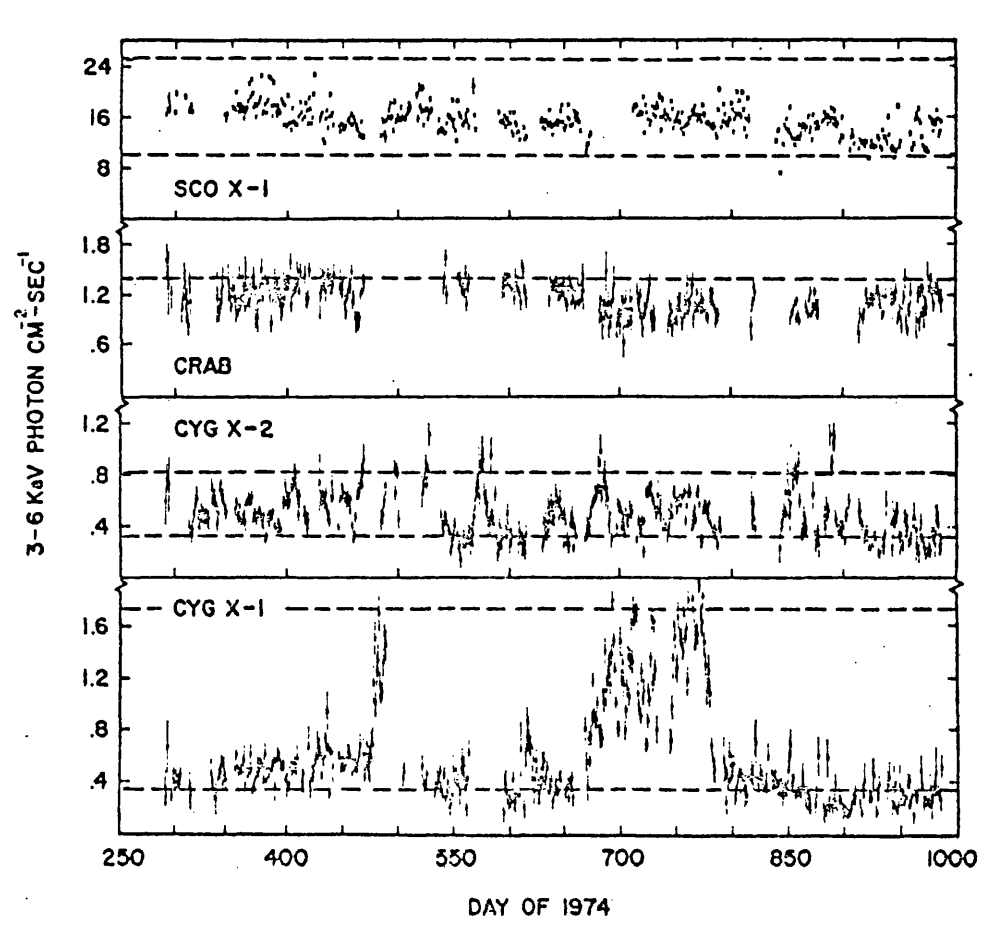

Fig. 1.5 (a) Short timescale variability of Her X-1, Cyg X-3 and Cyg X-1 as observed on a 1973 rocket flight (from Rothschild et al.1974).

(b) Long timescale variability of Sco X-1, the Crab, Cyg X-1 and Cyg X-2 as seen by the Ariel V ASM (from Kaluzienski 1977).

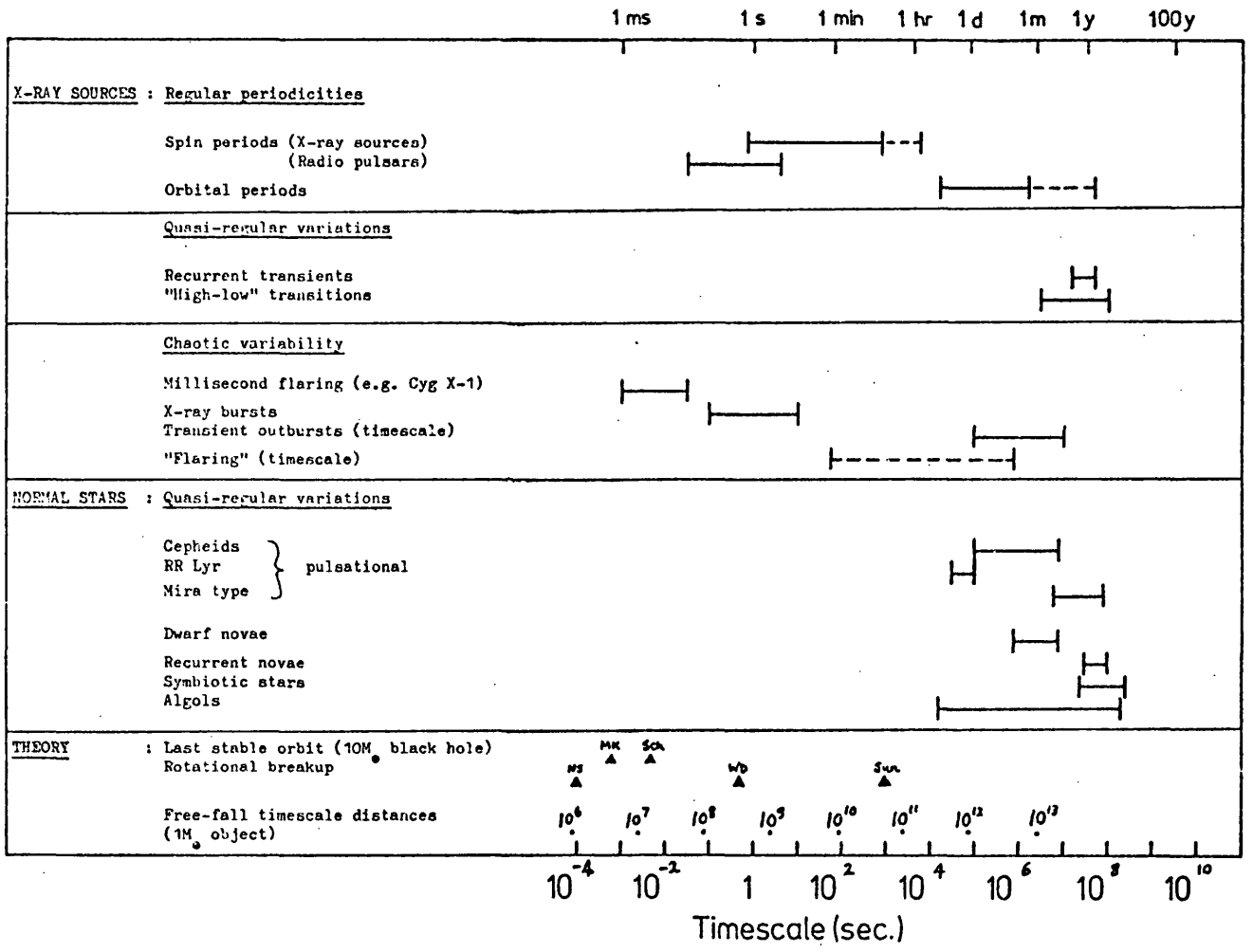

Fig. 1.6 Range of observed timescales for variability in both x-ray sources and normal stars, and as given by theoretical considerations. (MK, Sch refer to maximal Kerr and Schwarzchild black holes, NS, WD to neutron stars and white dwarfs. Free-fall timescale distances are given in cm.).

1.4.2 Theoretical Aspects

In general terms the regular periodicities seen in galactic sources are the most easily understood, since they must reflect some rotation (or conceivably free pulsations) within the system. Quasi-regular and chaotic variability is much more difficult to interpret since there are usually a number of mechanisms which might lead to the same behaviour. Nevertheless some constraints can be placed on the origin of the variations simply by considering the physical limitations implied by the timescale.

The ultimate limit is set by the light travel time considerations. If the x-ray emission comes from a region with dimension R, variability cannot occur on timescales shorter than t_{lt} given by:

$$t_{lt} = \frac{R}{c} \approx 2.3\left(\frac{R}{R_\odot}\right) \approx 3 \times 10^{-5} \left(\frac{R}{R_6}\right) \quad \text{sec} \qquad (1.14)$$

where R_6 is in units of 10^6 cm. A more realistic limit comes from considering the free-fall timescale from a radius R within the system (Ostriker 1977):

$$t_{ff} \sim \left(\frac{GM_x}{R^3}\right)^{-\frac{1}{2}} \approx 1.6 \times 10^3 \left(\frac{M_x}{M_\odot}\right)^{-\frac{1}{2}} \left(\frac{R}{R_\odot}\right)^{+3/2} \quad \text{sec} \qquad (1.15)$$

$$\approx 8.6 \times 10^{-5} \left(\frac{M_x}{M_\odot}\right)^{-\frac{1}{2}} \left(\frac{R}{R_6}\right)^{+3/2} \quad \text{sec} \qquad (1.16)$$

For example, a typical close binary system has dimensions $R \sim 10^{11}$ cm, with $M_x \sim 1\ M_\odot$. This gives $t_{ff} \sim 1$ hour. For free-fall from the magnetosphere of a neutron star ($R \sim 10^8$ cm), $t_{ff} \sim 0.1$ sec (this may be directly relevant to models for x-ray burst sources where $t_{rise} \sim 0.1$ sec). Note that the free-fall timescale also gives the maximum angular velocity for a spinning object before breakup occurs:

$$\omega_{max} \approx \frac{2\pi}{t_{ff}} \quad \text{Hz} \qquad (1.17)$$

For a star with $R \sim 1\ R_\odot$, the breakup angular velocity corresponds to a spin period of $\sim 10^3$ sec, for a white dwarf a period of 1 - 3 sec, and for a neutron star $\sim 10^{-4}$ sec.

For a black hole the relevant timescale is that which corresponds to the period of the last stable orbit. For a Schwarzchild hole this is:

$$t \approx 4.5 \times 10^{-4} \left(\frac{M_x}{M_\odot}\right) \quad \text{sec} \tag{1.18}$$

amd for a maximally rotating Kerr hole:

$$t \approx 6.4 \times 10^{-5} \left(\frac{M_x}{M_\odot}\right) \quad \text{sec} \tag{1.19}$$

(Ruffini 1975). (The constraints implied by eqns. 1.14 - 1.19 are also illustrated in Fig. 1.6).

It is clear that x-ray variability on the shortest timescales, for example the millisecond variability in Cyg X-1 and x-ray bursts (see Figs. 1.5 and 1.6), must originate at or near the surface of a compact object (regions with $R < 10^8$ cm). The general variability on timescales as short as 0.1 sec seen in a large number of galactic sources (e.g.Forman et al. 1976) must also originate in regions smaller than $\sim 10^{10}$ cm ($< 1\ R_\odot$). In terms of the breakup angular velocities given by equation 1.17, the shortest spin periods detected in x-ray sources ($\sim$ 1 sec, Fig.1.6) must be related to the rotation of a neutron star, whilst the longer periods ($\lesssim$ 1000 sec) demand an object at least as compact as a white dwarf.

On longer timescales (hours to days), periodic modulation is easily understood in terms of the orbital motion of the x-ray source. The origin of chaotic and quasi-periodic variability is more difficult to pin down, since both accretion instabilities (particularly within an accretion disc) and secular variations in the mass transfer rate may play their part. Instabilities in the accretion flow are almost bound to occur -

some of the possibilities are discussed by Ostriker (1977). As before the timescale for variability will be given approximately by the free-fall timescale.* Thus only instabilities in the outer disc regions are expected to give variability on longer timescales.

Variability in the mass transfer rate is known to occur for both Roche-lobe overflow and stellar wind mass-loss. For example, the repetitive outbursts in dwarf novae are believed to be a result of varying Roche-lobe mass-loss by the non-degenerate star (Bath 1976), although the underlying mechanisms are not well understood (Bath 1977). Dramatic changes in the stellar wind are thought to explain the long term variability of sources like Cen X-3 (Schreier et al. 1976), and recurrent "hard" transients like 4U0115+63 (Rappaport et al. 1978). At present the mechanisms which drive these secular variations in mass-loss rate are not generally well understood. One might expect however that such variations would show a spectrum of timescales similar to those apparent in ordinary stellar systems (e.g. recurrent novae, Algols, etc. - see Fig. 1.6).

With such a range of possibilities it is perhaps surprising that all galactic x-ray sources do not show variability on all timescales. One reason for the lack of short timescale variability (including coherent pulsations) in some sources (e.g. Sco X-1) may be the existence of a gas shell surrounding the x-ray source which is optically thick to electron scattering ($\tau_{es} \gtrsim 5$) (Maraschi et al. 1977). This shell will effectively smooth out any variability on timescales $t < (1 + \tau_{es}) \frac{R}{c}$, where R is the radius of the shell. Gas shells of this sort may exist preferentially in low-mass binary systems in which mass transfer occurs via Roche-lobe overflow, and may thus explain the lack of x-ray pulse periods in these sources.

---

* Note however that the radial infall timescale for a viscous accretion disc is $\gg t_{ff}$ leading to timescales of $\sim$ months for large discs, such as may result from Roche-lobe overflow.

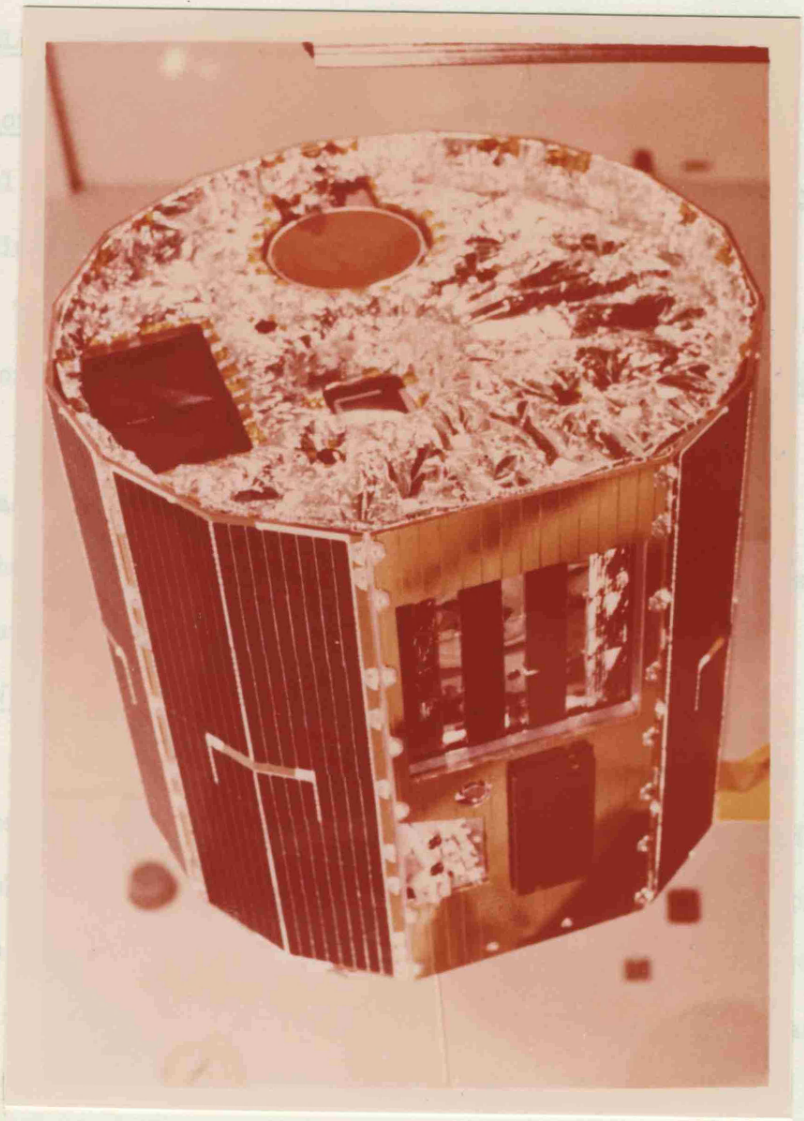

Fig. 2.1 Ariel V Satellite

Chapter 2

ARIEL V SATELLITE, SKY SURVEY INSTRUMENT AND DATA HANDLING

2.1 Introduction

The Ariel V satellite has a scientific payload of six x-ray astronomy experiments provided by four British and one American institutions. The experiments span the energy range 0.3 keV - 1.2 MeV with a variety of broadly complementary capabilities for determining source spectra, positions and variability. Since launch in 1974 October the satellite has operated remarkably successfully, despite a few minor problems, and the project is planned to continue until 1979 October (see Fig. 2.2 for history of operations).

2.2 The Ariel V Satellite

Ariel V, shown in Fig. 2.1, is the first British satellite devoted to x-ray astronomy. Its only true predecessor is the American UHURU satellite with which it has much in common, although a number of previous spacecraft, such as OSO-7 and Copernicus, have included cosmic x-ray astronomy experiments. The important features of the satellite are summarised in Table 2.1.

The low, nearly equatorial orbit of the satellite is designed to maximise the shielding of the experiments by the earth's magnetic field from the cosmic ray flux. In practice the particle background is adequately low except when the spacecraft passes near the South Atlantic Anomaly. This is catered for by use of a background rate veto flag, accessible to each experiment, to inhibit data collection if desired. Power for all spacecraft systems is supplied during the sunlit portion of the orbit by

TABLE 2.1

Ariel V Satellite : Main Parameters*

DIMENSIONS	Height 86.4 cm; width 95.9 cm.
WEIGHT	132 kg.
ORBIT	556 x 512 km; 2.9° inclination to equator.
LAUNCH	1974 October 15 from San Marco platform, Kenya by 4-stage Scout rocket.
ATTITUDE	
Sensing	2 pairs of sun slit-sensors, 2 pairs of Earth albedo-sensors (1 pair redundant). Sector generator supplies 1024 equi-spaced signals per satellite rotation.
Control	Spin-stabilised at ~ 10 rpm. Manouevres and spin-rate changes using pulsed gas jets fed by liquid propane tanks (or using magnetorquer system - see text).
Accuracy	Sensing: $\lesssim 0.5^\circ$. Drift: $\lesssim 0.2^\circ$ in one orbit; $< 1^\circ$ per day (can be corrected by small attitude changes on command).
POWER SUPPLY	Solar cells covering 7/8 of circumference of satellite. In eclipse power supplied by 3 Ah NiCd battery. Power consumption ~ 12 w.
DATA HANDLING	On-board computer with two 4096 word (8-bit) core stores.
TELEMETRY	Data dumps and satellite commands relayed via VHF link with NASA STDN ground stations (part of NASCOM network).

---

* Based on "The Scientific Payload for the UK-5 Satellite", SRC Report (1973).

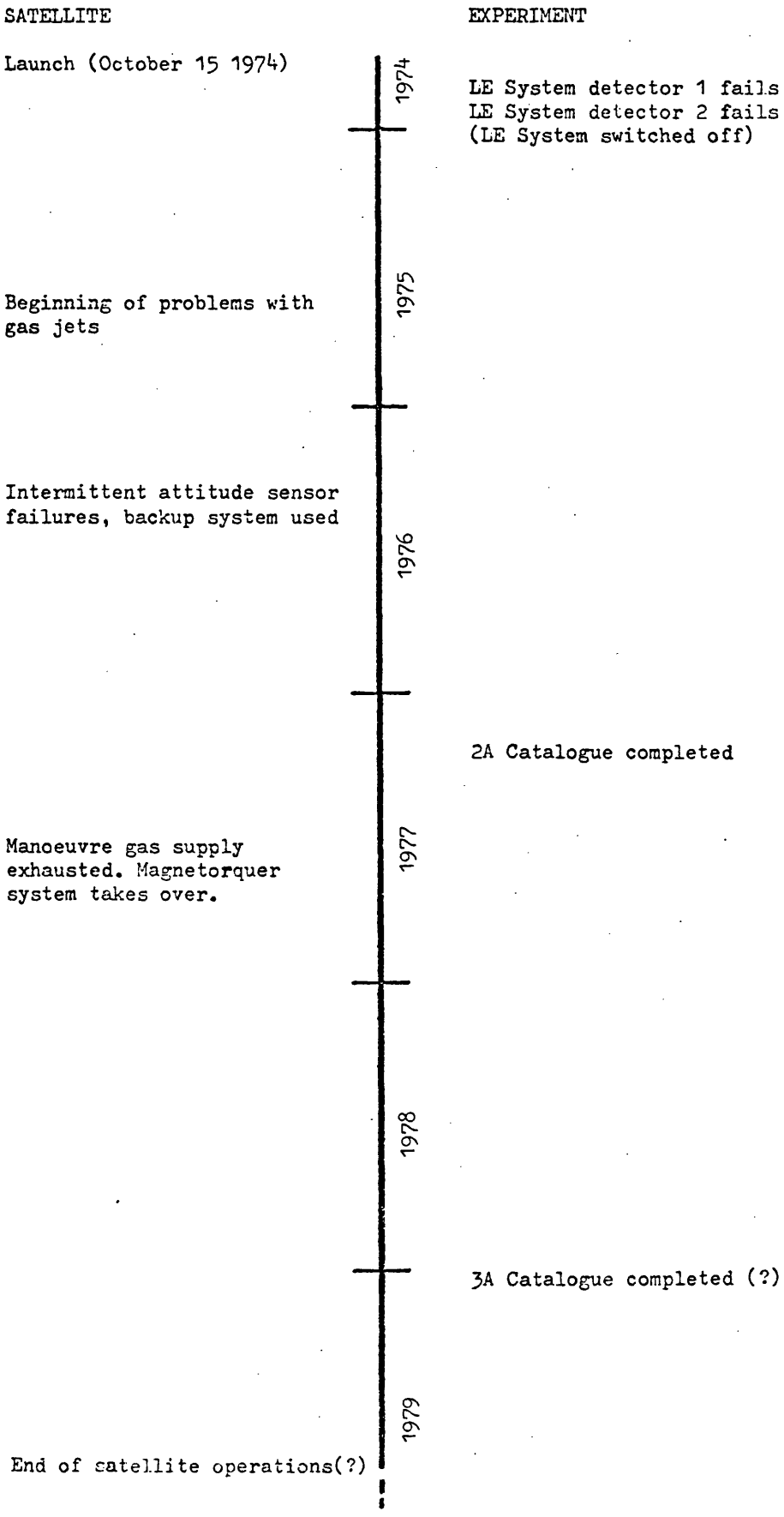

Fig. 2.2 History of Ariel V and the SSI since launch

solar cells which cover 7/8 of the periphery of the spacecraft. Power requirements constrain the solar vector to be within 45° of the normal to these solar cells, i.e. within 45° of the spacecraft spin plane (see Fig.2.3). During eclipse an on-board battery keeps the satellite "live" but cannot provide enough power for operation of the experiments.

Ariel V is a spin-stabilised satellite with a nominal spin-rate of 10 r.p.m. Control of the spacecraft attitude and spin-rate (at least for the first three years of operation) is achieved by use of three pairs of pulsed gas jets (see Fig.2.3) fed from a liquid propane tank via reducing valves. At launch the gas supply was estimated as being sufficient for a total of ~ 4000° of manoeuvre. Operational problems with the reducing valves have led to rather larger gas usage than expected, and at the time of writing the gas supply is exhausted (see Fig.2.2). Restricted manoeuvres can, however, still be made by powering the on-board magnetorquer coil thus inducing an attitude change by interaction with the earth's magnetic field. Attitude manoeuvres as large as 10° per day in R.A., but only ~ 0.5° per day in declination are possible with this method, but pointing directions are severely constrained by the requirement that the satellite spin-rate remains reasonably steady. (Large spin-rate changes can be induced by the magnetorquer - earth's field interaction).

The data-handling system for both the experiments, and the spacecraft house-keeping data, is based on two 4096 word (8-bit) core stores. The contents of both stores are dumped every orbit, on command, to a NASA STDN ground station (at Quito, Ascension Island, and more recently Guam). Manoeuvres and changes to the experiment command registers are also made on certain passes over the same ground stations. This results, in the case of manoeuvres, in the loss of experimental data for that orbit.

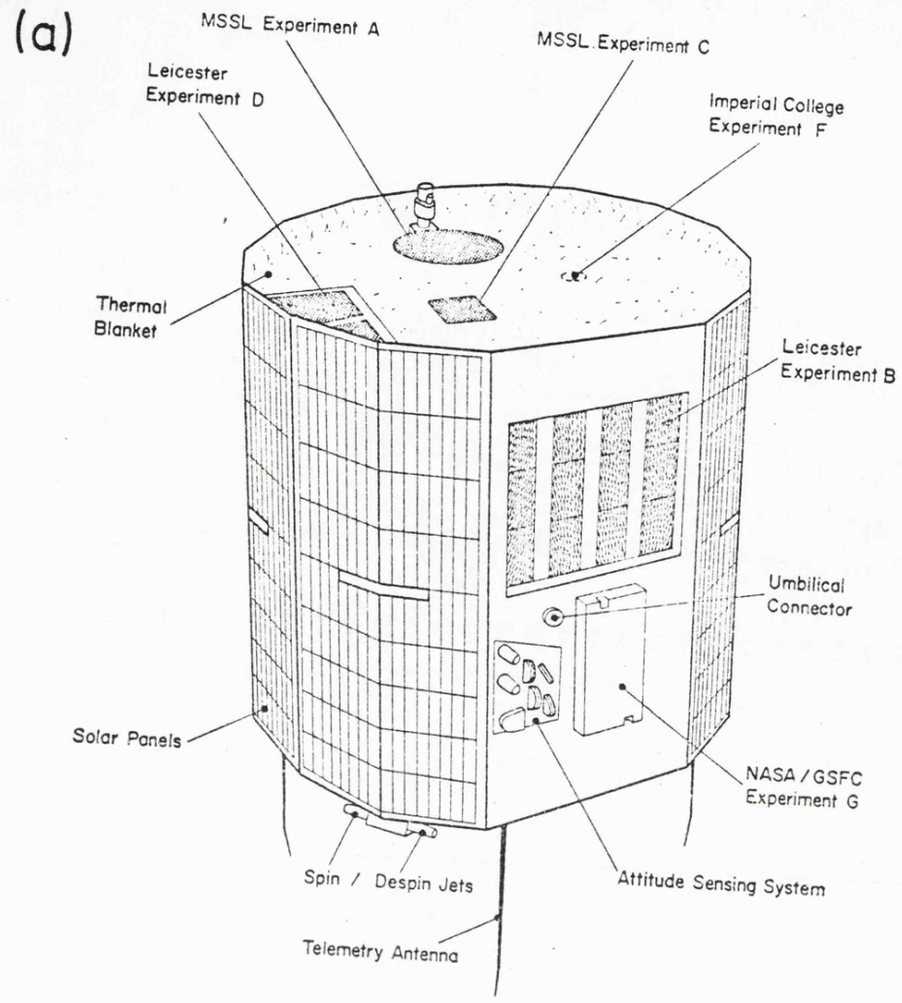

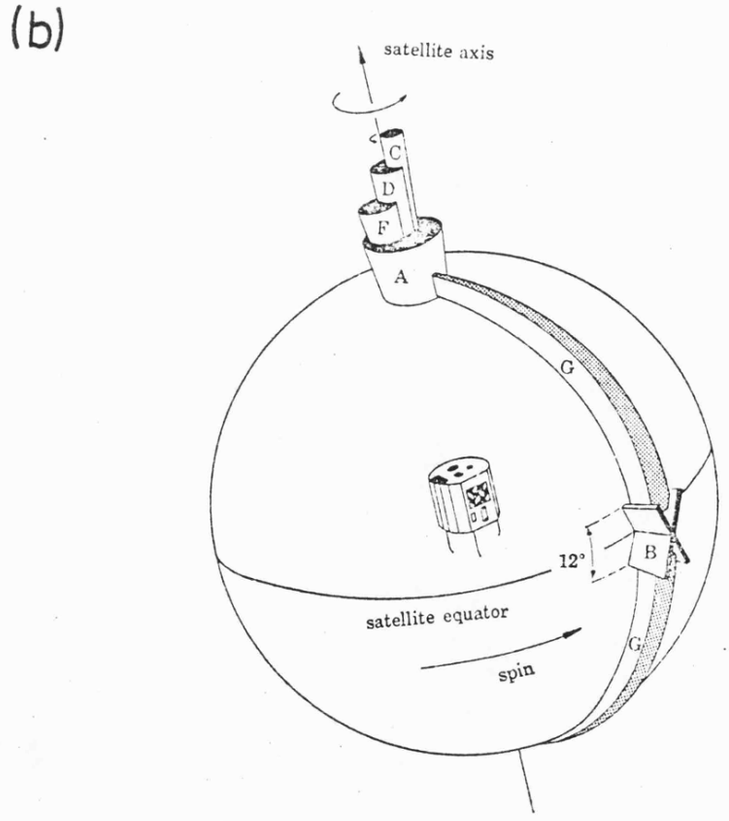

Fig. 2.3 (a) Line drawing of the Ariel V satellite showing the experimental payload and main spacecraft systems.

(b) Fields of view of the experiments. (Both figures from Smith and Courtier 1976).

Summary of Experimental Payload**

(1)	(2)	(3)	(4)	(5)	(6)	(7)			(8)
Expt.	Institution	Description	FOV (FWHM)	θ_{min}	Δt_{min}	Spectral Response Range	N	$\Delta E/E$	Objectives
A (RMC)	Birmingham Univ./MSSL [1]	Rotation modulation collimator using channel electron multipliers and prop.counters.	17°	$0^{\circ}.02$	32^{s}	0.3-6 2-18	1 3	>100 38	Positions of brighter sources to < 1 arcmin.
B (SSI)	Leicester University [2,3]	Sky survey instrument using slat-collimated scanning prop.counters.	$10^{\circ}.6 \times 0^{\circ}.75$	$0^{\circ}.2$	512^{s}	0.9-6 2.5-20	8 8	30 30	Sky survey to $\sim 10^{-3}$ Crab. Detailed study of individual source variability.
C	MSSL [4]	High resolution prop.counter spectrometer.	$3^{\circ}.5 \times 3^{\circ}.5$	$0^{\circ}.5$	64^{s}*	1.4-30	128	2	High resolution spectra and studies of time variability.
D	Leicester University [5]	Bragg crystal spectrometer/ polarimeter.	$7^{\circ}.5$	-	64^{s}*	2-8	8	1	Emission line spectra of bright sources plus polarisation studies.
F	Imperial College [6]	CsI Scintillator with active collimation.	$8^{\circ}.0$	2°	256^{s}*	26-1200	16	27	High energy spectra of bright sources.
G (ASM)	NASA GSFC [7]	All Sky Monitor incorporating two pinhole cameras and position sensitive prop.counters.	90% of celestial sphere	2°	100^{m} (one orbit)	3-6	1	100	All sky survey for bright transient phenomena. Long-term monitoring of bright sources.

** based on Smith and Courtier (1976)

Notes to Table 2.2

Column (2) : Name of institution operating experiment. (MSSL = Mullard Space Science Laboratory; GSFC = Goddard Space Flight Centre). Reference to expt. description given in brackets.

Column (4) : Field of view (full width at half maximum) in degrees.

Column (5) : Approximate optimum positional accuracy for a bright source in one orbit (degrees).

Column (6) : Minimum time resolution (seconds).

Column (7) : Range - Energy range in keV.

N - No. of energy channels.

$\Delta E/E$ - Approximate energy resolution (%).

These values are the launch characteristics of the experiments.

* These three experiments can operate in 'pulsar' mode in which x-ray counts are accumulated in 16 bins according to the phase of the preset 'pulsar' period. The time resolution in this mode is limited by detector characteristics and the stability of the on-board clock to about 1 ms.

References

1 Wilson (1977)

2 Cooke et al. (1978)

3 Villa et al. (1976)

4 Sanford and Ives (1976)

5 Griffiths et al. (1976)

6 Carpenter et al. (1976)

7 Kaluzienski (1977)

Four of the experiments on Ariel V are mounted on the top of the satellite and view along the spin-axis, i.e. are essentially "pointed". The other two, including the SSI, are side-mounted and thus scan the sky as the satellite rotates. The configuration of the experiments and their approximate fields of view are shown in Fig.2.3. Further details of the experiments are given in Table 2.2.

2.3 The Sky Survey Instrument

The Sky Survey Instrument is a scanning proportional counter system sensitive to x-rays in the energy range $\sim 2 - 18$ keV, with up to 16 PHA channels of spectral information and normal time resolution of ≈ 100 minutes (one satellite orbit). The instantaneous field of view of the experiment, set by the mechanical slat collimators, is a cross-shaped fan beam, one arm of the cross corresponding to the low-energy and the other to the high-energy detector system. Experimental data from the SSI is accumulated throughout each orbit in the 1024-word section of the satellite core-store allocated. The satellite sector-generator provides 1024 equi-spaced signals per satellite rotation. These signals are used to divide the scan into 1024 azimuthal sectors (width = $\frac{360^\circ}{1024} \approx 0.35^\circ$). In the simplest case of SECTOR 360° MODE operation each core-store location will correspond to one azimuthal sector. Data from the SSI in this observing mode are shown in Fig.2.5. Where spectral information is required the limited core-store available demands a trade-off between the arc of the scan covered and the number of energy channels stored. For example in SECTOR 45° MODE data from only 45° of the scan is used (i.e. 256 sectors) but for each sector 4 channels of spectral information is stored (making a total of 4 sets of 256 sectors). In order to make spectral mode observations of specific sources the start sector (sector zero) can be preselected to ensure that the correct arc of the scan is observed. Further details of the SSI are given in Table 2.3.

T A B L E 2.3

Sky Survey Instrument Parameters

COLLIMATORS	Stainless steel slats defining: FIELD OF VIEW : 10.6° x 0.75° canted at 65° to spin plane. Low energy (LE) and high energy (HE) systems collimators have fields of view which cross on the spin plane (see Fig. 2.4).
DETECTORS	Two pairs of proportional counters - one pair for LE, one pair for HE system. Windows : LE system 0.0086 cm Be HE system 0.0127 cm Be Filling gas: LE system 2 cm depth HE system 4 cm depth Ar(76%):Xe(16%): CO_2(8%) at 900 mm Hg. Energy range : LE system 0.8 - 6 keV HE system 2.4 - 20 keV (nominal values at launch) PHA divides counts in each system into 8 energy channels with geometrically spaced boundaries : $\frac{E_{upper}}{E_{lower}} = \frac{1.3}{1}$ Energy resolution ~ 60% at 6 keV. Effective area: 280 cm^2 for each system.
CALIBRATION	In-flight calibration by Fe^{55} K capture source irradiating detectors by removing masking shutters on command.
BACKGROUND REJECTION	(1) Each detector is surrounded on 3 sides by a guard detector in anti-coincidence with main detectors. (2) RTD rejects events with rise-time above selectable threshold. (3) Pulses outside range of PHA rejected. These 3 methods result in rejection of ~ 96% of non x-ray background. Contamination by solar x-rays is avoided by inhibiting data collection when the sun is within 15° of the spin plane (sun diode veto). Experiment is also provided with background rate veto flag from either Expt.C or D allowing inhibition of data collection during periods of high background (such as passage through the South Atlantic Anomaly).
DATA STORAGE	Experimental data is accumulated in 1024 16-bit core-store locations addressable by sector position, energy and time.

Continued ...

EXPERIMENT COORDINATES	Coordinate system has spin-axis as pole with spin plane as equator. The spacecraft has a sector generator which divides each spacecraft rotation into 1024 sectors. The zero sector starts when the sun is detected in the sun slit sensor. The fields of view of SSI and sun slit sensor are aligned so sector zero is also the zero point of experiment azimuth (unless offset by start sector).
EXPERIMENT CONTROL	Experiment is controlled by a 27-bit command register, set by signals from ground station. Control options : HT and pre-amps (ON/OFF) Calibration source shutter (OPEN/CLOSED) Coarse gain control RTD threshold select Select background veto flag (C/D) Select start sector Select observing mode
OBSERVING MODES	11 observing or diagnostic modes are available. Normal observations are made in SECTOR mode where data is accumulated according to sector position and energy. Restrictions in core-storage require a trade-off between energy channels and extent of azimuth scanned, i.e. 360° scan with no energy information; $22\frac{1}{2}^{\circ}$ scan with 8 energy channels. Azimuthal resolution stays constant at one sector $\approx 0.35^{\circ}$.
OPERATIONAL CHARACTERISTICS	Background count-rate ≈ 9 counts s^{-1} (estimated 50% diffuse and 50% non x-ray). Maximum observing time per 100 minute orbit is ≈ 60 min, due to switch-off during eclipse. Typical observing time for particular source is ≈ 30 min. due to effects of earth-screening, giving actual exposure times ~ 2 sec per azimuth sector.
SENSITIVITY	3σ sensitivity for one orbit (source on spin plane) ≈ 6 SSI counts s^{-1} ≈ 15 UHURU counts s^{-1} $\approx 3 \times 10^{-10}$ erg $cm^{-2}s^{-1}$ (2-10 keV). (See § 2.4.2 for more details).

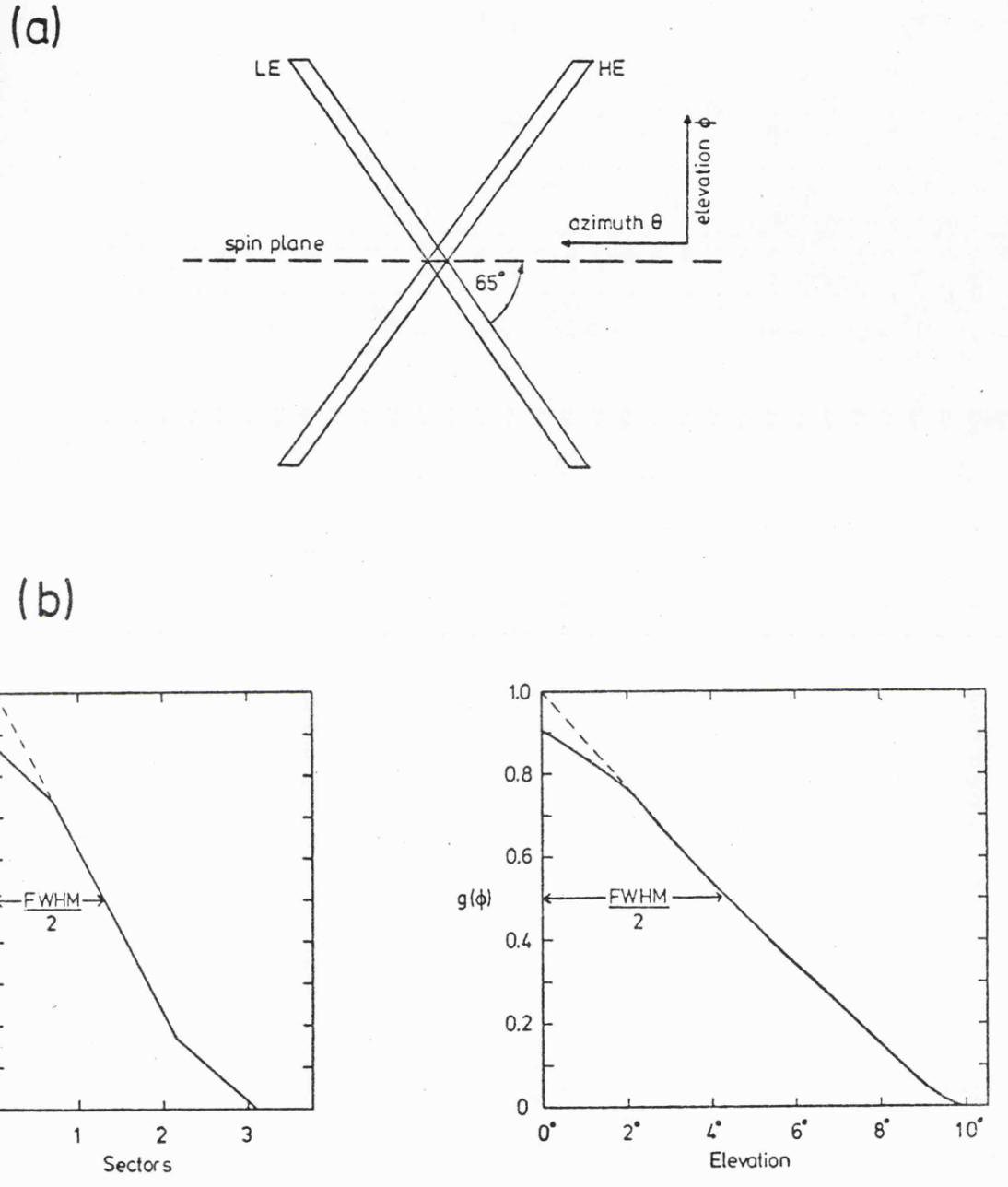

Fig. 2.4 (a) Instantaneous field of view of the SSI as defined by the slat collimator. Note definition of azimuth and elevation coordinates.

(b) Azimuth and elevation response functions of the SSI collimators (based on observations of the Crab). Departures from the theoretical triangular shape are due to random mechanical misalignment of the collimator cells.

At launch both detector systems were working normally but shortly afterwards both low-energy systems counters developed leaks which made them unusable after only a few months (see Fig.2.2). The low-energy system was switched off in 1974 December, thus the majority of the SSI observations have been made with the high-energy system alone.

The SSI is designed to perform two major tasks:

(i) to survey the whole sky with a sensitivity of 10^{-3} I_{Crab} with sufficient positional accuracy to make identifications possible;

(ii) to make a detailed study of the variability of individual sources.

The failure of the low-energy system has led to some changes in the observational strategy for the all-sky survey but has not seriously affected the study of individual sources (although simultaneous low-energy system observations would have been useful in monitoring spectral changes). The results of the sky survey for sources at high galactic latitudes ($|b| \geqslant 10^{\circ}$) have already been published as the '2A' catalogue containing 105 x-ray sources (Cooke et al. 1978). Detailed studies of individual sources have been published in a number of papers, some of these results being presented in Chapters 3, 4 and 5.

Observing time with the Ariel V satellite is divided more or less equally between five of the experiments (the sixth, expt.G, makes no special demands on the spacecraft attitude since its field of view covers most of the sky (see Table 2.2)). In the pre-agreed observing programme each experiment typically has control over the spacecraft attitude for several days continuously, during which period the spin-axis position will normally be kept approximately steady by making small attitude changes daily to correct for drift. The total attitude change during one observation is usually restricted to $\lesssim 3^{\circ}$. Thus the observations with the SSI consist of sets of orbits with nominally the same spacecraft attitude ("observing

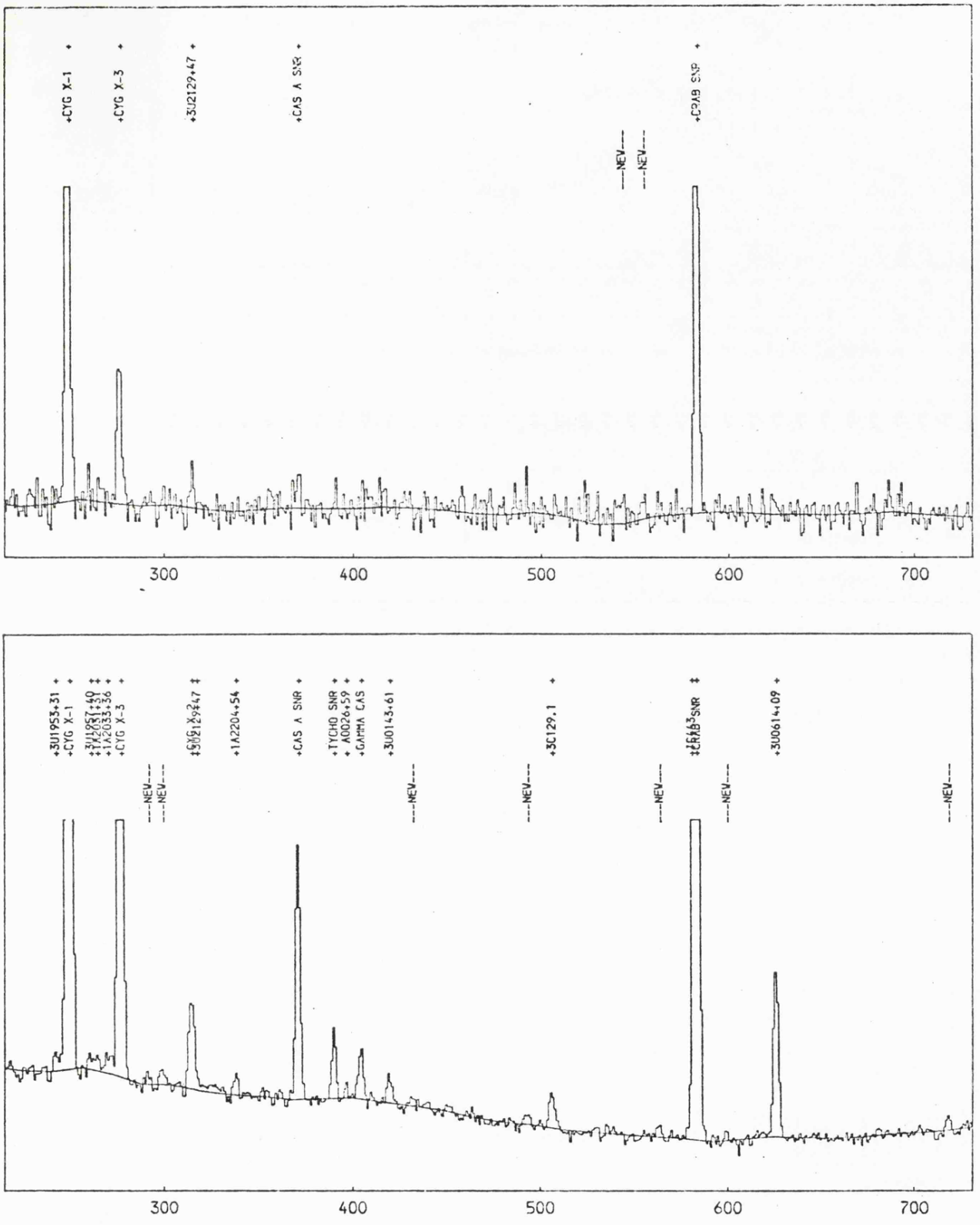

Fig. 2.5 SSI scans of the galactic plane made in 1976 November. Top histogram shows a section of the data accumulated in one orbit, bottom histogram shows the same section of the scan for data accumulated for 100 orbits with corresponding dramatic increase in sensitivity. The solid line is the fitted background level and the labels indicate the peak matching with catalogued source performed by the scan analysis.

slots") spanning typically 1 - 10 days. Approximately 80% of these slots will of course be made with the spacecraft attitude chosen by one of the other experiments, but because of the wide strip of sky scanned by the SSI, practically all this data will be of some value, at least for sky survey purposes. (Further details of the observing programme are given in Silk 1976 and Elvis 1978).

Provided the attitude change in each observing slot does not exceed $\sim 3^{\circ}$, the SSI data from each orbit within the slot can be coherently summed with little loss in spatial resolution by overlaying the sector data making allowance for the small attitude drift from orbit to orbit. Examples of both single orbit and summed data are shown in Fig.2.5. The sensitivity to weak sources is obviously much greater in the summed data (signal-to-noise ratio has a $\sim n^{\frac{1}{2}}$ dependence on the number of orbits summed) and the observations are normally analysed in this form for the determination of source positions, and for examining the variability of weak sources. Variability studies of strong sources can be made using the single orbit data with the advantage that the highest time resolution is then available.

In principle, observations with the SSI consist of 14 - 15 satellite orbits per day, the data from each orbit being relayed to Leicester via the NASA ground stations and OCC at the Appleton Laboratory. In practice about 20% of all orbits are lost due mainly to telemetry problems and scheduling priorities at the ground stations. The SSI data received at Leicester is stored in machine-readable form in one extensive data base which includes all the useful observations made since launch. The data are analysed on both a "quick-look" and long-term basis. The "quick-look" analysis is really no more than a preliminary scan of the data with the object of identifying transient events, etc., and is completed within about

a day (at most) of the time of the observation. The long-term analysis proceeds at a more leisurely pace and is discussed in the next section.

2.4 SSI Data Analysis

The essentially simple format of the SSI data for each satellite orbit lends itself particularly well to analysis with one standard program. This program, now known as "SCAN" has been continuously developed* since the start of Ariel V operations and now performs automatic processing of the SSI data with remarkably few problems. The program analyses the data on a single orbit basis, but if required will also coherently sum all orbits with nominally the same spacecraft attitude and perform a similar analysis on the summed data, deriving for each orbit and sum of orbits a flux and position for each peak detected in the data, associating these peaks with catalogued x-ray sources where possible. Almost all the data presented in this thesis rely on the "SCAN" analysis of the SSI observations.

The basic operation of the analysis program is illustrated in a simplified form in Fig. 2.6. The flow chart shown is for the analysis of a single orbit; analysis of summed orbits is essentially identical with the addition of a summing routine between steps (I) and (J) and additional checks on the experiment mode, start sector and attitude in step (C).

Points to note on the flow chart are:

(A): Data for each orbit consists of the timing, attitude and housekeeping information for that orbit, together with the contents of the 1024 word core-store allocation (the experimental data).

(B): (i) This routine evaluates the mean attitude and error estimates from the 7 independent attitude records in the data.

(ii) Total integration time is determined from the experiment event codes and event times which are a record of the switch on/off times corresponding to the start/end of orbit; entry/exit into Earth eclipse and start/end of background rate veto. In the event of the corruption of the event data the program can usually make an intelligent correction.

---

* The original program was mostly the work of G.R.Eadie, development since launch has been undertaken almost single-handedly by Dr.C.G.Page. Previous versions of the program were called "OSA".

Fig. 2.6 SCHEMATIC FLOWCHART FOR SINGLE ORBIT ANALYSIS OF SSI DATA

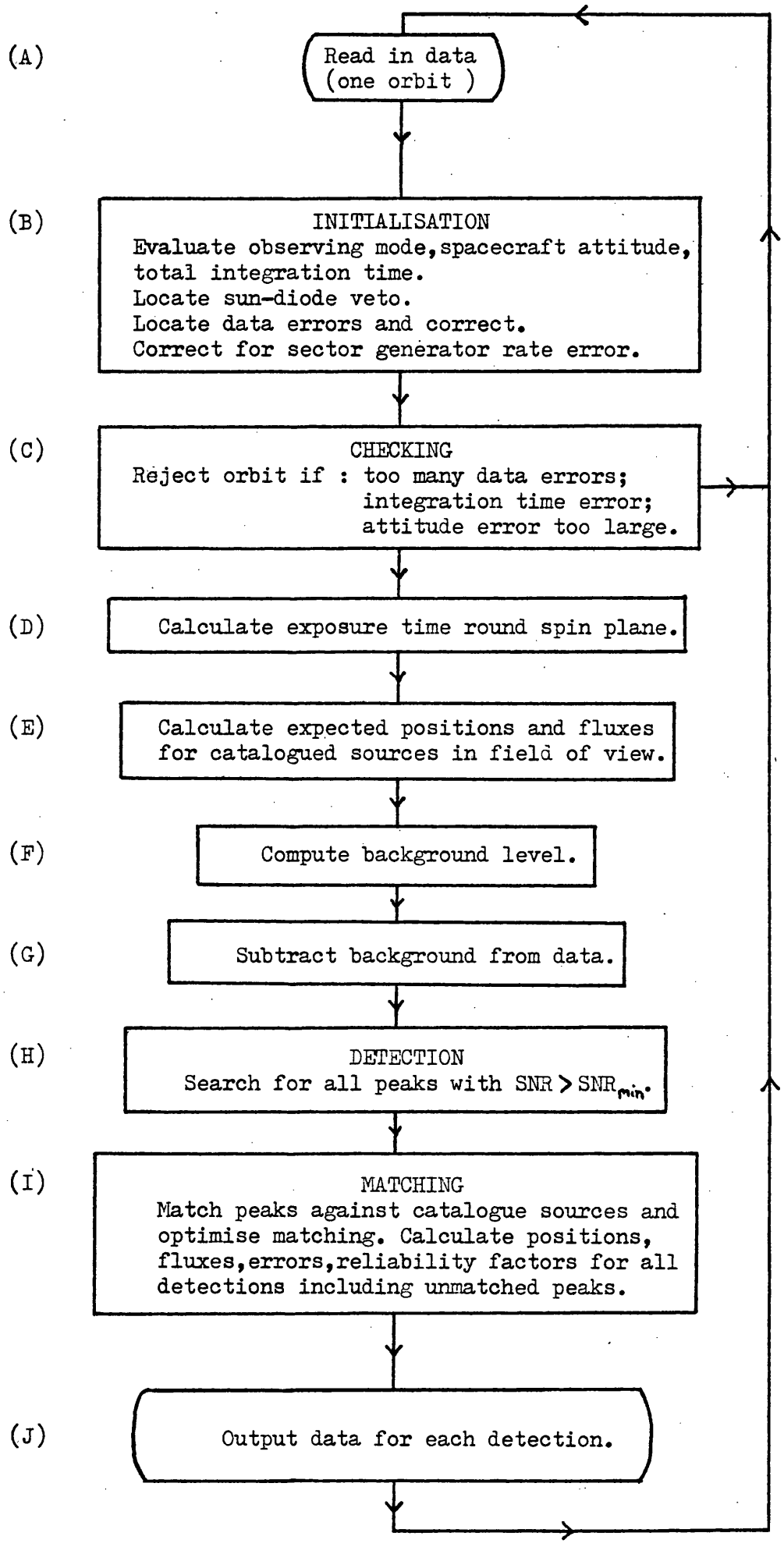

(iii) Parts of the data affected by the sun diode veto (see Table 2.3 and Fig. 2.8) are flagged to avoid background fitting problems, etc.

(iv) Telemetry problems, and more rarely faults in the spacecraft data handling system, can occasionally lead to corrupt core data. Simple corruptions can usally be rectified or, if necessary, the value reset by interpolation.

(v) A slight fault in the sector generator clock (see Table 2.3) leads to the last sector being only 0.4 sectors wide (i.e. one rotation ≡ 1023.4 sectors). This results in both a distortion in the azimuth scale and low exposure in the last sector. A correction for these effects is made at this stage.

(C): If the data quality is too low, either because of data corruption or large errors in the basic orbit parameters, the orbit cannot be analysed. These orbits are rejected.

(D): Exposure time is calculated from the total exposure time at a series of points every 16 sectors ($\sim 6^{o}$) around the spin plane by evaluating the Earth occultation factor, taking into account the on/off times for the experiment (see (B) above).

(E): The expected positions and fluxes for all catalogued sources in the field of view of the experiment are calculated using the spacecraft attitude. The source list used is a composite catalogue of known x-ray sources.

(F): The background level is estimated empirically from an examination of the data. The level is derived for apparently source-free regions and is extrapolated over the rest of the data, constrained by the requirement that it be a reasonably smooth function of azimuth. Except for regions of high source density the background fit is usually remarkably good (see Figs. 2.5 and 2.8).

(H): The detection routine searches for all peaks which have $SNR \geqslant SNR_{min}$ (usually 2.5 or 3σ). The peaks are located in decreasing order of size using a generalised least squares fitting algorithm to the azimuth response (note that a point-source will produce an azimuth response shaped peak in the data). The curve fitting is iterated until acceptable χ^2 values for the fit are obtained. Unacceptable χ^2 values will result from spurious peaks of various origins; these will be rejected at this stage. A list of all peaks and their associated parameters is passed to (I).

(I): Matching is achieved by comparing the set of detected peaks with the set of sources predicted to be in the field of view (see (E) above). The best match is evaluated by assigning a figure of merit to each association of peak with known source and iterating the procedure to achieve an optimum solution. The details of this procedure are somewhat complex, but in practice the results are reasonably consistent with a manual analysis. In the case of highly confused regions anomalous matches can occur and recourse to manual analysis is necessary. This routine also evaluates fluxes, positions and their associated errors for all matched sources, and also for all "new sources" (unmatched detections). Upper limits to the fluxes of undetected sources can also be determined.

(J): Output of the analysis results is usually in the form of lineprinter listings and histogram plots (e.g. Fig.2.5). The results can also be output in a condensed, machine-readable form in order to create a file for further analysis.

The SCAN analysis of the data is the basis for both immediate interpretation of the observations, and also for most further processing; for example, the production of x-ray light curves or the determination of source positions. Much of this further analysis can also be done automatically using a number of special purpose programs. Most of these programs rely on a "source data file" (SDF) produced by the SCAN analysis of all the SSI observations, either on a single orbit or summed orbit basis. The SDF is basically a machine-readable summary of the results output by the SCAN analysis (see step (J) above). The structure of the overall analysis scheme for SSI data is shown in Fig.2.7.

The two routes shown from the SDF indicate the two main areas of further analysis - determination of source positions and the study of time variability - which represent the bulk of all the analysis performed on the SSI data. Not shown are the routes corresponding to spectral analysis, or PST analysis, neither of these fit into the overall structure for somewhat complicated reasons.

Although much can be achieved with automatic processing of the data, a number of problems arise which are either difficult or impossible to allow for in the analysis programs and have to be solved externally, often manually. These problems include source confusion (especially in the galactic plane), spurious peaks in the data (e.g. due to solar x-rays), large background effects due to fluorescence x-rays produced in the Earth's atmosphere and bad background fits arising from unresolved source complexes near the galactic centre or from the steep background gradient encountered where the Earth's limb occults the x-ray sky. Some of these problems are shown graphically in Fig.2.8.

Fig. 2.7 OVERALL STRUCTURE OF SSI ANALYSIS

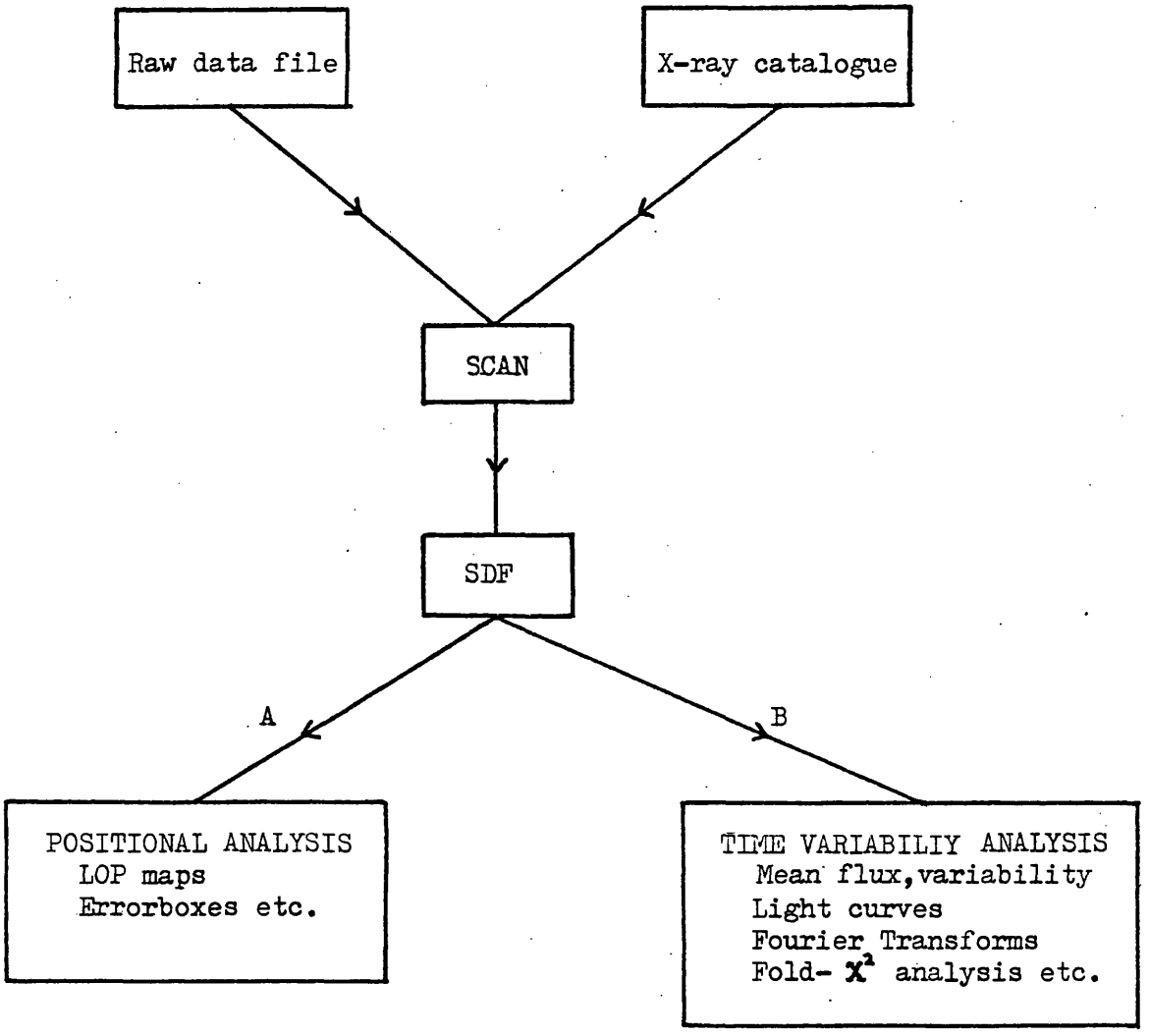

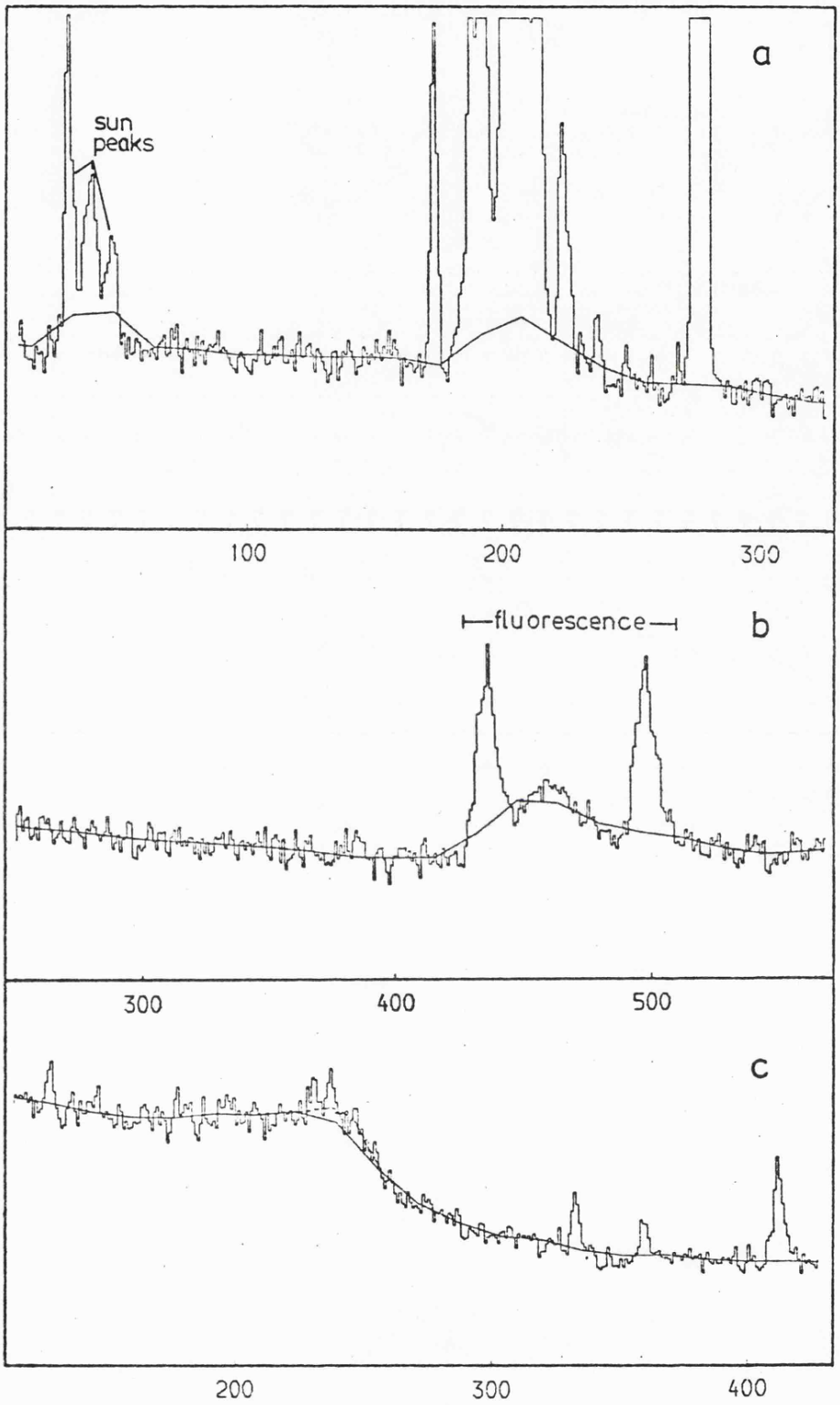

Fig. 2.8 Sections of SSI summed orbit histograms illustrating various problems with the data: (a) multiple sun peaks due to solar x-rays penetrating side of the collimators, and bad background fit (near sector 200) arising from unresolved source complex near galactic centre; (b) detection of atmospheric fluorescence x-rays resulting from enhanced solar activity; (c) steep background gradient (resulting in poor fit) at position where earth's limb occults sky.

2.4.1 Determination of Source Positions

The determination of source positions is an important facet of the analysis of SSI data, although it is not given much prominence in this thesis. Full descriptions of the procedures and problems are given in Cooke et al. (1978) and Elvis (1978).

The detection of a peak in the SSI data (normally a summed orbit data set for positional work) enables the one-dimensional position of the corresponding x-ray source to be determined with an accuracy $\Delta\theta \approx \frac{\theta_{\frac{1}{2}}}{SNR}$ where $\theta_{\frac{1}{2}}$ is the FWHM of the collimator azimuth response (see Fig.2.4), and SNR is the signal-to-noise ratio of the detection. The position in the elevation direction (i.e. approximately perpendicular - see Fig.2.4) is only determined to within $\pm \phi_{\frac{1}{2}}$, where $\phi_{\frac{1}{2}}$ is the FWHM of the collimator elevation response (Fig.2.4). The detection can thus be represented as a line of position (LOP) on the sky with dimensions $\sim 2\Delta\theta \times 2\phi_{\frac{1}{2}}$. Such LOPs can be plotted on a sky map directly from the data contained in the SDF. Scans over a particular x-ray source with different spacecraft orientations will yield LOPs intersecting at the position of the source with a range of positional angles. An LOP map for a single source is shown in Fig.2.9. Complications arise in regions of high source density since intersections of LOPs associated with different sources can easily arise, making the determination of new source positions in particular rather complex.

The precise position and errorbox for a source can be determined from the LOPs by evaluating the joint probability distribution in the region of overlap of the LOPs. The overall distribution is calculated by assuming that the probability distribution for each LOP is a Gaussian of standard deviation σ, where σ is given by:

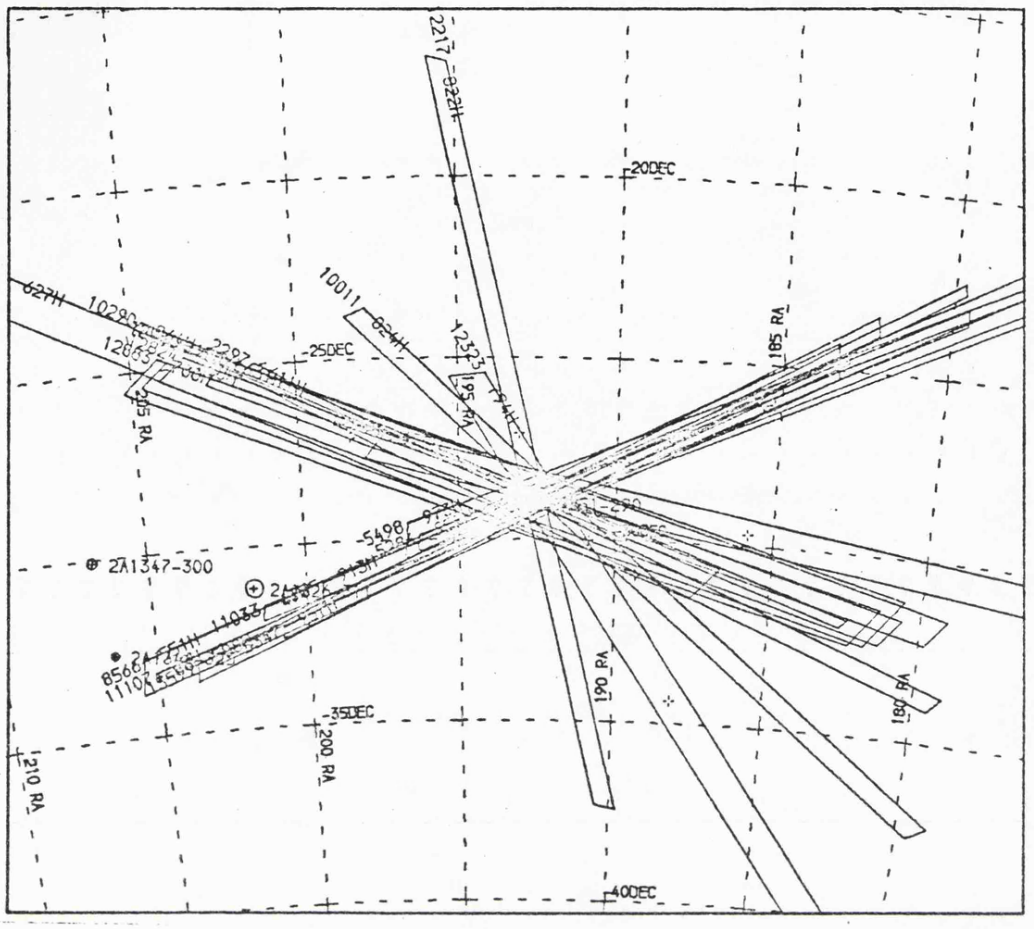

Fig. 2.9 Line of position (LOP) map for all SSI observations of 2A1251-290 (= EX Hydrae) plotted in celestial coordinates. (Numbers on lines refer to orbit and sector numbers of detections).

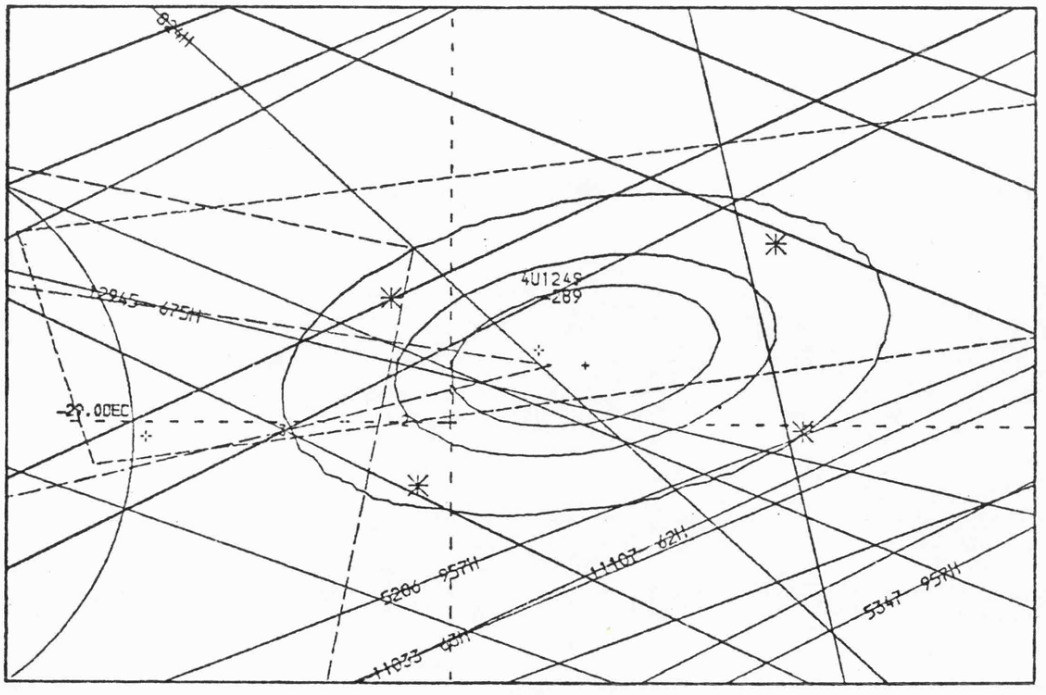

Fig. 2.10 Isoprobability contour map derived from the LOPs shown in Fig. 2.9 Approximately elliptical contours correspond to 67%, 90% and 99.7% probability respectively. Errorboxes (dashed lines) for 4U and original 2A position determinations are also shown, the solid lines are edges of the LOPs.

$$\sigma^2 = \frac{1}{3}\left(\frac{\theta_{\frac{1}{2}}}{SNR}\right)^2 + \theta_o^2 \qquad (2.1)$$

θ_o is an angle ($\approx 0.^\circ07$, empirically determined) which estimates the systematic uncertainty in the location of the LOP arising from errors in the spacecraft attitude, and the factor 1/3 comes from a detailed consideration of the statistics (see Cooke et al.1978).

The joint probability distribution is then just the product of the individual distribution (p_i) evaluated at each point in the region of interest:

$$P(x,y) = \prod_{i=1}^{N} p_i(x,y) \qquad (2.2)$$

where the product is taken over the N lines of position. The best estimate for the position of the source is the point of maximum probability, and the errorbox is the contour which encloses (traditionally) 90% of the total integrated probability. The probability distribution contours calculated from the LOPs in Fig. 2.9 are shown in Fig. 2.10.

Some idea of the positional accuracy possible using this analysis can be gained by considering the case where the errorbox is determined from N lines all of equal width σ_o. The errorbox dimensions will then be of order $\frac{\sigma_o}{N^{\frac{1}{2}}}$. For example, if each line has SNR = 5, $\sigma_o = 0.^\circ11$ (from eqn. 2.1 with $\theta_o = 0.^\circ07$), for 5 lines of position the resultant positional accuracy would be $\sim 0.^\circ05 \approx 3$ arc minutes. This assumes that the lines overlap perfectly; in practice this is unlikely to be the case and the true positional accuracy will be several times (~ 3) worse than that estimated. The <u>limiting</u> accuracy obtainable from the SSI data is set by the size of θ_o. If SNR is large enough, $(\frac{\theta_{\frac{1}{2}}}{SNR}) \ll \theta_o$, and the errorbox

size will depend only on the number of LOPs. The largest number of LOPs normally available for a well-observed, strong source is ~ 25, which would give a positional accuracy of ~ 1 arc minute. Again this is an overestimate of the recision available. The empirical limit, derived from the errorbox sizes of the strongest sources, is ~ 2 arc minutes.

2.4.2 Determination of Source Intensities

Time variability of x-ray sources is a major part of this thesis. It is important therefore to establish in detail the way in which intensities are derived from the data, and how various errors in the intensity measurement arise. The procedure discussed here for determining the intensity of a source, and for estimating the errors is mathematically very similar to that implemented in the SCAN program (i.e. as in step (I) of Fig. 2.6).

In general the total count accumulated at a particular point in one orbit's observation with the SSI will be made of contributions from three separate sources of x-ray photons - c_s the count from a discrete source in the field of view, c_d the count from the diffuse x-ray background and c_b the count from the non x-ray (particle) background events:

$$c = c_s + (c_d + c_b) \tag{2.3}$$

The total background contribution $(c_d + c_b)$ is estimated empirically (see § 2.4), giving c_s directly. The total count from the source, assuming it to be a point source, is given by the integral of c_s over the azimuth response $f(\theta)$ (see Fig. 2.4):

$$C_s = \int_{\theta_1}^{\theta_2} \frac{c_s}{\omega} \cdot f(\theta)\, d\theta \tag{2.4}$$

where ω is the angular velocity corresponding to the scan rate of the SSI, and θ_1, θ_2 are angles well either side of the source profile. Since the

azimuth response is well approximated by a triangular function (FWHM ($\theta_{\frac{1}{2}}$) $\approx 0.9^{\circ}$), eqn. (2.4) can be re-written:

$$C_s = g(\phi)\, t(\theta)\, I_s \qquad (2.5)$$

where $g(\phi)$ is the elevation response function (see Fig. 2.4), I_s is the source intensity*, and $t(\theta)$ is the source exposure time which takes into account both the factor $(\frac{\theta_{\frac{1}{2}}}{\omega})$ arising from the integral in eqn. (2.4), and the azimuth dependence arising from the variation in Earth screening of sources at different positions in the scan, i.e.

$$t(\theta) = \frac{\theta_{\frac{1}{2}}}{2\pi} \quad T(\theta) \qquad (2.6)$$

where $T(\theta)$ is the total exposure time at azimuth θ per orbit.

From eqn. (2.5) it is clear that the error in the derived intensity, I_s, is given by:

$$\frac{\delta I_s}{I_s} = \frac{\delta C_s}{C_s} + \frac{\delta g}{g} + \frac{\delta t}{t} \qquad (2.7)$$

The factor $\frac{\delta C_s}{C_s} = \frac{1}{SNR}$, where SNR is the signal-to-noise ratio for the peak (as in §2.4.1). In the case where the source is weak the Poisson fluctuations of the background dominate the noise giving $\delta C_s \approx \sqrt{C_d + C_b}$. Using the typical background intensity, and the exposure time values quoted in Table 2.3, δC_s for a source on axis ($g(\phi) = 1$) will be:

---

* The "intensity" used here, and extensively throughout this thesis, is just the corrected count-rate which is related to the flux density S from the source by:

$$I_s = \int_{E_1}^{E_2} \epsilon(E)\, A\, S(E)\, dE \qquad (2.8)$$

where ϵ is the efficiency, A is the effective area of the detectors and E_1 and E_2 are the lower and upper energy limits of the experiment. See Cooke et al. (1978) for further details. Intensities of this sort are commonly used in x-ray astronomy.

$$\delta C_s \approx 2 \text{ counts } s^{-1} \tag{2.9}$$

or for integration over N orbits:

$$\delta C_s \approx \frac{2}{N^{\frac{1}{2}}} \text{ count } s^{-1} \tag{2.10}$$

Thus eqn. (2.7) becomes

$$\frac{\delta I_s}{I_s} \approx \frac{2}{C_s N^{\frac{1}{2}}} + \frac{\delta g}{g} + \frac{\delta t}{t} \tag{2.11}$$

Errors in the exposure time ($t(\theta)$) arise from both the inherent accuracy of the timing data, and also from possible uncertainties deriving from the error in the spacecraft attitude. Both sources of error normally contribute only a few percent to the total error in the intensity ($\frac{\delta t}{t} \lesssim 0.02$) except in certain abnormal conditions (corrupt timing data, etc.). On the other hand errors in the spacecraft attitude can cause substantial errors in the elevation response factor ($g(\phi)$) for large source elevations. Fig. 2.11 shows the fractional error ($\frac{\delta g}{g}$) arising from an error in ϕ, $\delta\phi = 0.05\ \phi_{\frac{1}{2}} \approx 0.^{\circ}5$, as a function of ϕ. Errors as large as this will occur for certain regions of the spin plane if the attitude uncertainty has a value of $0.^{\circ}5$ (see Table 2.3). The average value of $\delta\phi$ over the whole spin plane will of course be rather less than this. Nevertheless the rapid increase in ($\frac{\delta g}{g}$) for $\phi \gtrsim 6^{\circ}$ seriously affects the accuracy of intensity measurements made at higher source elevations. This is illustrated in Fig. 2.12 which shows, for a variety of source elevations, the minimum intensity measurable to an overall accuracy of 20% as a function of the number of orbits over which the signal is integrated. It is clear that for high source elevations the intensity error is dominated by the effects of attitude errors on the collimator response factor. For this reason light curves of even strong sources at high elevations are nowhere nearly as useful as those obtained with the source near the spin plane.

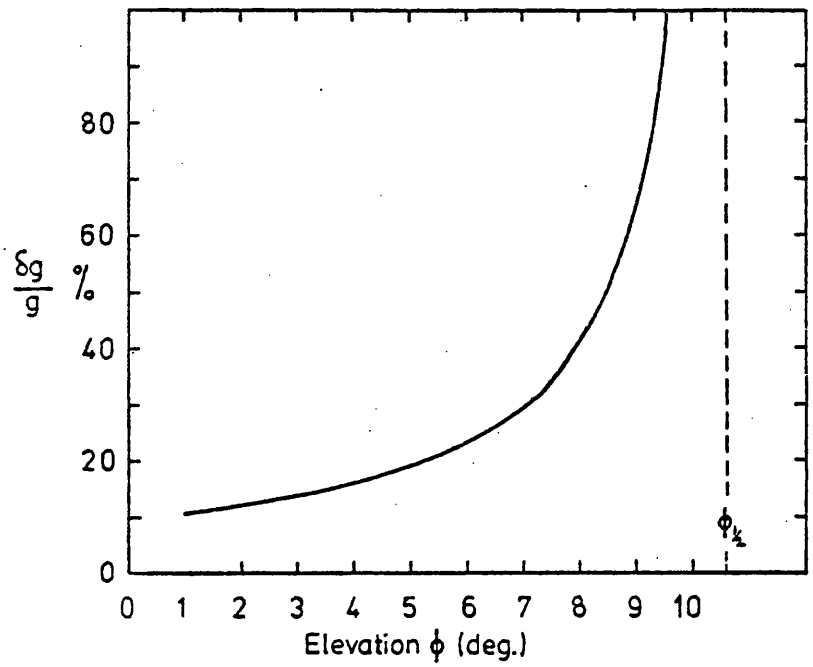

Fig. 2.11 The function $(\frac{\delta g}{g})$ plotted against source elevation ϕ assuming an error in ϕ of $\delta\phi = 0.05\,\phi_{\frac{1}{2}} \approx 0.5^{\circ}$ (see text for more details).

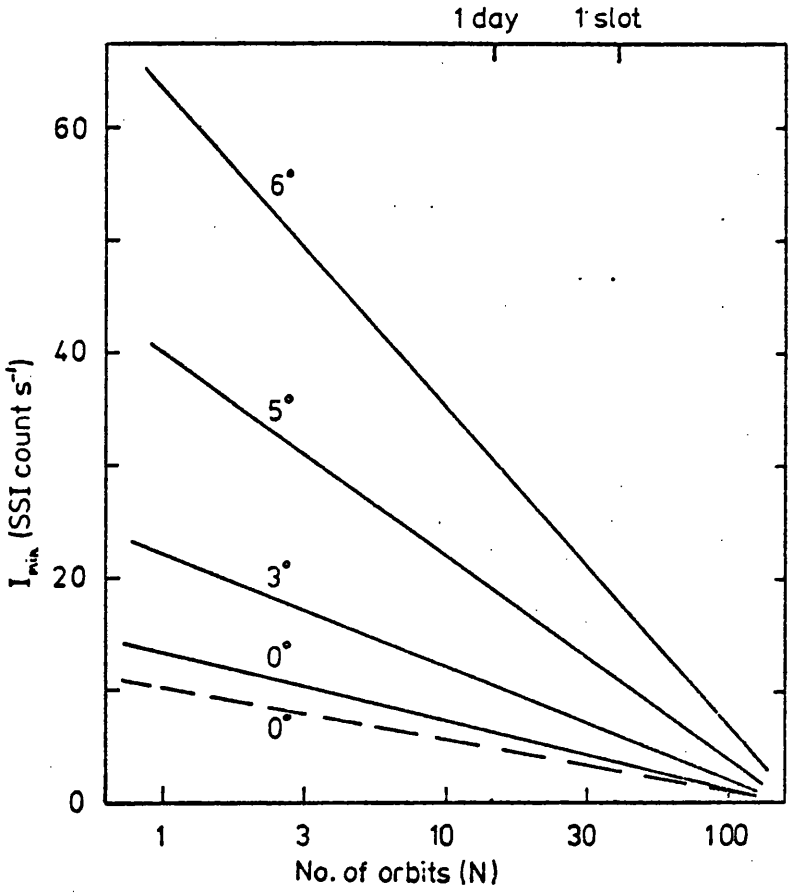

Fig. 2.12 Minimum source intensity I_{min} as a function of no. of orbits over which detection is integrated plotted for a variety of source elevations with $\delta\phi = 0.05\,\phi_{\frac{1}{2}}$. Dashed line corresponds to $\delta\phi = 0$ for $\phi = 0^{\circ}$ (see text for more details).

The final factor which can sometimes affect the accuracy of intensity measurements is source confusion. Since the FWHM response of the collimator in azimuth has a width of ≈ 2.75 sectors ($\approx 0^{\circ}.9$), sources will be confused if the separation of the centres of their peaks in the data is less than ~ 5.5 sectors. In the worst case, where the peaks are exactly aligned, no intensity determination (except for an upper limit) is possible unless the intensity of one of the sources can be independently estimated. In the less severe situation where the peaks overlap but can be resolved (separation ≥ 2.75 sectors) additional uncertainty in the intensity determination arises from the source fitting procedure since the intensities of the two peaks cannot be derived uniquely in the presence of background noise. The errors introduced by source confusion are only important, however, if confusion is with an approximately equal strength or stronger source.

Chapter 3

HIGH-MASS X-RAY BINARIES

3.1 Introduction

One of the most important discoveries to have emerged from x-ray astronomy since 1970 is the existence of a class of x-ray binary systems consisting of a high-mass star and an approximately solar mass compact object. Observations with the Uhuru satellite in 1971 revealed the existence of the first member of this class, Cen X-3 (Schreier et al. 1972). The binary nature of Cen X-3 was apparent, both from the eclipsing nature of the x-ray light curve, and from the cyclic variations in the period of 4.8 second pulses detected. Schreier et al.'s initial analysis indicated that the companion of the x-ray source had to be massive ($M \gtrsim 17\ M_\odot$). Subsequent optical identification of Cen X-3 with a 13^m O III star (Krzeminski 1973) confirmed this system as a high-mass binary.

Since then several new members of this class have been identified; they now number about 20 (cf. Table 1.5). As discussed in § 1.3.7 x-ray binaries with a high-mass companion star have a wide range of observational similarities. Theoretical models for systems of this type are successful in explaining the overall features of the x-ray emission (§ 1.2.2 - 1.2.6), and their relative abundance in the galaxy (§ 1.2.7).

For the small number of sources in this class which have been studied extensively both optically and at x-ray wavelengths, many properties of the binary system are well established (in particular the orbital elements and masses). For this reason the study of these sources no longer focusses on the nature of the system, the emphasis having shifted to an understanding of the physics of the mass-loss and accretion processes, and to the nature of the compact object.

3.2 4U0900-40 (Vel X-1)

3.2.1 Background

The binary nature of Vel X-1 was revealed by OSO-7 and Uhuru observations of the source made in 1972 (Ulmer et al. 1972; Forman et al. 1973) which established that the x-ray light curve showed an x-ray eclipse lasting ~2 days recurring with a period of ~9 days. Vel X-1 was subsequently identified with HD 77581, an early-type supergiant with photometric variability at precisely the same period (Hiltner 1973; Vidal et al. 1973a, b; Jones and Liller 1973).

Optical studies of HD 77581 (see excellent review by Vidal 1976) indicate a complex pattern of gas flows within the system. The photometric light curve shows two peaks per binary cycle as is expected from the ellipsoidal variations of the primary (which is close to filling its Roche-lobe), but also considerable scatter which has been attributed to circumstellar material in the system. High dispersion spectra, in particular of the Hα line, show a complicated profile composed of several phase-dependent components, which has been interpreted in terms of gas flows within the system (e.g. Bessel et al. 1975).

Early x-ray observations of Vel X-1 had indicated its variability on a range of timescales, but had failed to detect regular pulsations. Pulsations were eventually discovered in 1975 by the SAS-3 satellite (McClintock et al. 1976) at a period of ~283 seconds, almost two orders of magnitude longer than had previously been seen in a steady source (e.g. Cen X-3 or Her X-1), but of the same order as the periods established in the "transient" sources A1118-61 and A0535+26 by the Ariel V satellite.

X-ray and optical observations of Vel X-1 have provided the eclipse duration, x-ray and optical mass functions and the spectroscopic mass of the primary star, allowing the determination of the orbital elements of

the system with an accuracy mainly determined by the errors in the observed quantities, and our understanding of the ways in which the system departs from the simple binary model assumed.

3.2.2 SSI Observations and Analysis

Vel X-1 was scanned by the SSI on ~ 900 separate satellite orbits between 1974 November and 1976 April, including coverage in 17 binary cycles. The extended light curve of these observations is shown in Fig. 3.1. Table 3.1 summarizes the SSI observations, and includes some derived quantities discussed later.

All the data presented refer to single orbit observations in the SSI high-energy system (~ 2 - 18 keV) with a time resolution of 100 min. The gaps in the light curve arise principally from satellite orbits in spectral mode where Vel X-1 is out of the field of view, and also from calibration and command orbits. The fluxes have been corrected for both exposure time and the collimator response.

The characteristics of the light curve and their possible origin are discussed in Section 3.2.3.

(a) Binary Period

The binary nature of Vel X-1 was established by Ulmer et al.(1972), and the first accurate period was given by Forman et al. (1973) from Uhuru observations. The identification of Vel X-1 with HD 77581 (Hiltner 1973; Vidal et al. 1973 a,b) has allowed optical measurements of the period to be made from both the radial velocity and light amplitude variations. The most accurate optical period was quoted by Hutchings (1974b) based on radial velocity curves spanning 17 yr. He gave $P = 8^d.966 \pm 0^d.001$.

Accurate x-ray determinations of the orbital period have so far been based on the spacing between eclipse centres. Analysis of the orbital variations of the pulsation period will of course eventually provide the most accurate measure of the binary period. Until now the most accurate

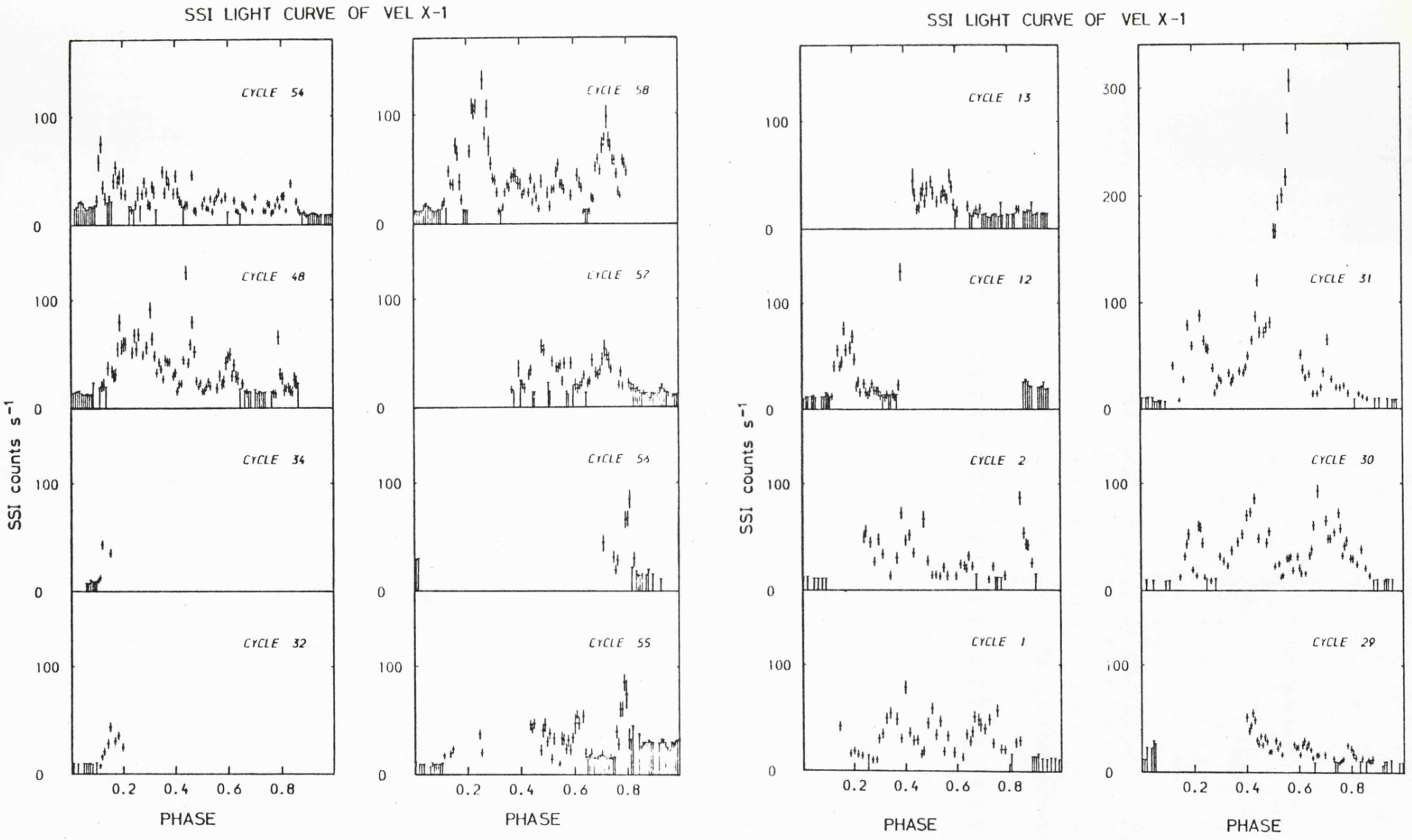

Fig. 3.1 Complete light curve of SSI observations of Vel X-1. Data points are plotted with $\pm$ 1σ error bars except for upper limits which are 3σ. Each frame corresponds to one binary cycle numbered as in Table 3.1.

TABLE 3.1

Summary of Vel X-1 observations

Cycle* (N)	Date+	N_{obs}++	Phase ranges	Mean flux (SSI cts s^{-1})	Max flux (SSI cts s^{-1})	T entry+++ (days)	T exit+++ (days)	Comments
1	Nov.74	53	0.15–1.00	30.3±0.7	162	–	–	) Published in Eadie et al.
2	Nov.74	44	0.00–0.90	28.9±0.8	87	−1.22±0.20	1.15±0.32	) (1975)
3	Dec.74	–	–	–	–	−0.94±0.20	–	Eclipse entry only
12	Feb.75	54	0.01–0.41 0.88–0.95	25.7±0.9	(78)	–	1.02±0.04	
13	Feb.75	56	0.44–0.95	24.3±1.0	(50)	–	–	
14	Mar.75	–	–	–	–	−1.32±0.30	–	Eclipse entry only
28	Jul.75	6	0.96–1.00	–	–	–	–	Not shown in Fig. 3.1
29	Jul.75	59	0.00–0.07 0.41–1.00	22.1±0.5	(51)	–	–	
30	Jul.75	66	0.02–0.96	32.0±0.5	93	−0.90±0.17	1.15±0.18	Phase zero = cycle 30
31	Aug.75	68	0.01–0.98	38.2±0.6	307	−1.07±0.07	0.97±0.13	Flare!
32	Aug.75	16	0.01–0.20	(23.0±1.3)	(44)	−1.06±0.13	0.92±0.07	
34	Sep.75	11	0.06–0.15	(30.2±1.5)	(43)	–	0.90±0.03	
47	Dec.75	11	0.91–0.99	–	–	–	–	Not shown in Fig. 3.1
48	Jan.76	97	0.01–0.87	32.9±0.6	126	–	1.03±0.04	
54	Mar.76	106	0.02–0.99	20.1±0.5	75	–	0.88±0.04	Low state, little variability
55	Mar.76	80	0.00–0.26 0.44–1.00	29.6±0.8	74	−0.87±0.10	0.96±0.04	
56	Mar.76	20	0.01–0.02 0.72–0.93	(41.8±2.1)	(85)	–	–	
57	Mar.76	69	0.37–1.00	29.4±0.8	(57)	−1.29±0.30	–	
58	Apr.76	94	0.01–0.80	37.1±0.6	132	−1.16±0.30	0.95±0.03	

* The observations are divided into binary cycles according to the period and epoch given in the text. The cycle no. (N) gives the time of the beginning of the cycle (=centre of occultation) according to T = (MJD 42620.303±0.04) + (N − 30) x ($8^{d}.964 \pm 0^{d}.0005$).

\+ Approximate dates – month of bulk of cycle.

++ No.of separate observations in this cycle.

+++ The eclipse entry/exit times are measured from the centre of occultation as given above.

() Figures given in brackets for the mean and maximum fluxes are uncertain due to the incomplete coverage of these cycles.

T A B L E 3.2

Observations of Vel X-1 eclipse centre 1968 - 1976

Cycle (N)*	Instrument	$T_{0.0}$(MJD)	Reference	Comments
-260	Skylark 723	40019.50[± 1.0]	Cooke, Griffiths & Pounds (1969)	Rocket flight. Not necessarily eclipse centre+.
-101	Uhuru	41446.04[± 0.05]	Forman et al.(1973)	Based on ~ 2 months data.
- 70	OSO-7	41723.83 [± 0.15]	Ulmer et al.(1972)	Single observation. Values estimated from published light curve.
- 56	(Optical)	41849.108[± 0.05]	Hutchings (1974)	Based on radial velocity measurements covering 17 years. See text ++
2	Ariel V/SSI	42369.28 ± 0.38	This paper	See Table 3.1
11	OAO Copernicus	42449.97 ± 0.04	Charles et al.(1976)	Based on Copernicus and Uhuru observations
29	SAS-3	42611.51 ± 0.12	Rappaport et al.(1976)	Based on 36 days data
30	Ariel V/SSI	42620.43 ± 0.25	This paper	See Table 3.1
31	Ariel V/SSI	42629.22 ± 0.16	This paper	See Table 3.1
32	Ariel V/SSI	42638.16 ± 0.15	This paper	See Table 3.1
55	Ariel V/SSI	42844.45 ± 0.20	This paper	See Table 3.1
58	Ariel V/SSI	42871.20 ± 0.30	This paper	See Table 3.1

Notes:

* Refers to cycle no. measured from epoch given in text. (See note on Table 3.1).

\+ Cooke et al. observation is the only pre-Uhuru measurement consistent with Vel X-1 being in eclipse; large estimated error reflects the size of the eclipse width (See Ulmer et al. 1972).

++ Hutchings optical measurement was omitted from the final analysis of the data.

Values in square brackets have been estimated.

x-ray period is $P = 8^d.963 \pm 0^d.001$ (Charles et al. 1976), determined from Copernicus and Uhuru eclipse centres.

Table 3.2 summarizes the time of the eclipse centres taken from published data and those determined from the SSI observations. A least squares fit to this data yields the following improved period (P) and epoch of eclipse centre (phase 0.0)

$$P = 8^d.964 \pm 0^d.0005 \ (1\sigma) \quad E_{0.0} = \text{MJD } 42620.30 \pm 0.05 \ (1\sigma)$$

These values are in good agreement with those quoted by Charles et al. but are not entirely consistent with Hutchings' result. The discrepancy between the periods suggests either that the errors have been underestimated or that the period is changing. If the difference is real, the change is of the same order ($\dot{P}/P \sim 10^{-4}$ yr^{-1}) as that observed in Cen X-3 (Tuohy 1976) and thus might arise through some form of tidal interaction (cf. Pringle 1974).

By extrapolating our epoch of phase zero (= superior conjunction of the x-ray source) back to Hutchings' (1974b) epoch, we get a minimum difference of $0^d.21$, corresponding to $\sim 4\sigma$ if our estimate of the errors on his epoch is correct. This discrepancy may be interpreted as a constant phase difference between the x-ray and optical eclipse centres amounting to $\Delta\phi = \phi_{o,x\text{-ray}} - \phi_{o,Opt} = 0.023$. A phase difference of this order could arise through mass flow within the binary system which is asymmetric relative to the optical primary (Rappaport et al. 1976).

(b) Eclipse Duration

The definition of the x-ray eclipse is beset with several problems which have led to a variety of values being quoted, ranging from 1.7 to 2.0 days. This range reflects:

(i) The intrinsic variability of the eclipse duration;

(ii) the energy dependence of the eclipse width;

(iii) the sensitivity and time resolution of the observations.

Recently Avni and Bahcall (1975b) have stressed the importance of the eclipse-width determination in deriving the mass ratio for the binary system. It was with this in mind that we attempted to obtain the best possible eclipse profile.

Fig. 3.2 shows the Vel X-1 data folded modulo $8^d.964$ and divided into 100 phase bins. Only those bins around the eclipse centre are shown. The transition is not abrupt for either eclipse entry or exit, so the phase of eclipse entry/exit has been determined from a linear fit to the bins defining the eclipse. To some extent the choice of bins is subjective, and the errors have been estimated with this in mind. The entry/exit phases are defined here as the points where the linear fit crosses I = 2 counts/s since this is the 3σ upper limit on the source intensity in eclipse (see later).

The eclipse width is $\Delta\phi = 0.188 \pm 0.007$ as a phase, or $\Delta T = 1^d.69 \pm 0^d.06$. This corresponds to an eclipse semi-angle $\theta_e = 33^\circ.8 \pm 1^\circ.3$. Since this value is derived from the folded-binned histogram of all the data, it is in a sense an average value, but the increased sensitivity obtained by binning allows us to regard it as a minimum value.

Our value is considerably smaller than either the Uhuru width $\theta_e = 38^\circ \pm 1^\circ$ (Forman et al. 1973), or the Copernicus result $\theta_e = 39^\circ.8 \pm 0^\circ.4$ (Charles et al. 1976). The difference must in part be due to the 'softer' energy range of both these experiments, since in general terms the eclipse width is expected to vary inversely with energy in the x-ray band. In addition the individual eclipse entry/exit times given in Table 3.2 illustrate the intrinsic variability of the eclipse width. Only by monitoring the source for many cycles can one hope to establish the minimum eclipse width.

Avni (1976) has generalised the analysis of the eclipse duration of Vel X-1 to include the effects of both eccentricity and departures

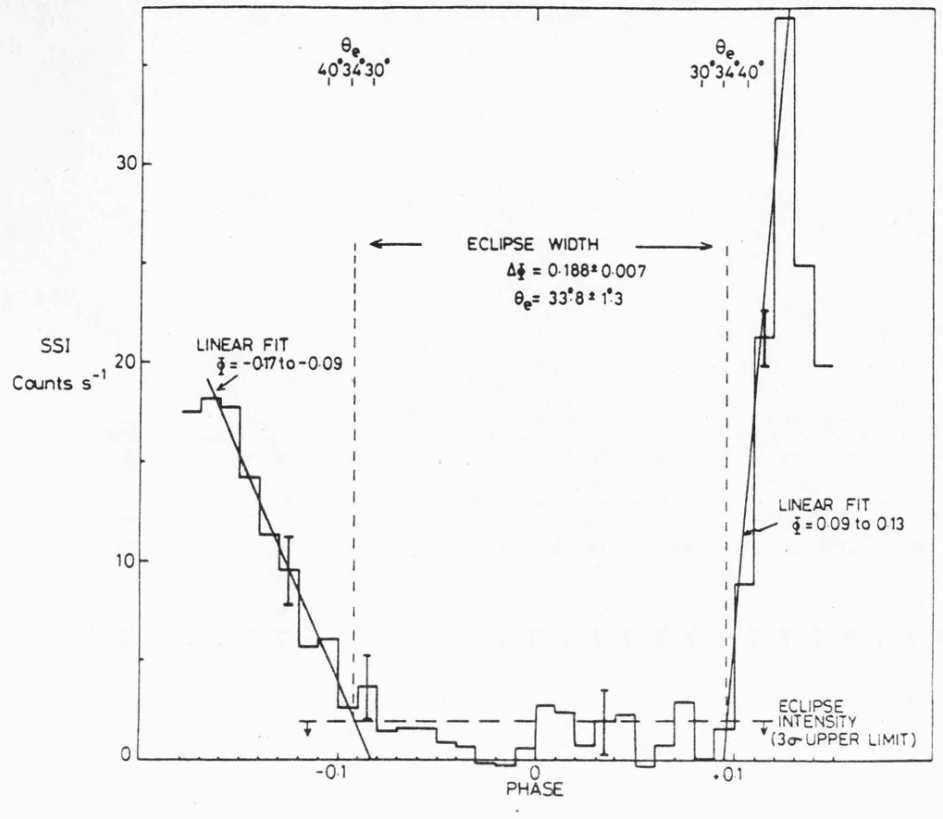

Fig. 3.2 Histogram of all Vel X-1 data folded modulo 8.964 days and divided into 100 phase bins. Solid lines are the best least squares fit to the histogram over the phase range shown. The dashed line is the 3σ upper limit to the in-eclipse intensity.

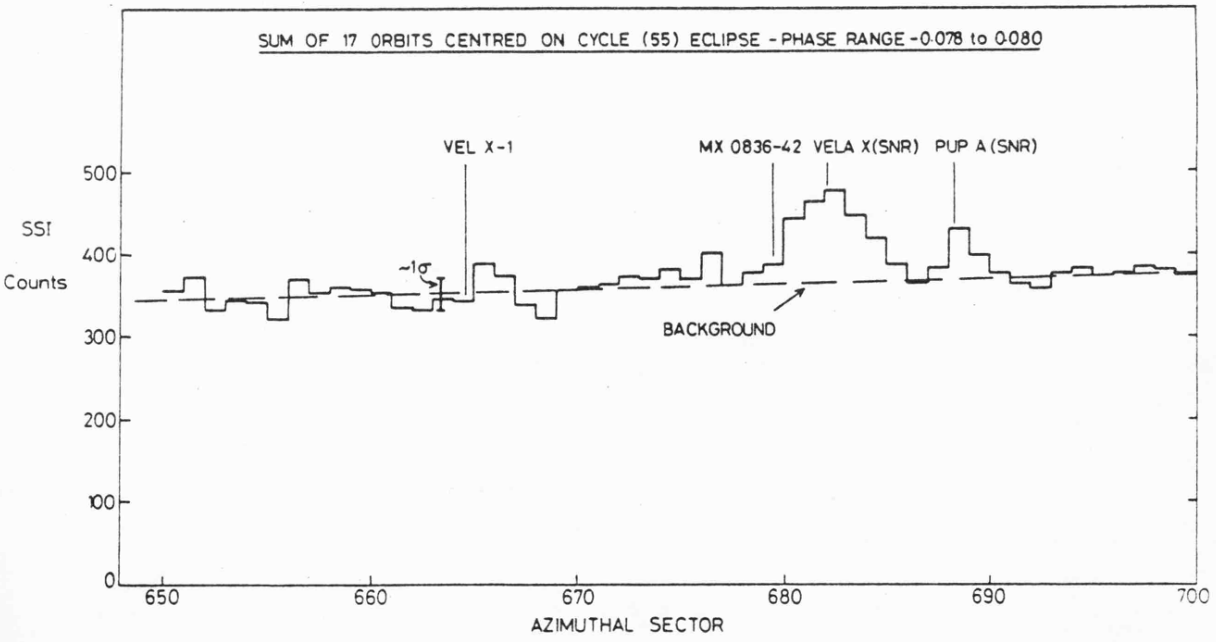

Fig. 3.3 Histogram of the sector data for the Vela-Puppis region from a sum of 17 orbits centred on mid-eclipse of cycle (25) covering phase range -0.078 to + 0.080.

from corotation. Referring to his Table 2, which is calculated using the most recent x-ray (McClintock et al. 1976) and optical (van Paradijs et al. 1976) radial velocity data, our central value $\theta_e \approx 34^\circ$ implies the following restrictions on the value of the inclination angle i:

$$\text{for } \left(\frac{M_x}{M_{opt}} = 0.072\right)$$

(i) For no primary rotation ($\omega_{rot} = 0$), $i \geqslant 68^\circ$;

(ii) For 'average' corotation ($\omega_{rot} = \omega_K$), $i \geqslant 77^\circ$;

(iii) For corotation at periastron ($\omega_{rot} = \omega_{peri}$) $i \geqslant 82^\circ$.

We note that for $\omega_{rot} = 0$ the range of inclination angles is somewhat larger than is usually considered for Vel X-1.

During eclipse Vel X-1 is never seen above the 3σ detection level (~ 5 SSI counts s^{-1} at best) on single satellite orbits. The x-ray intensity in eclipse can be better estimated by summing the data from individual orbits. Fig. 3.3 shows the histogram of the sector data from a sum of 17 orbits centred on phase zero of cycle (55) where the source elevation from the satellite spin plane was $\sim 1^\circ$ giving near optimum sensitivity. The nearby supernova remnants, Vela X and Puppis A, are clearly resolved, but there is no apparent emission from Vel X-1. The 3σ upper limit to the source flux is 2.0 SSI counts s^{-1}. Assuming a distance of ~ 2 kpc for Vel X-1 (Zuiderwijk et al. 1974), this implies $L_x \lesssim 6 \times 10^{34}$ erg s^{-1} in eclipse.

(c) Characteristics of the Light Curve

From an inspection of the light curve presented in Fig. 3.1, the following features emerge:

(i) some cycles are very "quiet", characterized by both a low intensity level and little variability, e.g. cycles (2) and especially (54); on the other hand evidence of flaring is seen on several cycles, particularly cycle (31) where a flare lasting ~ 1 day reaches a peak intensity of 307 SSI counts s^{-1} (corresponding to ~ 0.8 of the Crab intensity). The overall average out-of-eclipse intensity is ~ 30 SSI counts s^{-1};

(ii) the range of intensities seen on most cycles is about an order of magnitude;

(iii) although some features are common to consecutive cycles, this is by no means the rule and there is little similarity in observations separated by more than a few binary periods;

(iv) whereas many cycles show evidence for intensity dips (e.g. cycle (58)), which have previously been interpreted as absorption features due to an accretion wake near the compact secondary (Eadie et al. 1975; cf. Jackson 1975), the overall pattern is highly variable with little evidence for stable absorption dips on individual cycles. The interpretation of high- and low-intensity states in terms of absorbing material is provided by spectral data taken at the end of cycle (57) and during cycle (58), clearly showing that the high-intensity states are characterised by little absorption ($E_a < 1$ keV), whereas the low-intensity states are characterised by heavy absorption ($E_a \sim 5$ keV), where E_a is the energy at which the source intensity is reduced to e^{-1} of the radiated value. Similar evidence was found in the earlier SSI spectral data (Eadie et al. 1975).

Fig. 3.4 shows the histogram of all the Vel X-1 data folded modulo $8^d.964$ and divided into 50 phase bins. Obviously many individual features are smoothed out by this technique, but the gross features which emerge are:

(i) general absorption regions between phases 0.2 - 0.4 and 0.5 - 0.7. We cannot exclude the possibility of a secondary maximum phase ~ 0.6, as found for CenX-3 (Pounds et al.1975), though the evidence for this is very weak;

(ii) the mean intensity is higher in the first half of the folded data; the mean flux over phases 0.5 - 0.8 is 23 percent lower than the mean flux over phases 0.12 - 0.5;

(iii) eclipse entry has a longer timescale ($\sim 0^d.7$) than eclipse exit ($< 0^d.4$) (see also Fig. 3.2). This behaviour is also seen on several individual cycles, e.g. cycle (30).

3.2.3 Interpretation

The primary star, HD 77581, is a ~ 21 $M_\odot$ supergiant of spectral class B0.5 Ib and mass-loss of approximately 10^{-7} $M_\odot$ yr^{-1} is expected by stellar wind (Lamers et al. 1976). This is possibly confirmed by optical observations (see review by Vidal 1976). Such a wind will be focussed in the gravitational field of the secondary giving rise to x-ray emission

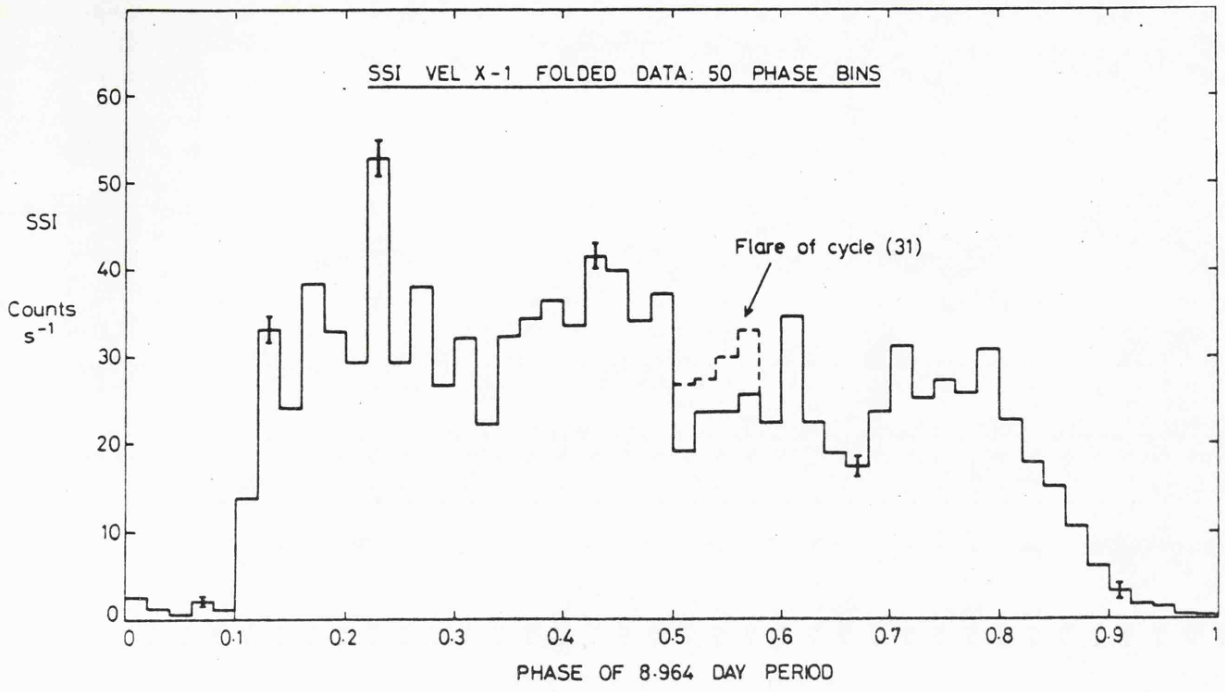

Fig. 3.4 Histogram of all the Vel X-1 data folded modulo 8.964 days into 50 phase bins. Representative ± 1σ error bars are shown.

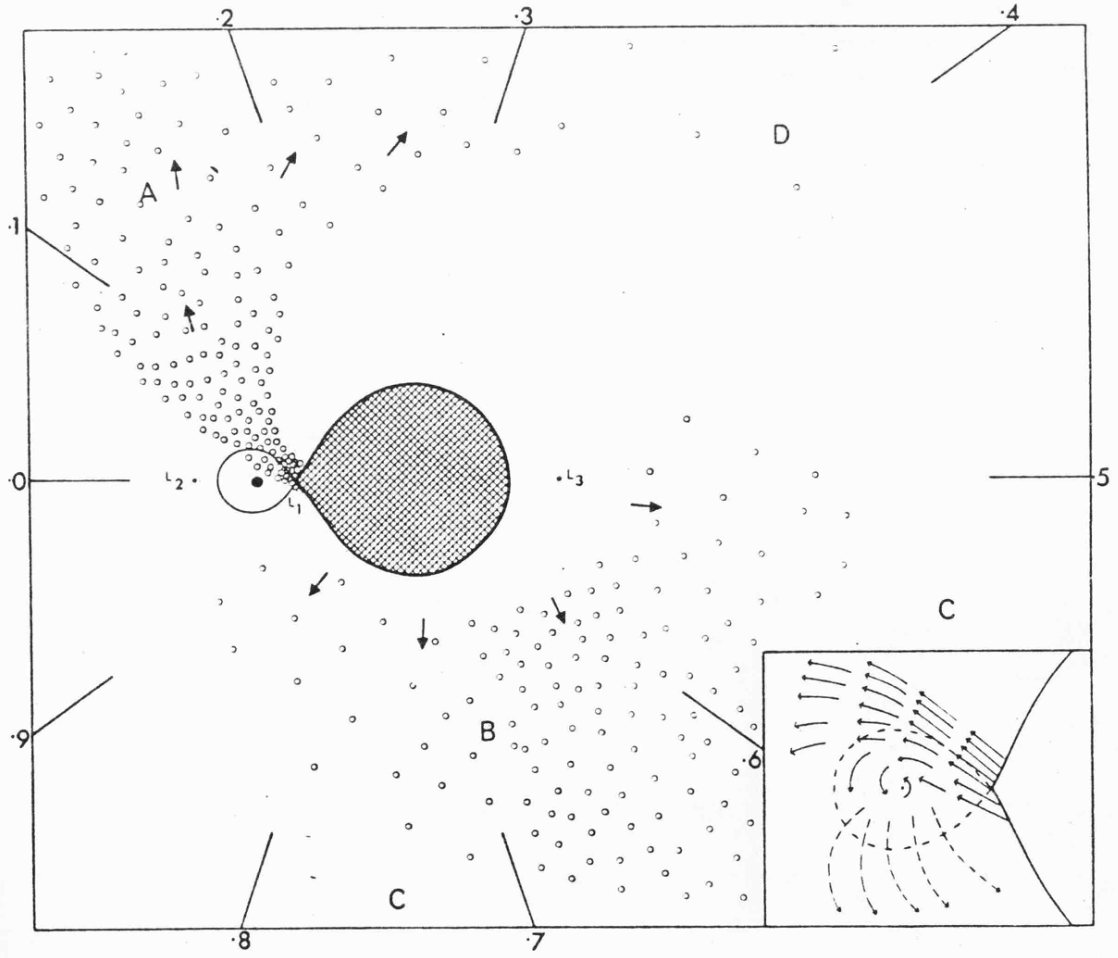

Fig. 3.5 Distribution of absorbing material in the Vel X-1 system inferred from optical spectra (from Bessel et al. 1975).

(Pringle and Rees 1972; Davidson and Ostriker 1973) and the supersonic passage of the secondary through this wind will result in a bow shock and accretion wake (Pounds et al. 1975; Jackson 1975). The accretion-wake model was developed by Eadie et al. (1975) for Vel X-1 to predict an up-stream (i.e. preceding the orbiting secondary) as well as a down-stream accretion wake, and this can explain the absorption structure between phases 0.2 and 0.4, as well as the more general absorption between phases 0.5 and 0.7. A phase difference of 180° between these two absorption regions, as predicted from the geometry of the shock cones, is difficult to confirm from the observations since the broad absorption features have no clear structure, comprising the summation of many phase-independent absorption dips over many cycles.

The simple model of the stellar wind and static shock cone is, however, clearly inadequate to explain the variability in the x-ray emission from cycle to cycle. Complications to the stellar wind model result from considerations of the radiation pressure-driven mass-loss from the outer regions of an accretion disc (Wickramasinghe 1974). In particular, the relatively long decay time leading into eclipse could be caused by the optically thick gas streams falling back on to the primary surface. Furthermore, radiation pressure from the flat x-ray spectrum of Vel X-1 will tend to reduce the stellar wind from that part of the primary en face, except near the equatorial plane. A shock region is predicted to arise from the interaction of the primary stellar wind and the out-flowing material from the outer parts of the accretion disc.

Evidence for Roche-lobe overflow in the Vel X-1/HD 77581 system is provided by high-dispersion measurements of the Hα emission and absorption profiles (Bessell et al. 1975) and observations of He II λ 4686 emission from the region between the two stars (Hutchings 1974b). Such overflow may

occur only at periastron (Hutchings 1974a). Bessell et al. (1975) form a picture of the main gas streams in the system by an interpretation of the complex Hα absorption profiles as a function of phase (shown in Fig. 3.5). The main gas stream is found to flow from the inner Lagrangian point L1, though there appears to be further material roughly on the opposite side of the primary to the main stream, and emanating either from L3 (unlikely, since this would mean far more activity) or else from the accretion disc around the secondary. Kondo et al. (1976) consider the effect of radiation pressure upon the Roche equipotential surface and conclude that material leaving L1 will have access to the whole system, thus supporting the gas stream model of Bessell et al. The main stream, leaving L1 and flowing past the secondary (with some capture and accretion) would tend to disrupt any standing shock wave formed by a stellar wind, and would cause any absorption dips to become irregular from cycle to cycle, both in depth and phase.

The material suggested by Bessell et al.(1975) to be concentrated roughly in region B (Fig. 3.5) on the opposite side of the secondary from the main gas stream would tend to produce x-ray absorption centred near phase 0.1. The emergence from x-ray eclipse is, however, often sharp and a broad absorption feature is evident over phases 0.2 - 0.4. This would place the absorbing material closer to the accretion disc and tend to support its origin there (cf. Wickramasinghe 1974).

The possibility of a large part of the absorption being caused by material in the outer regions of the accretion disc would tend to further enhance the irregularity of individual dips in the x-ray light curves. If the overall absorption features were mainly due to this material, however, the phase dependency would presumably not be as great, and there would be no observed lack of absorption near phases 0.1 and 0.5.

The appearance of flares, both in the present data and in that of Uhuru (Forman et al. 1973) perhaps supports the suggestion of at least some accretion by Roche-lobe overflow. The luminosity of these flares reached a maximum of $\sim 10^{37}$ erg/s, still well below the Eddington limit of $\sim 2.10^{38}$ erg/s for a 1.5-$M_\odot$ compact object. Shakura and Sunyaev (1973) and Pringle (1973) pointed out that Roche-lobe overflow would lead to 'smothering' of the x-ray emission, but Kondo et al. (1976) have investigated the effect of radiation pressure on the Roche equipotential surface and found that the amount of matter accreted will be decreased by this effect. Excessive Roche-lobe overflow may, however, be invoked to explain the low intensity of the source during some cycles.

The combination of stellar-wind accretion with the associated shock regions and accretion wakes, together with major disturbances by material driven off the accretion disc by radiation pressure and material accreted from Roche-lobe overflow near periastron thus explains qualitatively most of the observed features in the x-ray light curve.

A greater understanding of the x-ray light curves will have to await detailed theoretical computer simulations of the complex gas flow in this system, similar to those performed by Prendergast and Taam (1974) for U Cep binaries.

3.3 4U1538-52

3.3.1 Introduction

The known high-mass x-ray binaries are predominantly bright sources in the x-ray band with typical count rates $\gtrsim$ 100 U.F.U. This is probably purely a selection effect since high quality observations of bright sources are easier to obtain. It is only recently, with the detailed study of several weaker galactic sources, that their binary nature has been revealed,

the most notable example being 4U1538-52, which is now known to be an eclipsing, binary x-ray pulsator.

Regular pulsations with a period of 529 seconds from a source in the region of 4U1538-52 were discovered independently by two satellite experiments: Ariel V Expt.C and the cosmic x-ray spectroscopy experiment on OSO-8 (Davison 1977a, b; Becker et al. 1977a,b). The OSO-8 observations also revealed a clear orbital modulation of the pulsation period throughout their 9-day scan, and good evidence for an eclipse lasting ~ 0.6 days recurring with a period of ~ 3.75 days*.

The report by Davison indicated that the pulsar was $\sim 1^{\circ}$ from 4U1538-52, but emphasised the difficulties in deriving a reliable position for a weak source with the instrument concerned. This difficulty is resolved in this section by making use of data from the SSI.

The SSI data, and recent observations from Ariel V Expt.C (a proportional counter spectrometer; Sanford and Ives 1976, see also Chapter 2) also allow certain refinements to the orbital elements, and indicate the variability of the x-ray eclipse profile.

4U1538-52 has very recently been optically identified with an early-type supergiant. This identification, which broadly confirms the possibilities discussed in § 3.3.4, is briefly considered in § 3.3.5.

3.3.2 Observations

The observations presented in this section were made by two of the six experiments in the Ariel V satellite - Expt.C and the SSI+. The fields of view of these instruments are mutually exclusive, thus the observations were necessarily made at different times.

---

*The binary nature of the source was also discovered (independently) by the author in the SSI data. Unfortunately this discovery was made somewhat later

+The analysis and interpretation of the Expt.C data presented here was performed by Peter Davison whilst at MSSL.

The region near 4U1538-52 has been scanned many times by the SSI since launch, typically for periods of ~ 3 days. The position and errorbox for the single x-ray source seen near 4U1538-52 was determined by combining all the statistically significant sightings to give the isoprobability contour shown in Fig.3.6* (see § 2.4.1 for details of the method). Only sightings which were not confused by nearby catalogued sources were employed to produce the final errorbox. The overlap with the 4U catalogue errorbox (Forman et al. 1978) is large enough for us to be confident that the Ariel and Uhuru sources are identical. In addition the Ariel V RMC errorbox(A.Wilson and G.Carpenter, private communication 1977) also shown in Fig.3.6 is entirely consistent with both Uhuru and SSI positions, and suggests that the source lies in the overlap region of the three errorboxes. Table 3.3 gives the centroid of the SSI errorbox, and the corners of the rectangle which just encloses the 90% confidence contour. (Note that the position given by Davison (1977a) for the source designated A1540-53 is in error - see Davison et al. (1977)).

In order to establish the light curve periodicity, all the reliable single-orbit (~ 100 min time resolution) SSI data for 4U1538-52 were folded modulo a range of trial periods from 0.5 to 8 days, and the folded data tested against the hypothesis of source constancy by evaluating the χ^2 value at each trial period. This technique revealed a strong (~ 100%) modulation at 3.73 ± 0.01 days. The error quoted was estimated from the shape of the χ^2 peak.

Fig.3.7 shows the "average" light curves for two long SSI observations made over a year apart. The data were folded modulo 3.73 days and divided into 20 phase bins. In both light curves the eclipse is clearly seen and the general structure of the out-of-eclipse portion is

---

* The SSI errorbox for 4U1538-52 was obtained by John Pye in conjunction with the author.

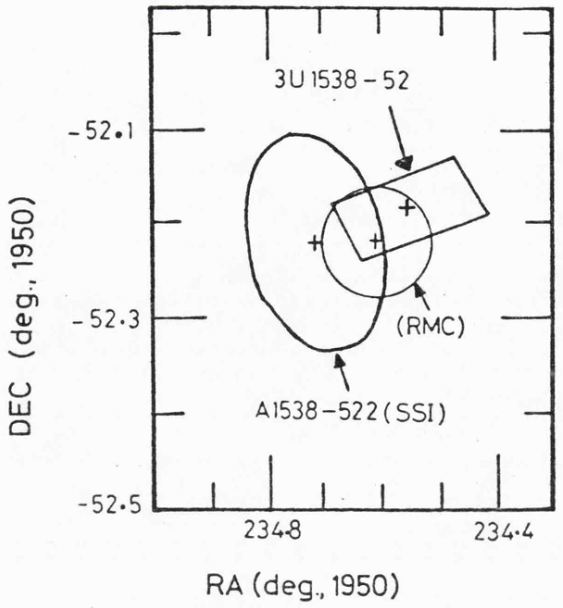

Fig. 3.6 SSI errorbox for 4U1538-52. The 3U/4U and Ariel V RMC error-boxes are also shown. The SSI and RMC errorboxes are 90% confidence regions.

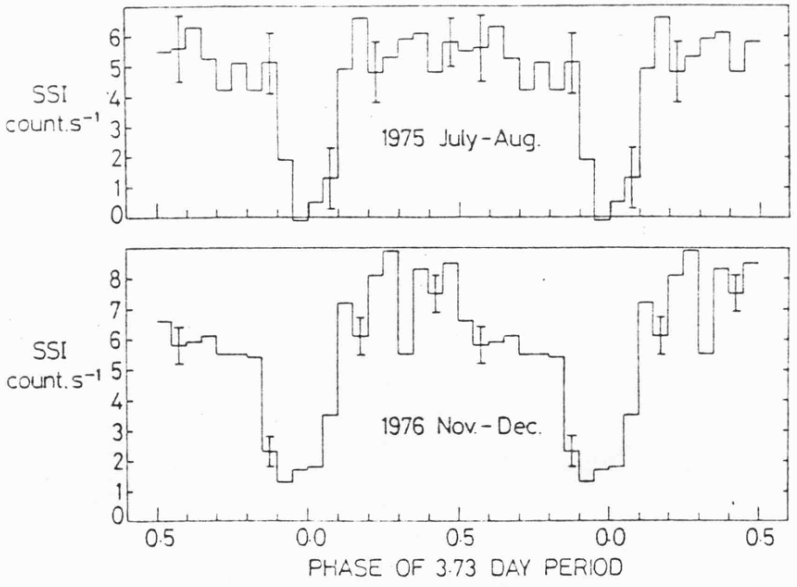

Fig. 3.7 SSI observations of 4U1538-52 folded modulo 3.73 days for data obtained in (i) 1975 July-August; (ii) 1976 November. Several representative $\pm$ 1σ error bars are shown. Phase zero corresponds to value given in Table 3.4.

TABLE 3.3

SSI Errorbox for A1538-522 (= 4U1538-52)

	$\alpha_{1950.0}$	$\delta_{1950.0}$
	$234^{\circ}.53$	$-52^{\circ}.30$
	$234^{\circ}.66$	$-52^{\circ}.09$
	$234^{\circ}.88$	$-52^{\circ}.14$
	$234^{\circ}.74$	$-52^{\circ}.35$
centroid (max. probability)	$234^{\circ}.72$	$-52^{\circ}.22$

TABLE 3.4

Orbital parameters for 4U1538-52

(a) Orbital elements

Pulse period (p)	528.929 ± 0.040 s	528.928 ± 0.036 s
Orbital period (P)	3.714 ± 0.083 d	3.730 d (fixed)
$a_x \sin i$	55.2 ± 4.3 lt-sec	55.2 ± 3.7 lt-sec
Phase zero	MJD 43015.80 ± 0.12	MJD 43015.78 ± 0.07

(b) Other parameters

Revised orbital period (see text)	3.7299 ± 0.0012 d
Eclipse semi-angle (θ_e)	$28^{\circ}.0 \pm 3^{\circ}$
$-\left(\frac{\dot{p}}{p}\right)$ (pulse period)	$\lesssim 9.7 \times 10^{-4}\ y^{-1}$

similar. Some differences in the eclipse profile are evident, the first eclipse being somewhat narrower. We estimate the total eclipse widths (i.e. measured at the top of the eclipse) to be 0.75 and 0.84 days respectively for the two data sets. Variability of the eclipse width is an established feature of several of the known eclipsing x-ray binaries, e.g. Vel X-1 (§ 3.2.2) and Cen X-3. The minimum eclipse width, quoted in Table 3.4, was obtained by summing the two data sets shown in Fig. 3.7, and measuring the width at the base of the eclipse profile, giving $\Delta T_{ecl} = (0.58 \pm 0.06)$ days, or for the eclipse semi-angle $\theta_e = 28^\circ \pm 3^\circ$. This value is consistent with, but slightly lower than, that derived from the OSO-8 data (Becker et al. 1977b).

Fig. 3.8 shows part of one binary cycle of 4U1538-52 observed by Ariel V Expt.C in 1977 April. In this light curve a rapid transition into eclipse occurs in $\lesssim$ 2 minutes. This timescale is comparable to that seen for some eclipse exits in the Her X-1 data (Pravdo 1976; Davison and Fabian 1977), and presumably indicates that this is the actual moment of geometrical eclipse.

Becker et al. (1977b) have listed pulsation periods on six days in 1976 August and September, together withtheir estimates of orbital parameters. The Expt. C pulse periods have been combined with the values from Becker et al. to provide revised estimates of the parameters. In making the least squares fit, we have taken due account of the rather large range of binary phase over which each data point is averaged. The results are listed in Table 3.4 for a four parameter fit to the data, the fitted parameters being pulse period, orbital period, a_x sini and phase zero (eclipse centre) of the binary period. We also list the marginally improved values that result if we repeat the fit withthe orbital period fixed at 3.73 days.

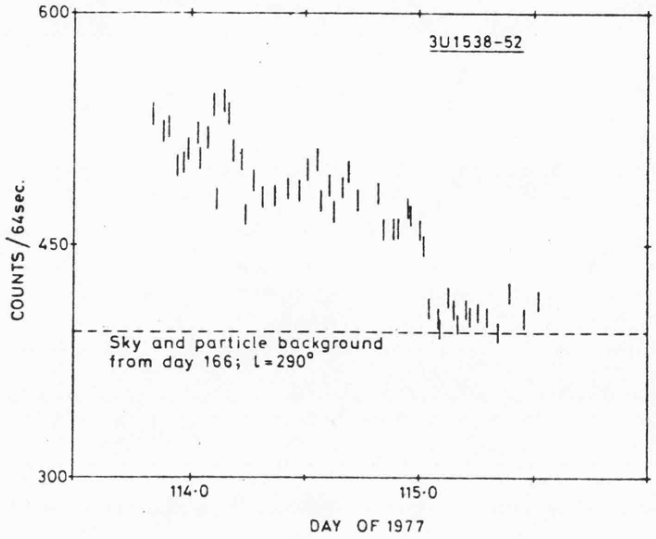

Fig. 3.8 Ariel V Expt.C light curve for 4U1538-52 for the period 1977 April 23 - 25. Data points are averages over 640 seconds. The background level is approximate, having been derived from data taken when no known x-ray source was in the field of view. Error bars are $\pm$ 1σ .

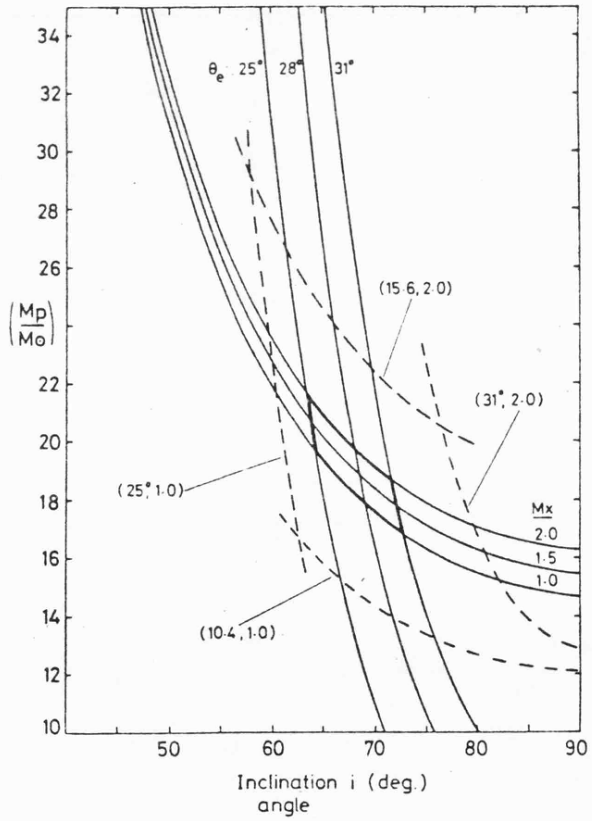

Fig. 3.9 The regions in the M_p - i plane allowed for the 4U1538-52 system for Roche-lobe geometry with (R_p / R_{Crit}) = 0.95, constrained by the measured values of f(m) and θ_e. The solid, approximately diagonal, lines correspond to eqn.3.1 with f(m) = 13 $M_\odot$. The solid approximately vertical lines correspond to eqns.3.2 and 3.3 with (M_x / $M_\odot$) = 1.5. The dashed lines represent the outer bounds of the allowed region for the range of ($f(m)$, θ_e, M_x) values assumed.

This latter value was derived from the data-folding technique outlined earlier, and also from the longest time base of data which we have available (see below). Either way, the binary period is measured to much higher accuracy than the fit to the Doppler curve allows.

Pulsations were also observed by Expt.C in 1977 April; we can derive a useful period measurement for only approximately one day of data, due to the intensity decrease and source eclipse shown in Fig. 3.8. The period was found to be 529.60 $\pm$ 0.34 seconds, averaged over the time MJD 43256.73 to MJD 43257.72. Assuming that the rapid intensity transition shown in Fig. 3.8, occurring a few hours after the period measurement, is due to the start of geometric eclipse, and taking the eclipse width indicated by the SSI and OSO-8 data, we can derive a binary phase zero applicable to the 1977 April observations, namely MJD 43258.35 $\pm$ 0.1. The uncertainty here is based on the known eclipse width, and its changes from one data set to another. Using this phase zero in conjunction with the binary period given in Table 3.4 and the observed pulsation period, we find that the centre of mass pulsation period was 529.13 $\pm$ 0.34 seconds in 1977 April. We note that there has been an insignificant change in pulse period since 1976 August, amounting to +0.20 $\pm$ 0.34 seconds. Thus we conclude that $-\left(\frac{\dot{P}}{P}\right)$ is less than $9.7 \times 10^{-4}\ y^{-1}$ for the x-ray pulsations.

In addition to the orbital parameters derivable from the Doppler shifts in pulse period, we can make a separate estimate of the binary period by measuring the time interval between eclipses. This is in effect what is done when testing folded data against the hypothesis that the light curve at the period concerned is constant. The results of using such a folding technique on the SSI data have been given earlier. Inclusion of Expt. C data from 1977 April gives us the longest time base possible. In addition, these data apparently do not suffer from the perturbing effects

of severe absorption prior to the geometrical eclipse. Likewise, the SSI data for 1975 July show a clean eclipse. The eclipse centres for these data are at MJD 43258.35 and MJD 42628.00, with an uncertainty of at most ± 0.1 day for both times. The resulting binary period, at 3.7299 ± 0.0012 days is consistent with that derived from all other pairs of eclipse centres of which we have knowledge.

3.3.3 Interpretation

The measurement of the amplitude of the radial velocity curve for the x-ray pulsations in 4U1538-52 allows, as in the case of a single-lined spectroscopic binary, the determination of the mass function for the binary system f(m):

$$f(m) = \frac{M_p^3 \sin^3 i}{(M_p + M_x)^2} = (13 \pm 2.6)\, M_\odot \qquad (3.1)$$

where M_p, M_x are the primary and secondary (x-ray source) masses, and i is the orbital inclination. Apart from indicating that the system is reasonably massive, this alone gives no further information. However, there is overwhelming evidence from observation and theoretical viewpoints that slow pulsators such as 4U1538-52 contain, as the compact secondary in a binary system, a rotating neutron star. Estimates of neutron star masses lie in the range $(1 - 2.5)\, M_\odot$, with best estimates $(1.5 - 2.0)\, M_\odot$ (Joss and Rappaport 1976). Thus using (3.1) with $M_x \sim 1.5\, M_\odot$ we derive $M_p \gtrsim 12\, M_\odot$ irrespective of any other assumptions.

Further constraints can be placed on the primary mass by using the determination of the eclipse semi-angle θ_e, and relating this to the orbital inclination. We have

$$\frac{R_p}{a} = (\sin^2 \theta_e \sin^2 i + \cos^2 i)^{\frac{1}{2}} \qquad (3.2)$$

where R_p is the primary radius, and a is the orbital separation. The critical, or Roche-lobe surface for a close binary system can be estimated as (Paczynski 1971):

$$\frac{R_{crit}}{a} \approx 0.38 + 0.2 \log_{10} \left(\frac{M_p}{M_x} \right) \qquad (3.3)$$

If we make the assumption that the primary star almost fills its Roche-lobe, by analogy with other massive x-ray binary systems (Avni and Bahcall 1975a), i.e.

$$\frac{R_p}{R_{crit}} \sim 1$$

then (3.2) and (3.3) lead to another relationship betwen M_p, M_x and i.

In Fig. 3.9 these two relations between the orbital parameters are plotted in the M_p - i plane. The region in this plane allowed is of course dependent on both the values assumed for M_x and (R_p/R_{crit}) and also the uncertainties in θ_e and f(m). The values estimated from the outer bounds shown in Fig. 3.9 are:

$$12 \lesssim \left(\frac{M_p}{M_\odot} \right) \lesssim 30 \quad \text{and} \quad 60^\circ \lesssim i \lesssim 90^\circ$$

The large range arises principally from the uncertainty in f(m) and in particular is not very sensitive to the value of $\left(\frac{R_p}{R_{crit}}\right)$ assumed. For the central values $M_p \sim 19\ M_\odot$ and $i \sim 70^\circ$, the primary radius $R_p \approx 16\ R_\odot$, consistent with the primary being an early supergiant (Allen 1973). Becker et al. (1977b) came to a similar conclusion.

3.3.4 Discussion

From this analysis it would seem very likely that 4U1538-52 is a high-mass binary system similar in many respects to Cen X-3, Vel X-1 and SMC X-1 where the dense stellar wind from the supergiant primary results in accretion onto the neutron star and the emission of keV x-rays. Indirect evidence for the existence of an extended atmosphere around the primary comes from the variation in eclipse width with x-ray energy noted by Becker et al. (1977b).

If the primary is a supergiant with $M_v \sim -6^m$ then the prospects for discovery of the optical counterpart are good, providing the distance and reddening are not too large. The upper limit placed on the rate of change of pulsation period $-(\frac{\dot{P}}{P}) \lesssim 9.7 \times 10^{-4}$ yr^{-1} may be used to set a rough upper limit to the luminosity of this source following the analysis of Rappaport and Joss (1977) and Mason (1977), since, if the dominant torque on the neutron star is that due to the mass accretion onto it, we expect a correlation between $-(\frac{\dot{P}}{P})$ and $pL_x^{6/7}$. The empirical fit found by Rappaport and Joss to the data for 7 x-ray pulsars is quite good, although caution must be exercised in applying it to new data because of the uncertainties involved in the relationship. Using this, we derive an upper limit $L_x \lesssim 1.8 \times 10^{36}$ erg s^{-1}. Combined with the average out-of-eclipse SSI intensity of ~ 7 count s^{-1}, equivalent to $\sim 3.6 \times 10^{-10}$ erg cm^{-2} s^{-1} (2 - 10 keV). This gives a distance estimate of $d \lesssim 6.5$ kpc. The requirement that the system lie within the galactic disc ($h \lesssim 300$ pc) gives, at a galactic latitude $b = 2^\circ.2$, a similar limit $d \lesssim 8$ kpc.

Reddening in this region has been discussed by Whelan et al. (1977b) for Cir X-1 ($\sim 5^\circ$ away), and for 4U1538-52 by Cowley et al. (1977). If we adopt a value of $A_v \sim 1$ mag/kpc, consistent with both authors, we estimate $m_v \lesssim 16^m$ for the optical star.

3.3.5 Postscript: Optical Identification

An optical search down to $m_B \sim 16^m$ for the optical counterpart of 4U1538-52 has already been completed by Cowley et al. (1977). Their work identified several possible candidates in the region of overlap of the Uhuru and Ariel V errorboxes on the basis of their having the appropriate colours for a reddened OB supergiant. Recent accurate x-ray positions, determined from SAS-3 and HEAO-1 A3 observations, have reduced the number of

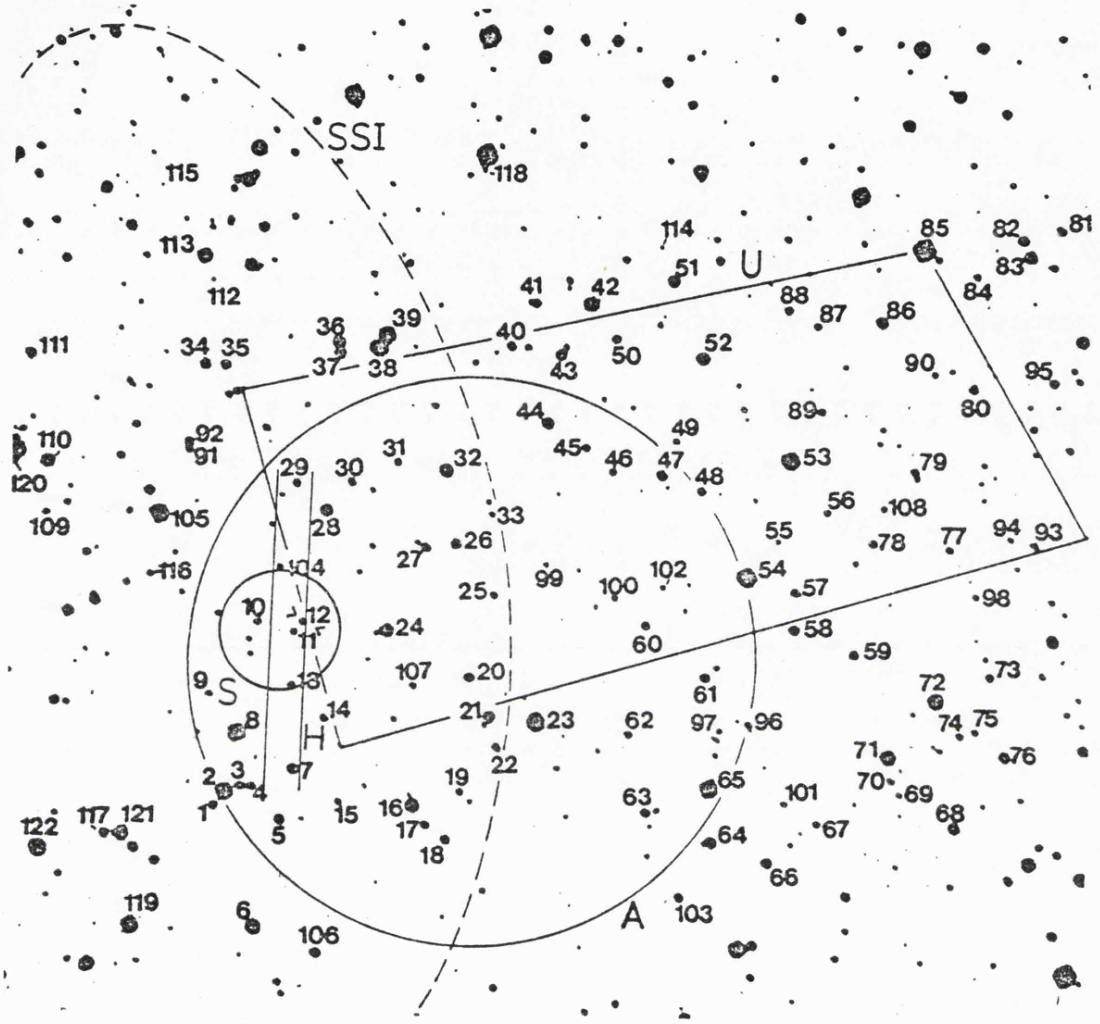

Fig.3.10 Errorboxes for 4U1538-52 overlaid on the optical field (based on Cowley et al. 1977) as follows:
U - Uhuru (4U/3U); A - Ariel V RMC (see text);
SSI - SSI (see text); S - SAS-3 (Schwartz et al. 1978);
H - HEAO-1 A3 (Schwartz et al. 1978). The candidate (now confirmed) is star 12 (arrowed).

potential candidate stars (see Fig. 3.10) (Apparao et al. 1978; Schwartz et al. 1978). One of these candidates, star 12 from the Cowley et al. list, has been suggested as the optical counterpart on the basis of its early spectral type and unusual spectroscopic features (Parkes et al. 1978). The identification is confirmed by a spectroscopic study performed by Crampton et al. (1978) which revealed radial velocity variations at the same period as the x-ray modulation.

The spectral type of the optical counterpart is quoted as BO Ia (Parkes et al. 1978); both Parkes et al. and Crampton et al. estimate a distance of ~ 5.5 kpc. From their radial velocity measurements Crampton et al. give $M_p = (20 \pm 4)\ M_\odot$, $M_x = (2.0 \pm 0.4)\ M_\odot$ with an inclination angle $i \approx 70^\circ$.

It is gratifying to see how many of the predictions made in § 3.3.4 have been confirmed. This must surely reflect the maturity of the study of high-mass x-ray binaries.

3.4 Cir X-1 (4U1516-56)

3.4.1 Introduction

Although it is now optically identified and established as a binary system, the detailed nature of Cir X-1 remains obscure. X-ray observations over a number of years have revealed a picture of chaotic variability with little coherent structure. Early observations by the Uhuru satellite (Jones et al. 1974) showed evidence for eclipse-like features in the x-ray light curve (see Fig.3.12) but the tentative periodicity suggested was ruled out by subsequent OSO-7 and Copernicus observations (Canizares et al. 1974; Davison and Tuohy 1975). The binary nature of Cir X-1 was established by observations with the Ariel V ASM which yielded a ~ 16.6 day period between sharp intensity transitions in the light curve (Kaluzienski et al. 1976). On shorter timescales Uhuru observations indicated variability down to 100 ms,

and the results from rocket-borne experiments provide evidence for chaotic behaviour, similar to that seen in Cyg X-1, on timescales as short as 1 ms (Spada et al. 1974; Toor 1977). On the longest timescales Cir X-1 shows long periods of inactivity ("off-states") where the x-ray flux is barely detectable. A suggested 200 day period modulating this behaviour has been ruled out by the extensive ASM data (Kaluzienski et al. 1976).

Cir X-1 has a radio counterpart+, first noted by Clark et al. (1975), which has recently been shown to flare with the same period as the x-ray modulation (Whelan et al. 1977b; Thomas et al. 1978). An optical counterpart+ of Cir X-1 has been discovered within a few arcseconds of the radio source showing strong Hα emission. The candidate is a faint ($m_J \approx 22^m.5$*) red star which suffers considerable interstellar extinction ($E_{B-V} \approx 3^m.5$). Both the Hα and the weaker HeI emission lines are variable, although observations have not yet been obtained at a wide enough range of binary phases to be certain whether this variability is orbital in origin. The radial velocity given by the Hα line measurements is $\approx$ 300 km s^{-1} (Glass 1978).

At radio wavelengths the light curve is characterised by a flare occurring just after the time of the x-ray transition. At short wavelengths (6 cm) the flare is quite prominent, but is much less noticeable at longer wavelengths (75 cm). The time delay between x-ray transition and onset of radio flare also appears to be wavelength dependent (in the sense $\Delta t \propto \lambda$). Recent radio observations at 2 cm, reported by Thomas et al.(1978) show a peak only a few minutes after the predicted time of x-ray transition, and a more complicated pattern of radio emission in general. In the infrared, photometric observations by Glass (1978) show the same 16.6 day modulation, with a light curve similar to that obtained at longer wavelengths.

+ The optical and radio properties of Cir X-1 are discussed fully in Whelan et al. (1977b) on which these comments are based.

* Here the subscript J refers to a magnitude from a IIIaJ plate ($\sim$ blue).

The distance of Cir X-1 has been estimated from both optical and radio studies. The results of Whelan et al.(1977b) and Goss and Mebold (1977) are consistent with d $\approx$ 10 Kpc. At this distance, with $E_{B-V} \approx 3^{m}.5$, a value of $M_J \approx -4^{m}.5$ can be derived for the optical counterpart. This would certainly be consistent with the star being an early-type giant or supergiant as is found with many other x-ray binaries. The IR colours are similar to those found for symbiotic stars (Glass 1976) but other properties of Cir X-1 do not support this interpretation (Whelan et al. 1977b).

3.4.2 SSI Observations

Although the Circinus region has been scanned by the SSI many times since the launch of Ariel V, Cir X-1 has only been unambiguously detected for a short period around the end of 1976. This is consistent with the Ariel V ASM observations which show that Cir X-1 was in an extended "low state" from 1974 October to 1975 September (> 300 days, Kaluzienski et al. 1976). The only observations of Cir X-1 by the SSI since 1976 (1978 May) show that the source has returned to this low intensity level.

Fig. 3.11 shows the observations of Cir X-1 made by the SSI in the period 1976 November to 1977 February. Plotted are single orbit fluxes corrected for both exposure time and collimator response. Cir X-1 lies in a crowded region of the galactic plane, and some parts of the light curve affected by source confusion (particularly with 4U1543-62) have been excluded. Other gaps in the light curve occur where satellite manoeuvres have taken the source out of the SSI field of view (elevation $> 8^{\circ}$ was the criterion for exclusion).

The light curve in Fig. 3.11 clearly shows the periodic flaring noted by Kaluzienski et al. (1976). The overall behaviour within each binary cycle is characterised by an extended period at low intensity ($\sim$ 10 - 14 days), a gradual rise to peak intensity ($\sim$ 1 day), and an abrupt fall in intensity

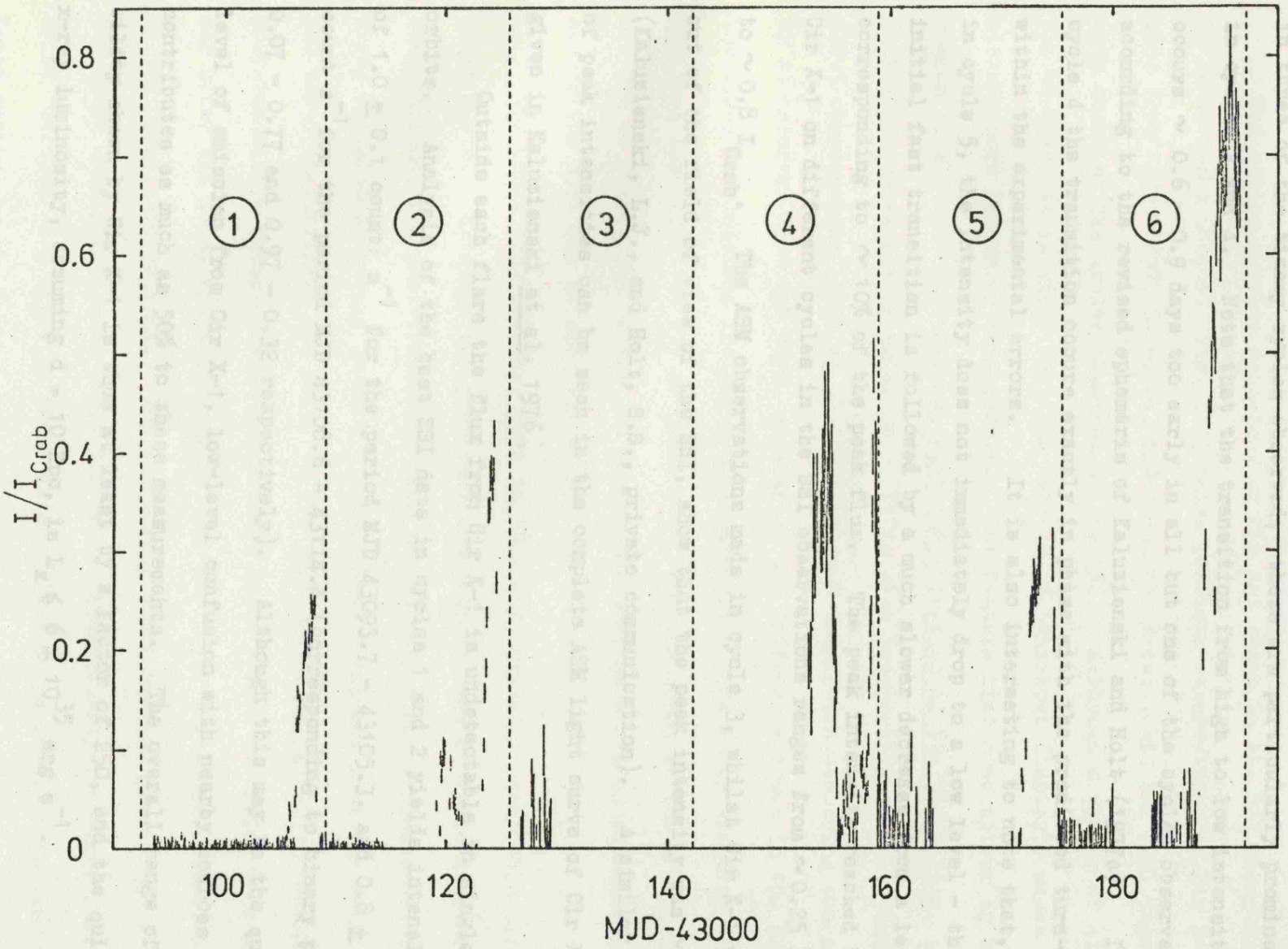

Fig. 3.11 SSI light curve for Cir X-1. Each data point is a single orbit flux with $\pm 1\sigma$ error bar for all the unconfused observations obtained from 1976 November to 1977 February. The dashed lines indicate the times of the predicted transitions on the basis of the ephemeris of Kaluzienski and Holt (1977a). Note that the vertical axis is marked in units of ~~10^{-3}~~ I_{Crab}.

(the x-ray "transition") occurring with an orbit or two ($\lesssim$ 0.14 days), the whole flare lasting 3 - 6 days. Within the flares dips are apparent in three of the binary cycles observed; these are particularly prominent in cycles 2 and 4. Note that the transition from high to low intensity occurs $\sim$ 0.6 - 0.9 days too early in all but one of the cycles observed according to the revised ephemeris of Kaluzienski and Holt (1977a). In cycle 4 the transition occurs exactly in phase with the predicted turn-off within the experimental errors. It is also interesting to note that, in cycle 5, the intensity does not immediately drop to a low level - the initial fast transition is followed by a much slower decrease from a level corresponding to $\sim$ 10% of the peak flux. The peak intensity reached by Cir X-1 on different cycles in the SSI observations ranges from $\sim 0.25\ I_{Crab}$ to $\sim 0.8\ I_{Crab}$. The ASM observations made in cycle 3, whilst Cir X-1 was out of the field of view of the SSI, show that the peak intensity was $\sim 1.5\ I_{Crab}$ (Kaluzienski, L.J., and Holt, S.S., private communication). A similar range of peak intensities can be seen in the complete ASM light curve of Cir X-1 given in Kaluzienski et al. 1976.

Outside each flare the flux from Cir X-1 is undetectable in single orbits. Analysis of the best SSI data in cycles 1 and 2 yields intensities of 1.0 ± 0.1 count s^{-1} for the period MJD 43093.7 - 43105.3, and 0.8 ± 0.1 count s^{-1} for the period MJD 43108.6 - 43114.4 (corresponding to binary phases 0.07 - 0.77 and 0.97 - 0.32 respectively). Although this may be the quiescent level of emission from Cir X-1, low-level confusion with nearby sources probably contributes as much as 50% to these measurements. The overall range of variability shown by Cir X-1 is thus at least by a factor of 250, and the quiescent x-ray luminosity, assuming d = 10 Kpc, is $L_x \lesssim 6 \times 10^{35}$ erg s^{-1}.

3.4.3 Discussion

(a) Light curve structure

The rather complex behaviour of Cir X-1 shown in the SSI observations is by no means unique. Fig. 3.12 shows previous observations of Cir X-1 made from 1972 - 1977 by Uhuru, SAS-3 and the Ariel V RMC and ASM, together with three of the cycles observed by the SSI. Although a number of similarities can be seen, it is clear that the variety of behaviour displayed makes the picture more confusing than before. One feature that does appear to be common to all the observations, with the exception of the Uhuru data, is the lack of post-transition emission. It is also interesting to note that the SAS-3 observations (Buff et al. 1977) show a transition occurring too early by an interval of ~ 0.8 days, similar to the difference found in the SSI data. The SAS-3 observations include a crude measure of the x-ray spectrum which indicate that both the dip at phase 0.85, and the onset of the transition, are due to absorption of the low energy photons, as would be expected if the absorption were due to cool gas within the system.

The Uhuru observations, made in 1972 May, reveal a remarkably different light curve. Although the pre-transition data resembles cycle 4 of the SSI observations, the post-transition data is the only clear evidence of significant x-ray emission at binary phase 0 - 0.5. Recent reports from the Ariel V ASM and SAS-3 (Kaluzienski and Holt, 1977b, 1978 , Dower et al. 1977) indicate that post-transition emission at a significant level is now occurring less than a day after the x-ray transition, i.e. that the light curve now resembles that of the Uhuru observations. The similarity could be even greater if a few of the Uhuru data points near phase 0.0 were systematically too high, i.e. if a brief "eclipse" did exist in their data. This seems possible in view of the large scatter in the light curve.

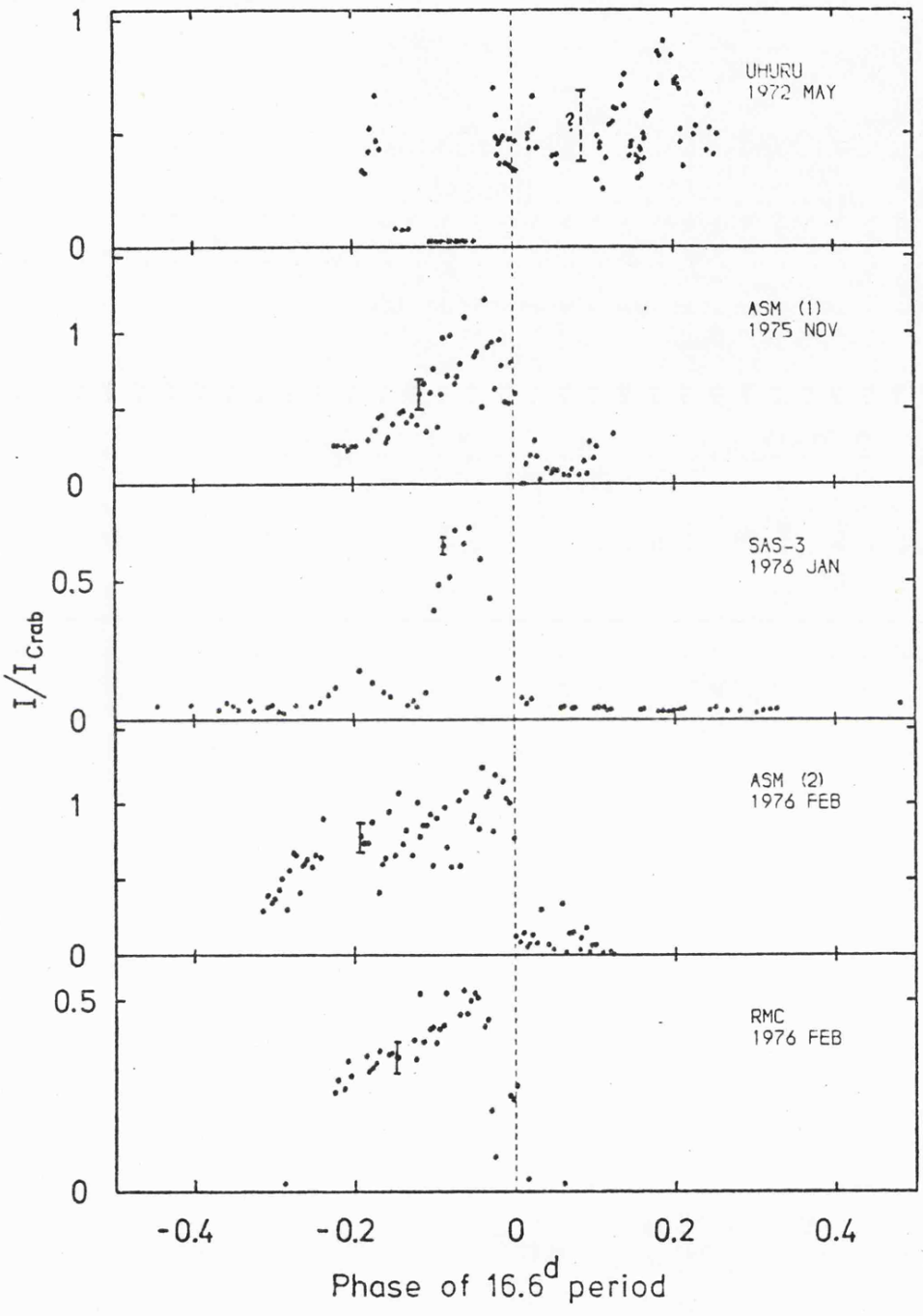

Fig. 3.12(a) Previous x-ray observations of Cir X-1 plotted as a function of phase of the 16.6 day period using the same ephermeris as Fig. 3.11. Data are from: UHURU - Jones et al. (1974); ASM(1) and ASM(2) - Kaluzienski et al. (1976); RMC - (Ariel V RMC) - Wilson and Carpenter, 1976; SAS-3 - Buff et al.(1977); ASM(3) - Kaluzienski L.J., private communication; SSI - this work (nos. refer to cycles as marked in Fig. 3.11). Intensity is shown relative to Crab, representative $\pm 1\sigma$ error bars are marked.

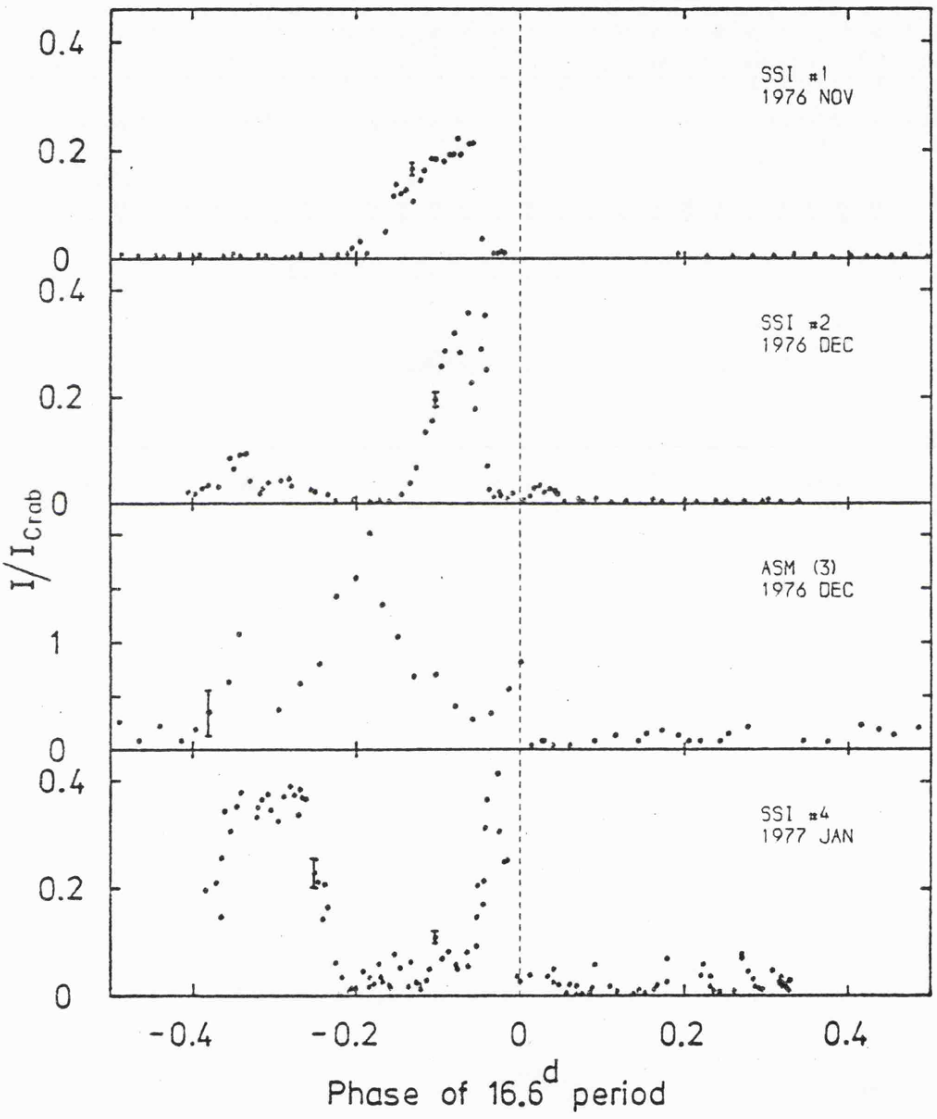

Fig. 3.12(b) Previous x-ray observations of Cir X-1 plotted as a function of phase of the 16.6 day period using the same ephermeris as Fig. 3.11. Data are from: UHURU - Jones et al. (1974); ASM(1) and ASM(2) - Kaluzienski et al. (1976); RMC - (Ariel V RMC) - Wilson and Carpenter, 1976; SAS-3 - Buff et al.(1977); ASM(3) - Kaluzienski L.J., private communication; SSI - this work (nos. refer to cycles as marked in Fig. 3.11). Intensity is shown relative to Crab, representative $\pm 1\sigma$ error bars are marked.

(b) Binary period

The x-ray period of Cir X-1 has been established by using the times of the x-ray transitions observed by the ASM over a baseline of ~ 1.75 years (~ 40 cycles), giving a mean period of 16.595 ± 0.001 days (Kaluzienski and Holt 1977a). Radio observations over a slightly shorter baseline yield a period and epoch which agrees with the x-ray ephemeris (Thomas et al. 1978). There seems little doubt that this period is due to orbital modulation of the x-ray (and radio) emission in a binary system. The shape of the light curves does not however resemble that of known x-ray binaries. The most reliable feature of the light curve, the transition from high to low intensity, is most easily interpreted as entry into x-ray eclipse. If this is the case the stability of the period is easily understood, but one must then find an explanation for the lack of observed eclipse exit in 1976 - 1977, as discussed above. If the transition is not due to an eclipse there are problems in explaining the long-term phase stability of this feature. (Period errors quoted by Kaluzienski and Holt (1977a) imply a mean stability in phase to better than 0.02% over ~ 2 years).

Further complications arise in explaining the increase in radio and infra-red flux immediately after the x-ray transition since this phenomenon would not be expected to be correlated with the time of geometrical eclipse of the x-ray source.

(c) Models

It is probably premature to discuss detailed models of Cir X-1 which may explain the wealth of observational data, especially as the source has not yet been adequately studied at optical wavelengths. It seems clear however that the correct picture of this source must be based on a binary system (of the type discussed in Chapter 1) with a period of 16.6 days. The complex structure of the light curve probably reflects the varying pattern of absorbing gas flows within the system, since the spectral data

from SAS-3 implies that at least one dip is due to low-energy absorption*.

The interpretation of the x-ray transition as the entry into eclipse is perfectly tenable, in which case the "early" transitions seen in the SSI and SAS-3 observations indicate variability of the eclipse width, a feature which is established in several x-ray binaries (e.g. Vel X-1, § 3.2). If this interpretation is correct the remaining problems lie in explaining the lack of observable eclipse exit over a number of binary cycles, and in explaining the radio and infra-red results. The lack of eclipse exit might be explained in terms of a large amount of obscuring matter in the system so placed as to absorb most of the x-rays between phases 0 and 0.5. Such a "cloud" could result from mass-loss by Roche-lobe overflow where not all the mass is accreted by the compact object; indeed the interpretation of the optical results on Vel X-1 (Bessel et al. 1975, see Fig. 3.5) includes matter in this region.

Alternatively the interpretation of the radio and infra-red results would seem to demand a model where the x-ray transition is not due to geometrical eclipse. For example, the model of Hatchett and McCray (1977) for Cen X-3 successfully explains the changing shape of the x-ray light curve as the source emerges from a "low-state" in terms of a small x-ray-transparent region near the x-ray source in the dense stellar wind. Applied to Cir X-1 the repetitive flare-like x-ray outbursts might be explained by a similar model in which the density gradients at the edges of this region reproduce the assymetry in the light curve. The leading edge of this region, responsible for the fast x-ray cut-off, would be a shock-front (i.e. high density gradient). The radio and infra-red emission might then originate from particles accelerated in the shock. The position of this region with the system is controlled by the wind velocity, density and the x-ray luminosity, all of which are likely to be variable (x-ray luminosity certainly is). This raises doubts as to whether this picture could produce the observed phase stability of the transition feature in the x-ray (and radio) light curves.

---

* Note however that recent SAS-3 observations (Dower et al. 1978) show large intensity variations in Cir X-1 with no spectral changes.

Chapter 4

LOW-MASS X-RAY BINARIES

4.1 Introduction

Low-mass x-ray binary sources have received relatively little attention to date, even though, as argued in Chapter 1, they are likely to be the most numerous class of luminous x-ray source ($L_x \gtrsim 10^{35}$ erg s^{-1}) in the galaxy, far outnumbering the high mass binaries discussed in Chapter 3. The principal reason for this is the difficulty in establishing the optical identifications for such systems due to the intrinsic faintness of the optical counterparts ($m_v \gtrsim 15^m$ is expected for d > 1 Kpc). In addition these sources rarely reveal their binary nature through a clear modulation of the x-ray or optical flux. Only two x-ray sources are known unambiguously to involve a low mass star in a binary system - Her X-1 and Sco X-1. Her X-1 is somewhat exceptional in that the optical counterpart is slightly evolved ($M \sim 2M_\odot$) and shows obvious eclipses in the x-ray light curve. In many respects it is closer in its overall properties to the high mass binaries. On the other hand Sco X-1 is a typical member of the low mass class, showing a soft x-ray spectrum, no evidence for an x-ray pulsation period, and no evidence for modulation of the x-ray light curve at the binary period. It is identified with a low-mass late-type dwarf ($M \lesssim 1\ M_\odot$). The binary period of 0.78 days was not established until 1975, nine years after the original identification with V818 Sco was proposed (Gottlieb et al. 1975). Cyg X-2, which is similar to Sco X-1 in many ways, still does not have a unique binary period, despite having been identified eleven years ago by Giacconi et al. (1967).

In this chapter observations by the SSI of five sources are discussed, all of which are very probably low-mass binary systems on the basis of their optical identifications. Three of the sources (A0620-00, A1524-61 and

H1705-25) are x-ray transients which have shown (to date) a single outburst with a peak intensity > 500 times that of the quiescent level, and the typical fast rise and slow decline of such objects. Of the other two, Aql X-1 is a "recurrent transient" which has shown repetitive transient-like outbursts with a total variability by a factor > 50; the other, 2A0042+323, is a weaker high galactic latitude source which has been observed to flare by a factor $\gtrsim$ 20 and shows structure in its x-ray light curve which may be periodic. The optical identification of four of these five sources was in fact accomplished as a result of optical activity of the counterpart correlated with x-ray outbursts, the fifth (2A0042+323) has been identified mainly on positional grounds.

About 30 transient or transient-like x-ray sources are now known (see Table 1.7). As is stressed in § 1.3.9 many of these sources may turn out to be "recurrent transients" or "long period variables" when better studied, i.e. that the transient outbursts recorded may simply be part of a more complex time variability. The three transients discussed in this Chapter represent one extreme of a spectrum of properties for transient-like sources, since they show such a high degree of variability. Sources like Aql X-1 and 2A0042+323 may represent an important link with the steadier sources such as Sco X-1 and Cyg X-2.

Transient sources seem to fall into two distinct observational categories on the basis of x-ray spectra (and possibly also in terms of outburst time-scales and x-ray luminosity - see discussion in § 1.3.9). The three transients discussed here are all indubitably Type I (Kaluzienski's category), indeed A0620-00 is the prototype of this class, as is expected if they are all low-mass binaries.

4.2 A0620-00 = Mon X-1

4.2.1 Introduction

The outburst of A0620-00 in 1975 August was one of the most dramatic events ever to occur in x-ray astronomy, comparable in many ways with the

appearance of a nearby nova in terms of the impact it had on the astronomical community. For months after the initial outburst, A0620-00 was monitored by dozens of astronomers using both satellite-borne and ground-based instrumentation which have yielded a wealth of observations at x-ray, ultraviolet, optical, infra-red and radio wavelengths. The resultant extensive literature (Webbink has compiled a bibliography containing over 130 entries, complete up to the end of 1977) is only summarised here; indeed most of the emphasis is placed on x-ray and optical observations.

(The purpose of this discussion of A0620-00 is primarily to set the scene for the discussion of other similar sources which have not been as extensively observed. The only unpublished results reported in this section concern the SSI light curve of the x-ray decline, in particular the observations in 1976 January which are discussed in terms of the reported 8 day periodicity seen by SAS-3 in partially overlapping observations).

4.2.2 X-ray Observations

A0620-00 was discovered by the Ariel V SSI on 1975 August 3 during the second long scan of the galactic plane (Elvis et al. 1975). Within a few days its intensity equalled that of the Crab and continued to rise over the next week to reach a maximum of $\sim 50\ I_{Crab}$ on August 13, interrupted only by a brief precursor at an intensity of $\sim 2.5\ I_{Crab}$ (the overall light curve is shown in Fig. 4.1). The source intensity remained steady for about 2 days and then started to decay quite smoothly with an initial e-folding timescale of $\sim$ 29 days. This smooth decay was interrupted in October by an unexpected increase in intensity ($\gtrsim$ 50% increase over extrapolated value) which lasted for $\sim$ 15 days. The exponential decay then continued with a shorter e-folding timescale of $\sim$ 21 days until December. The next part of the light curve is poorly monitored but it appears that the source intensity levelled out and was reasonably steady until mid-January (1976), when a further increase in

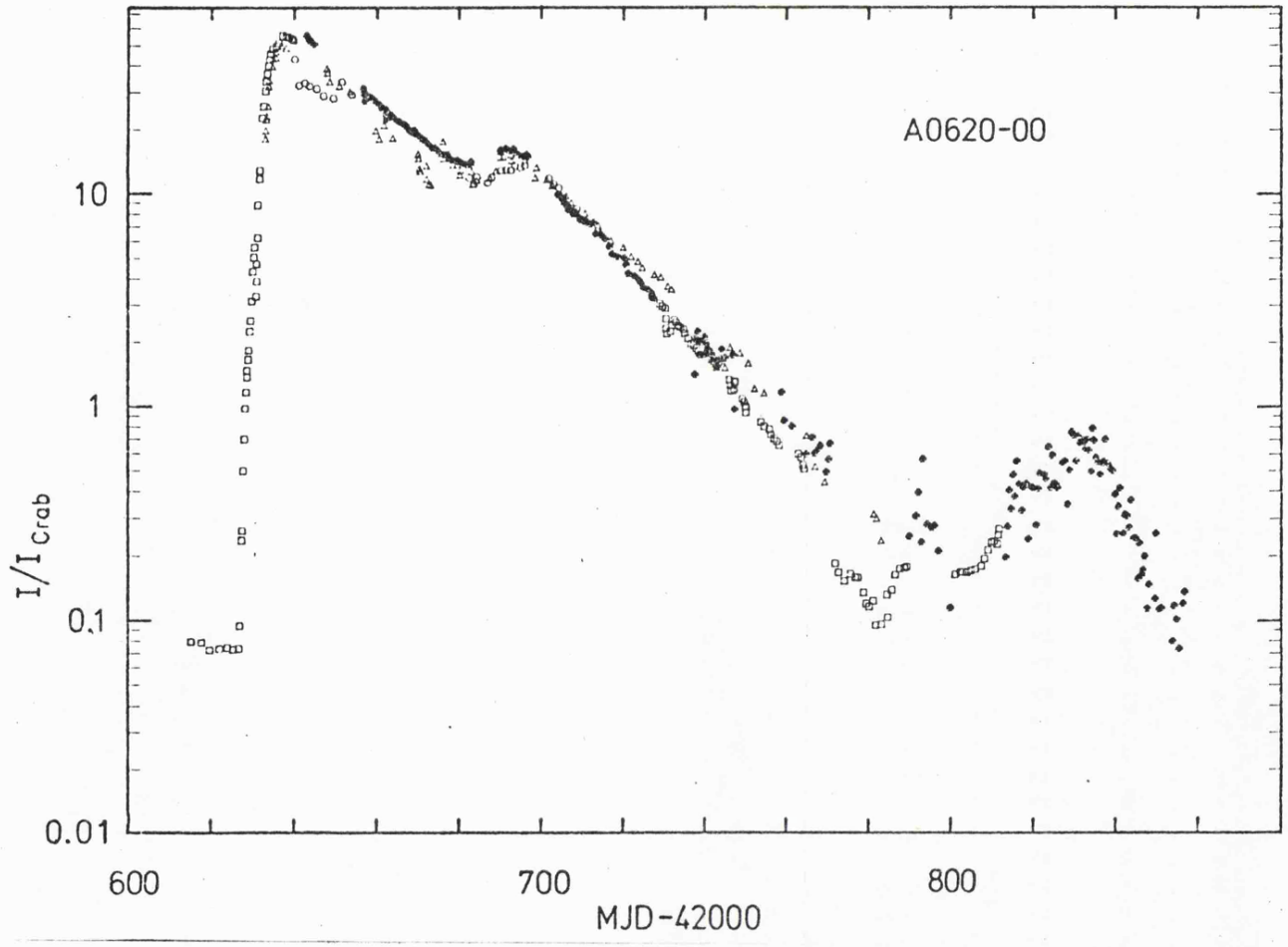

Fig. 4.1 Composite x-ray light curve for the outburst of A0620-00 (Mon X-1). Data are from

- □ : SSI (this work (~ 2 - 18 keV)
- △ : SAS-3 (~ 1.5 - 6 keV) (Matilsky et al. 1976)
- ○ : Ariel V RMC (~ 3 - 7.5 keV) (Carpenter et al. 1976)
- ● : Ariel V ASM (~ 3 - 6 keV) (Kaluzienski et al.1976)

The points shown have been replotted from the original figures by digitising them at approximately 1 day intervals, with some resulting loss in accuracy. Because of the problems of normalisation, accentuated by the strong spectral evolution of Mon X-1, the data have been arbitrarily normalised to agree between MJD 42700-740. Note that the intensity scale is logarithmic.

intensity occurred (by an order of magnitude) which lasted for ~ 30 days. Subsequently the intensity dropped rapidly with an e-folding timescale of ~ 4 days. Mon X-1 was undetectable at x-ray wavelengths by the beginning of 1976 April.

Most of the light curve of Mon X-1 is remarkable for its smoothness. Day to day variability is apparent in the observations made by SAS-3 between MJD 42650 and 42690 and again in the later stages of the light curve decay (MJD 42785-820) (Matilsky et al. 1976, also Fig.4.1). The SSI observations reveal a clear intensity dip near MJD 42730 but little other variability until MJD 42770, when the intensity had fallen to ~ 0.2% of its maximum value (see Fig. 4.3). Searches for periodic modulation during the initial rise, and around the time of maximum intensity, yielded upper limits of 2% for periods between 0.2 ms and 0.25s and 0.4% for periods between 0.8 and 435s (Doxsey et al. 1976), and 3% over timescales of 200s - 2d (Elvis et al. 1975).

Mon X-1 shows remarkable changes in its x-ray spectrum during outburst. From an initial kT ~ 30 keV prior to the precursor peak, the bremsstrahlung temperature fell to kT ~ 1.3 keV near maximum intensity, followed by a slight hardening to kT ~ 1.8 keV before the x-ray decline (Ricketts et al. 1975, Matilsky et al. 1976). Throughout the decay the spectrum softened gradually (kT fell below 1 keV ~70 days post-maximum). This complex spectral behaviour presents problems of normalisation when comparing intensities derived from different experiments - note that the composite light curve in Fig. 4.1 is not corrected for spectral changes (see Figure caption).

4.2.3 Optical Observations

The optical counterpart of Mon X-1 (= V616 Mon) was discovered on the basis of a preliminary position from SAS-3 as a normally faint ($B \sim 20^m$) star which showed an optical outburst by $\sim 9^m$ coincident with the x-ray flare (Boley et al. 1976). The optical light of V616 Mon, shown in Fig. 4.2,

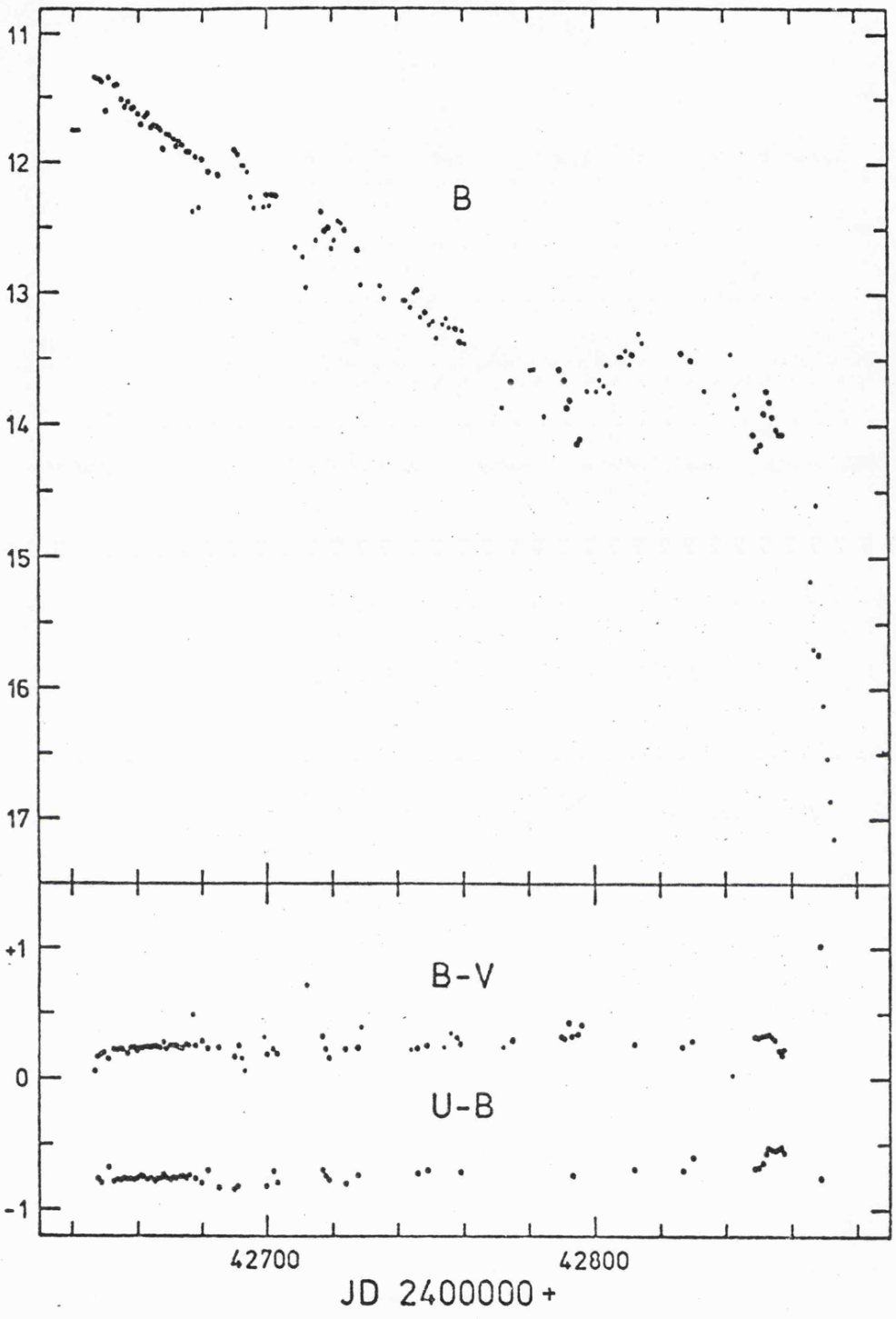

Fig. 4.2 Composite optical light curve for the outburst of V616 Mon (A0620-00) compiled by Webbink (preprint, 1978).

shows close similarities with the x-ray behaviour, including optical brightening in 1975 October and 1976 February. The February increase appears to occur ~10 days before the x-ray rise, and the final rapid decline ~ 20 days after the x-ray drop-off. The e-folding timescale for the B-band flux is ~70 days for the initial part of the decay (~ 3 times longer than that in x-rays). Eachus et al. (1976) have noted a previous optical outburst of Mon X-1 which occurred in 1917. This outburst appears from the data available to be remarkably similar to the present event.

At maximum light the spectrum of V616 Mon shows a featureless blue continuum similar to that of Sco X-1 (Whelan et al. 1977a). Post-maximum observations show a developing absorption and emission spectrum, particularly λ4686 HeII, λ4640 NIII (both in emission), Hα and Hβ (absorption with superimposed emission) and several interstellar lines (Whelan et al. 1977a; Oke and Greenstein 1977). Observations in 1976 November show the underlying spectrum of ~ K5 V, confirming early suggestions that the star was a late-type dwarf (Oke 1977). Estimates have been made by several authors of both the reddening and distance to V616 Mon. A distance of ~1 Kpc with $E_{B-V} \approx 0.39$ is consistent with the corrected apparent magnitude of the K dwarf as given by Oke (1977).

Spectrophotometry of V616 Mon in 1975 September and 1976 March shows that the optical emission is dominated by an approximately black-body source at 25,000 - 30,000 K (Oke and Greenstein 1977). This hot source has been associated with the heated face of the dwarf star (e.g. Wu et al. 1976). Because the intensity of this hot source is not strictly proportional to the x-ray intensity, Oke and Greenstein (1977) argue that the emission is more likely to originate within an accretion disc surrounding the compact object. X-ray heating of the dwarf star almost certainly is taking place

but the dominant emission comes from the disc. The emission lines seen in the post-maximum spectrum may also arise in the x-ray heated region (Whelan et al. 1977a).

4.2.4 Periodic Modulation

A variety of modulation periods have been suggested for Mon. X-1 on the basis of both optical and x-ray observations, including 3.9, 7.4 and 7.8 day periods in optical light (Duerbeck and Walter 1976, Tsunemi et al. 1977, Chevalier et al. 1977), and a 7.8 day period in the x-ray flux (SAS-3 observations, Matilsky et al. 1976). The only direct evidence that Mon X-1 is a binary system derives from these observations, hence it is important to examine critically the reported modulation.

Fig. 4.3 shows the SSI light curve of Mon X-1 for the period MJD 42772-812. Because of the lower source intensity, and high source elevation for some parts of the observation, the points shown are ~ 10 orbit sums (~ 0.7 day integrations). Clearly evident are two intensity minima centred on MJD 42774.0 and 42783.0 (i.e. 9 days apart) superimposed on quasi-linear decrease in intensity. After the gap in the data (due to high source elevation) no obvious modulation is present and the intensity is beginning to increase (initial stages of the 1976 February maximum - see Fig. 4.1). In the SAS-3 observations (which partially overlap - Fig. 4.3) two further intensity minima are apparent at MJD 42791.5 and 42799.0 (Matilsky et al. 1976). Matilsky et al.'s analysis gave a period of 7.8 $\pm$ 0.7 days for the modulation in this data. The modulation in the SSI light curve is consistent with this period, but it is clear that the minima observed are significantly displaced with respect to the times predicted from the SAS-3 observations. We have also attempted to confirm this periodicity by performing a fold-χ^2 analysis on the SSI data. The results are shown in Fig. 4.4 where the χ^2 deviation from source constancy is plotted against folding period (data folded in 5 bins). Although a χ^2 peak occurs at a period of 8.0 days, this peak is

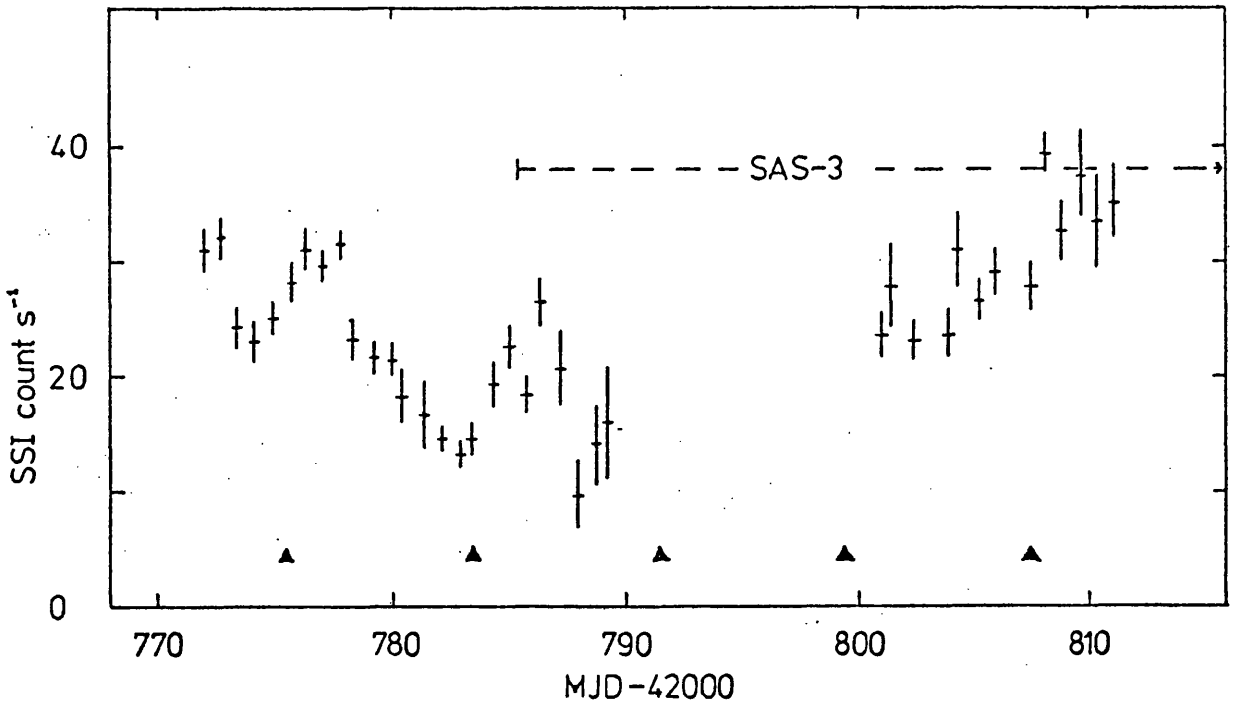

Fig. 4.3 SSI light curve of the observations of A0620-00 made in 1975 December and 1976 January. Each data point represents a sum over ~ 10 satellite orbits (~ 0.7 days) plotted with $\pm 1\sigma$ error bars. The times of the minima expected on the basis of the SAS-3 7.8 day period are shown by small triangles.

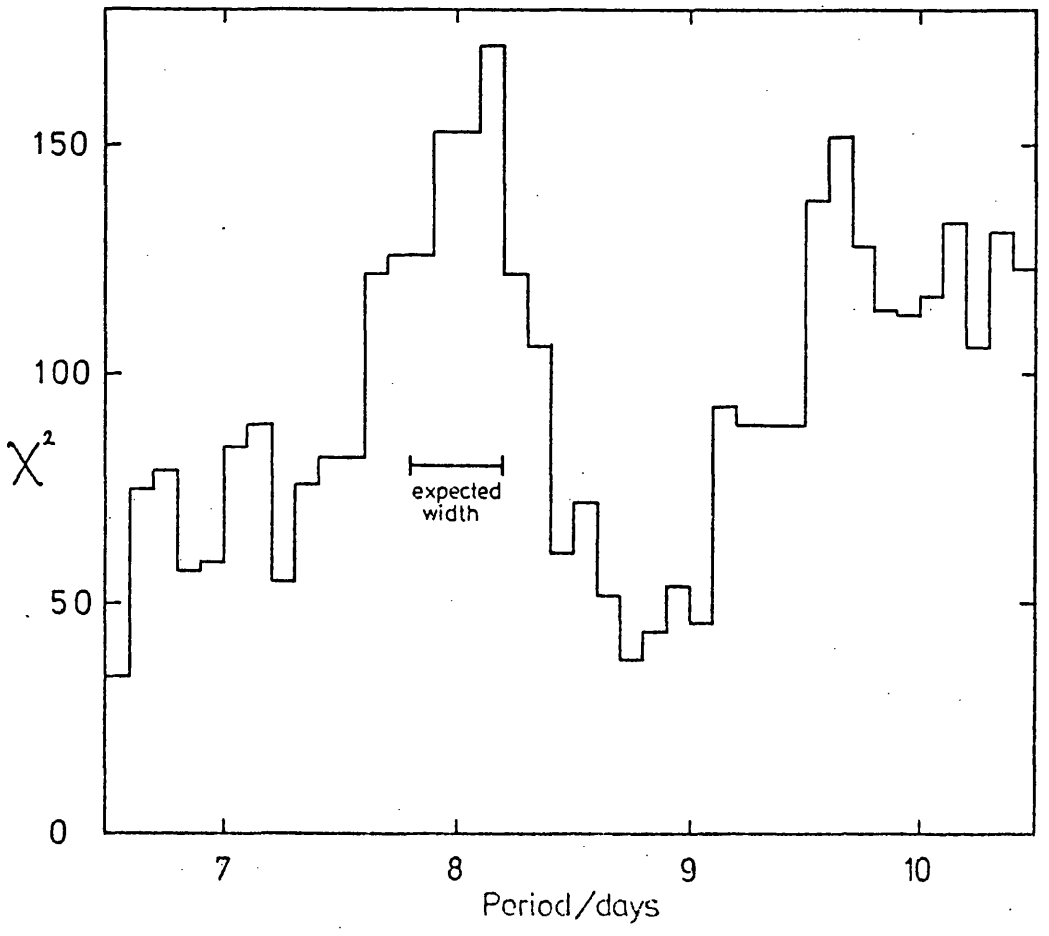

Fig. 4.4 Detail of the χ^2 vs. period plot for the SSI observations of A0620-00 folded at a range of trial periods from 6.5 - 10.5 days. χ^2 value is calculated for the data folded into 10 phase bins against the hypothesis of source constancy.

not prominent and would not be picked out in an unbiassed search for periodic modulation.

The SSI results seem to suggest that, although a modulation with a timescale of ~ 8 days is apparent for 4 cycles in the SSI and SAS-3 data, this is not a strictly periodic phenomenon. The amplitude of the modulation in the SSI data is ± 28% of the mean flux at a period of 8 days, whereas it is ± 50% in the SAS-3 observations. This difference may be due to the different energy bands of the experiments, if the modulation is primarily in low energy x-rays, since the SAS-3 detectors have a "softer" response (results quoted are in the 1.5 - 6 keV energy range).

4.3 A1524-61 - TrA X-1

4.3.1 Introduction

A1524-61* was the first of a remarkable series of bright x-ray transients discovered by Ariel V. It appeared shortly after launch of the satellite, in 1974 November, when the SSI was making its first extended observation of the galactic plane (Pounds 1974). The x-ray emission reached its precursor peak on 1974 November 22, followed about 12 days later by a more intense peak when the source intensity was comparable with that of the Crab Nebula, and a subsequent slow decay characterised by a e-folding timescale of ~ 52 days (Kaluzienski et al. 1975, Murdin et al. 1977).

On the basis of a series of optical plates covering the period of the x-ray outburst, A1524-61 has been identified with a faint ($m_v \sim 17^m$) optical nova (Murdin et al. 1977).

4.3.2 X-ray Observations

A1524-61 was extensively observed by both the SSI and ASM on Ariel V. The SSI observations, shown in Fig. 4.5, cover the smooth rise of the transient to its precursor peak and subsequent decline to a lower plateau for ~ 10 days; the ASM observations span the second, more intense, peak about 12 days after

---

* Also called, erroneously, A1524-62

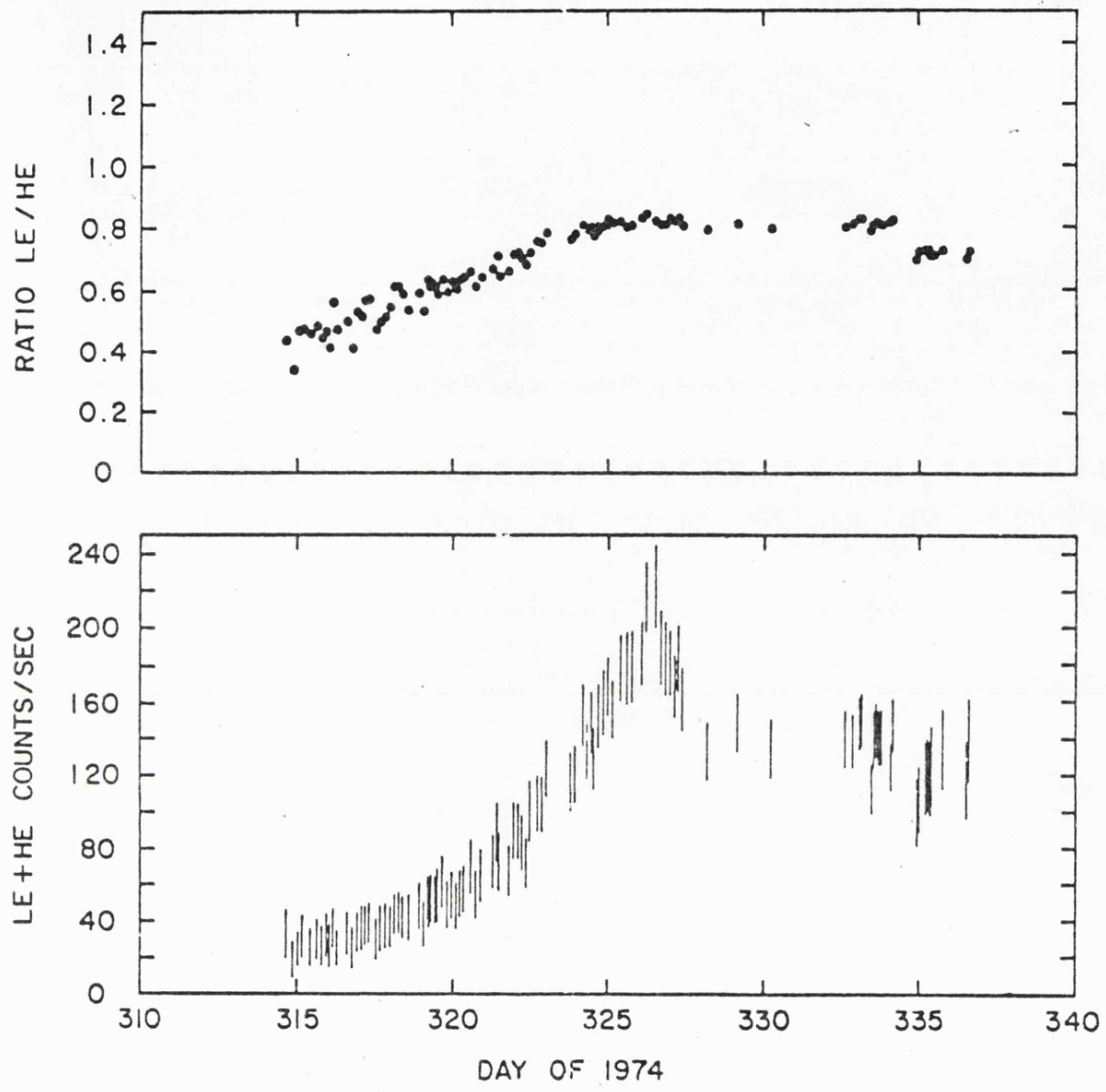

Fig.4.5 SSI light curve for A1524-61. The top frame shows the ratio of counting rates in the low energy and high energy detector systems which were still functioning at the time of this observation.

the precursor and the irregular decline of the source for over 100 days. (The ASM observations are shown schematically in Fig. 4.8). During the SSI observations the experiment was mainly in 180° SECTOR mode giving two-channel spectral information on this source, shown as a "hardness" ratio in the top panel of Fig. 4.5. Clearly the ratio implies a spectral softening of the source up to the precursor maximum, with apparently steady spectral ratio thereafter. The spectrum of A1524-61 was also measured with the SSI using four-channel spectra obtained over two days near the precursor peak. The best fit spectra were to a simple power law with photon index $\alpha = 2.5 \pm 0.1$ and no measurable low energy cutoff ($E_a \leqslant 4.2$ keV (3σ)). Thus in terms of the spectral classification discussed in Chapter 1, A1524-61 is undoubtedly a "soft" source.

A search for periodic modulation of this source was carried out using the ASM observations. No significant periods were found in the range 0.5 - 10 days with an upper limit of $\sim 5\%$ to any modulation (Kaluzienski 1977). A similar search in the SSI data shown in Fig. 4.5 extending down to periods of 0.2 days also revealed a lack of significant modulation.

4.3.3 Optical Identification*

Fig. 4.6 shows a photograph of the region containing the x-ray source, taken at the prime focus of the Anglo-Australian 3.9m telescope on 1974 December 15, during commissioning tests, this plate being badly fogged by the dawn. It was possible then to determine that there was no large change amongst the brighter stars by reference to the Franklin-Adams charts, but it was not until a second epoch plate was obtained at the AAT in March 1976 that the fading of 17th magnitude nova was noticed within the SAS-3 and Ariel V error boxes at R.A. 15hr 24m 05.3s, dec - 61° 42' 35" (1950).

Fig.4.7 was prepared from an SRC Schmidt IIIaJ plate taken 1975 June 30 when the nova had faded to 19th magnitude. Superimposed on Fig. 4.7 is the

---

* The optical results reported in this section are the work of Paul Murdin and Andy Longmore.

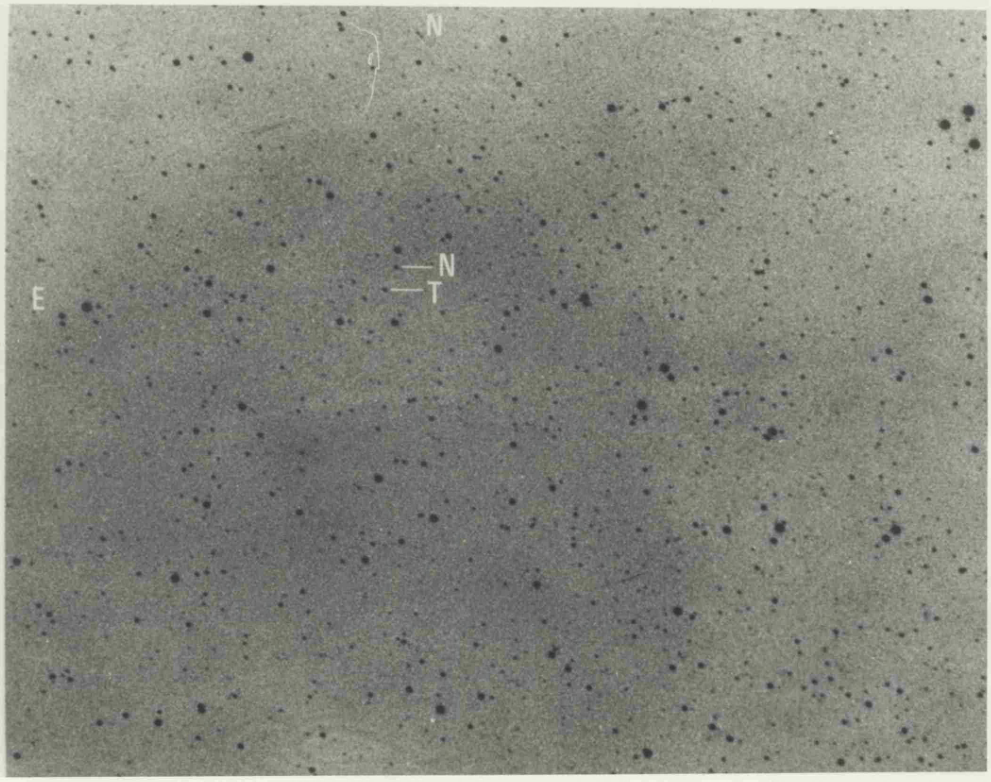

Fig. 4.6 AAT photograph of the A1524-61 field showing the nova N as bright as the 17^m star T. (1974 Dec.15, IIaO, 10 min exposure).

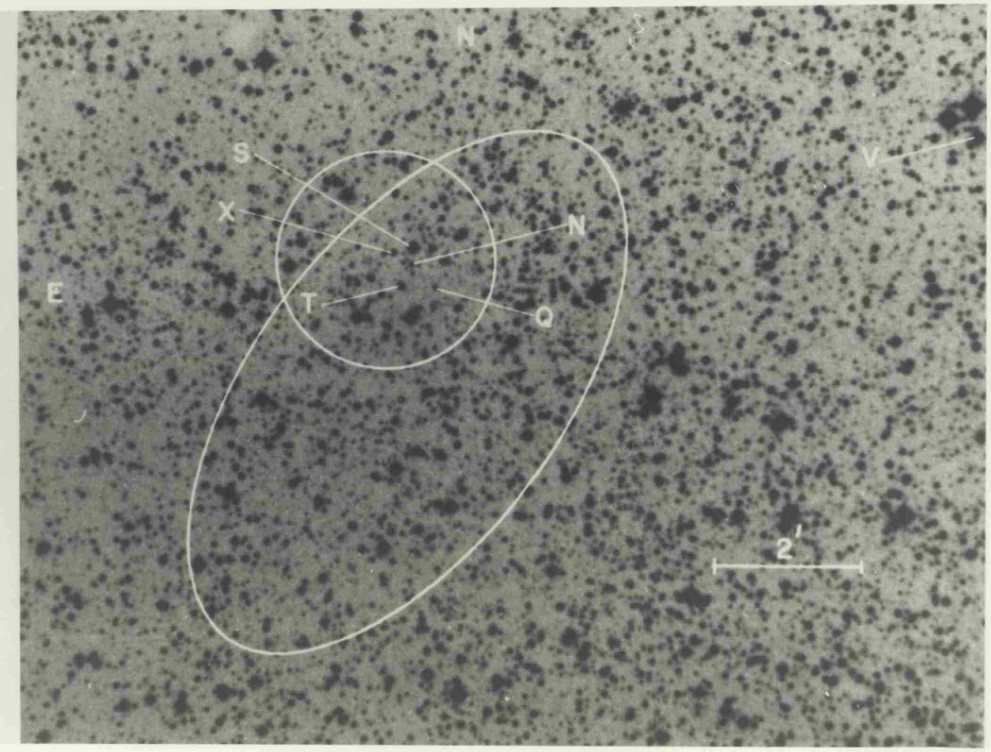

Fig. 4.7 SRC-Schmidt photograph showing the nova N almost as fainst as 19^m star Q. Also shown are 90% confidence regions for A1524-61 from SAS-3 (circle), and the SSI (ellipse). (1975 June 30, IIIaJ).

position of the x-ray transient obtained with the SAS-3 satellite (Jernigan 1975)* and a revised position from the Ariel V Sky Survey Instrument (SSI). The latter position has been obtained using all the positive sightings of A1524-61 with the SSI, each corrected for spacecraft attitude errors using sightings of the nearby bright sources Cen X-3, Ara X-1 and Nor X-1. (Note an intermediate SSI position, Watson (1975) contained an error and is replaced by the new position given here.) The proposed optical counterpart, N in both plates, lies within the region of overlap of the SAS-3 and revised Ariel V 90% confidence contours, and is also quite close to the centre of the original Ariel V SSI position.+ The x-ray and optical star positions are also listed in Table 4.1.

4.3.4 Comparison of Optical and X-ray Light Curves

In Fig. 4.8 the composite x-ray light curve of A1524-61 is shown, including later SSI observations made between 1975 April and 1976 May. The last positive detection by the SSI was in 1975 July-August (the second extended galactic plane scan) at a level of 2.9 SSI count s^{-1} ($\sim$ 1% of maximum intensity). The optical light curve, derived from AAT observations and plates taken with the SRC and ESO Schmidt telescopes, is shown in the upper section of Fig. 4.8, and is summarised in Table 4.2. The recent AAT magnitudes were observed with the television acquisition system and are conservative upper limits. (These magnitudes are based on the colour response of an unfiltered extended S20, excluding UV, and lie midway between R and V magnitudes). The plate calibrations were determined from a photoelectric sequence of four faint stars in the field of the nova. The stars are labelled in Fig. 4.7.

The optical and x-ray light curves of Fig. 4.8 peak at the same time. This temporal correlation is further strong evidence that the two are associated with the same event. The decay of the optical light (0.008 $\pm$ .002 mag/day) is

---

* A more accurate later position from SAS-3 (Bradt et al. 1977) is also available.

+ The candidate lies within 14" of the centroid of the Bradt et al. errorcircle.

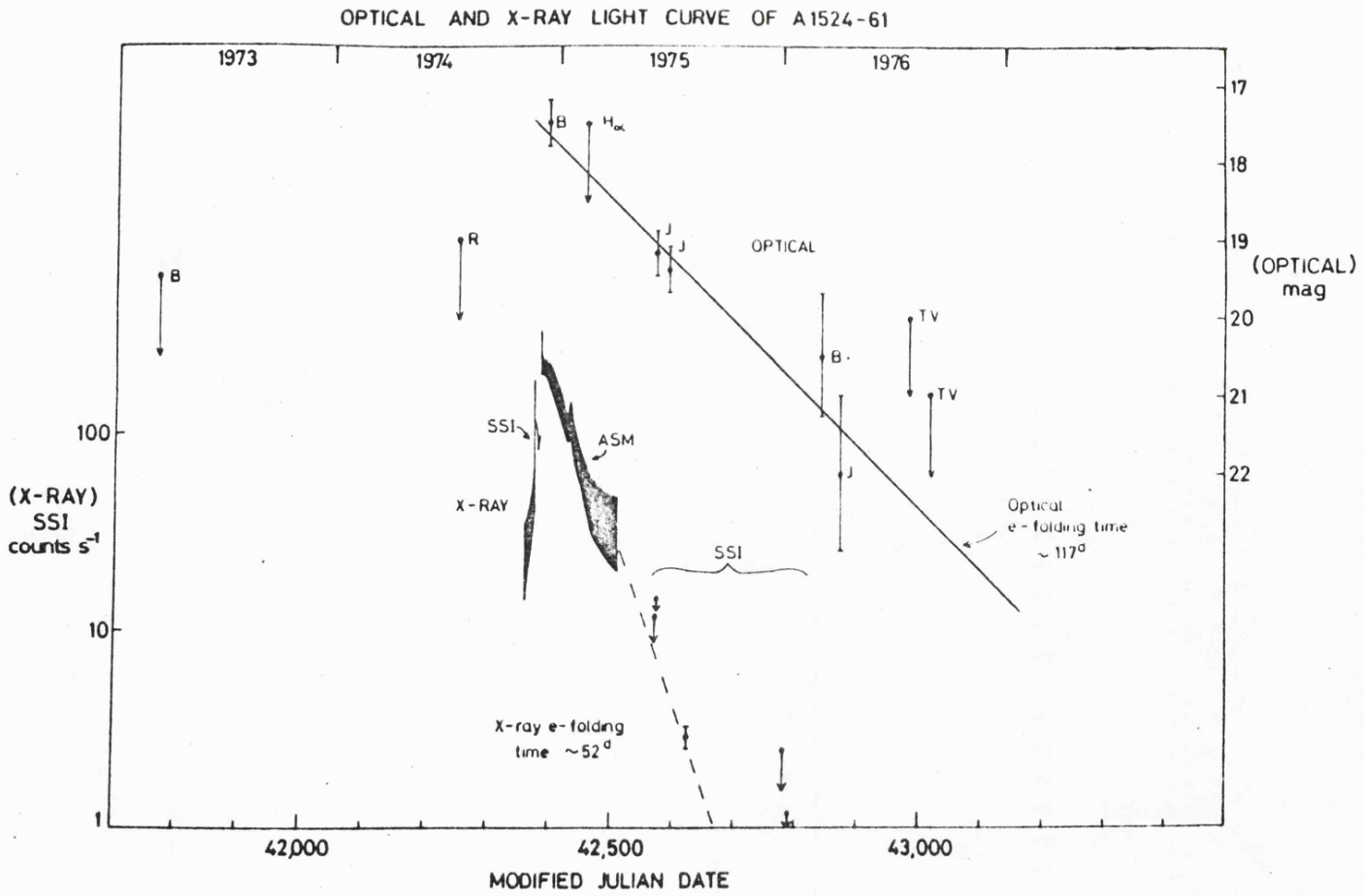

Fig. 4.8 The x-ray and optical light curves of A1524-61. X-ray upper limits are 3σ.

TABLE 4.1

X-ray and Optical Star Positions

	Position: R.A., Dec.(1950)		Error Box
(1) Ariel V SSI - initial position	15^h24^m	$-61^\circ42'$	Circle, radius 10'.
(2) Ariel V SSI - revised position	$15^h24^m05^s$	$-61^\circ44'.4$	Ellipse, major axis 9', P.A. 145° minor axis 4'.5
(3) SAS-3 (i)	$15^h24^m08^s$	$-61^\circ42'.5$	Circle, radius 1'
(4) SAS-3 (ii)	$15^h24^m06^s.9$	$-61^\circ42'.68$	Circle, radius 20"
(5) Optical star	$15^h24^m05^s.3$	$-61^\circ42'.58$	Circle, radius 5"

TABLE 4.2

Optical magnitudes of A1524-61

Date	Observatory	Bandpass	Magnitude
1973 Mar 29	ESO	B	>19.5
1974 July 24	SRC	R	>19
1974 Dec 15	AAT	B	17.5 ± 0.3
1975 Feb 1	SRC	H	≳17.5
1975 June 9	SRC	J	19.2 ± 0.3
1975 June 30	SRC	J	19.4 ± 0.3
1976 Mar 4	AAT	B	20.5 ± 0.8
1976 April 3	SRC	J	22 ± 1
1976 July 27	AAT	TV	>20
1976 Aug 29	AAT	TV	>21

B and R correspond to standard wideband photometric blue and red magnitudes.

J = IIIaJ emulsion.

TV = AAT Television acquisition system (see text)

unusually slow for an optical nova, but reminiscent of the only other securely identified transient x-ray source, namely A0620-00, for which $dB/dt \sim 0.015$ mag/day (Lloyd et al. 1977).

The optical radiation in such x-ray novae may arise from the x-ray emission region ($\sim 10^7$K). In the case of A0620-00 (B ~11.8 on 25 September 1975) the severely restricted x-ray line emission (Griffiths et al. 1976) implies a large electron scattering depth in the x-ray source and consequently substantially less optical output from the x-ray emission region than the optically thin case. Alternatively the optical radiation may arise from the heated photosphere of a non-degenerate companion star (assuming that the system is indeed a close binary). This is not contradicted by the different rates of decay of optical and x-ray intensities.* The slower decay of the optical light curve comes about from changes in the bolometric correction of the reprocessed x-radiation, a larger fraction of the re-processed energy leaving the system in the visible region as the x-ray nova fades.* Endal et al. (1976) have analysed the observed decay rates for A0620-00 and obtained a mean effective black-body temperature for the companion star's photosphere of 3.4×10^4 K, close to the value of 2.8×10^4 K derived from fitting the de-reddened UV spectrum (Wu et al. 1976). Whelan et al. (1977a) offer a plausible binary model of A0620-00 based on x-ray reflection. Though no x-ray line observations were obtained for A1524-61, the ratio F_{opt} to F_x and the respective decay rates, with the optical decay again being slower, suggest a very similar situation to A0620-00. Following the analysis of Endal et al., the rates of decay of A1524-61 shown in Fig. 4.8 (viz. e-folding times $\tau_x \sim 52d \pm 5$, $\tau_{opt} \sim 117d \pm 20$) yield a value of $T_{eff} \sim 2.7 \times 10^4$ K for the heated companion star in A1524-61. Although we have no optical spectra of A1524-61 to compare with A0620-00, the Hα plate taken 60 days after maximum with the SRC Schmidt was exposed through a 100Å band-

---

* See § 4.2.3 however.

pass interference filter. Clearly the nova spectrum did not have Hα strongly in emission at this time (less than about 70Å equivalent width). Hα in the spectrum of the optical counterpart of the x-ray nova A0620-00 never achieved this strength and was undetectable 60 days after maximum (Whelan et al. 1977a).

The similarity of the distance-independent x-ray characteristics of A1524-61 and A0620-00 (Table 4.3) have previously been taken (Pounds 1976) to indicate they are both in the same class of transients. All we know of the new optical identification of A1524-61 supports this view. The distance of the A1524-61 candidate star is difficult to estimate directly since no colour information for the star is available and the reddening is unknown. The nearby field in Circinus studied by Bok et al. (1972) shows a reddening of $E_{B-V} \sim 0.3$ to 0.5 magnitudes. Inspection of the SRC Schmidt plate containing the Circinus field and the field of the nova shows that the reddening is patchy, but the x-ray nova is in an area somewhat more obscured than the Circinus field. Star S however has a spectral type of early G (from an AAT spectrum taken with the Image Dissector Scanner). Thus its reddening is $E_{B-V} = 0.2$. The three fainter stars of the photoelectric sequence in the field of the nova are all redder than S($0.8 \leqslant B-V \leqslant 1.7$). In view of the foreground reddening $E_{B-V} \gtrsim 0.5$ is a rational guess for the nova. Hence the blue absorption is at least 2 magnitudes. Thus the ratio of optical fluxes near maximum of A0620-00 and A1524-61 (6 magnitudes or less) is consistent with the ratio of a factor of fifty between the x-ray fluxes of the two stars, although the evidence is not compelling.

If we assume that the ratio of x-ray to optical flux is the same in both A0620-00 and A1524-61 then the unabsorbed apparent blue magnitude of A1524-61 would be 14.0. Hence the blue absorption would be 3.5 mag., corresponding to a distance near the plane of the galaxy ($b = -3.^{\circ}8$) of about 3 Kpc.

TABLE 4.3

Comparison of A0620-00, A1524-61 and H1705-25

	A0620-00	A1524-61	H1705-25
X-ray flux (maximum)/I_{Crab}	50	1	3.5
X-ray flux ($\sim 12^d$ post maximum)/I_{Crab}	30	0.5	1.25
" " " /erg $cm^{-2}s^{-1}$	5×10^{-7} +	1×10^{-8}	2×10^{-8}
Apparent blue magnitude (12^d post-maximum) (m_B)	11.3	17.5	~16*
Absorption (A_B)/mag.	1.6	$\gtrsim 2$ (~ 3.5)	$\lesssim 4$
$m_B - A_B$ (de-reddened)	9.7	$\lesssim 15.5$ (~ 14)	$\gtrsim 12$
Optical flux/erg $cm^{-2}s^{-1}$ ++	8×10^{-10}	$\sim 1.6\times10^{-11}$	$\lesssim 1\times10^{-10}$
Ratio F_x/F_{opt}	600	~ 600	$\gtrsim 200$
X-ray decay time/days	27	52	~ 30-35
Optical decay time/days	69	117	-
Distance/Kpc	≈ 1	~ 3	~ 3
X-ray luminosity (maximum) erg s^{-1}	$\approx 1.2\times10^{38}$ +	~ 2×10^{37}	~ 8×10^{37}
Quiescent m_B	20.5	> 22	$\gtrsim 21$
Quiescent M_B	≈ 9	$\gtrsim 6$	$\gtrsim 4.5$

+ Energy band ~ 2-10 keV. (In the 0.3 - 10 keV band flux was ~ 1×10^{-6} erg. cm^{-2} s^{-1} and luminosity $\approx 3\times10^{38}$ erg s^{-1}).

* Estimated from $m_B = 16^m.5 \sim 30^d$ post-maximum (Griffiths et al. 1978).

++ Optical flux for A1524-61 and H1705-25 assumes colours similar to A0620-00 during outburst.

The faintness of the quiescent system ($m \gtrsim 22$) at this distance with 3.5 mag. absorption suggests that the primary star is a dwarf with absolute magnitude M_B fainter than + 6. Alternatively, if we assume that the peak 2 - 10 keV x-ray luminosity of the x-ray transients is the same, A1524-61 is seven times more distant than A0620-00, which is at least 1 Kpc away (Whelan et al. 1977a). With an absorption of 7 magnitudes and distance modulus of 14, the faintness of the quiescent system of A1524-61 places a limit of M_B fainter than + 1 on the primary star, again indicating it is a dwarf. Finally, assuming that the total energy in the outburst is 1.0×10^{45} ergs (Gallagher and Starrfield 1976), A1524-61 is at a distance of 5.5 Kpc, corresponding to a limit of M_B fainter than + 2 for the quiescent system, again consistent with the primary being a dwarf.

This is further evidence that A1524-61 and A0620-00 are in the same low mass binary class of galactic x-ray transients (see Chapter 1).

4.4 H1705-25 (Nova Ophiuchi 1977)

4.4.1 Introduction

The bright x-ray transient H1705-25 was discovered independently by the HEAO-1 Modulation Collimator (MC) (Griffiths et al. 1977, 8) and the Ariel V All Sky Monitor (ASM) (Kaluzienski and Holt 1977) at the beginning of 1977 September. The source first appeared in the Ariel V SSI data on August 8th and reached a peak intensity of $\sim$ 3.5 times that of the Crab Nebula by August 10th.*

On the basis of the small MC errorbox an associated optical nova (Nova Ophiuchi 1977) was discovered on plates taken at the Anglo-Australian Telescope and UK Schmidt Telescope (Longmore et al. 1977; Griffiths et al. 1978) thus making it the third successfully identified transient x-ray source.

---

* The presence of this transient in the Ariel V data was not immediately noticed, unfortunately, due to confusion with the strong galactic centre source GX9+9, and the weaker source 4U1709-23.

4.4.2 X-ray Observations

The source H1705-25 was in the field of view of the Ariel V SSI from 1977 July 31 to 1977 August 31. At the end of this observation a satellite spin axis manoeuvre took the source out of the field of view of the SSI (and into that of the ASM).

The data points plotted in Fig. 4.9 are single orbit SSI intensities in the 2 - 18 keV band corrected for both collimator response and exposure time. The error bars shown reflect both the statistical errors and the additional errors introduced through the collimator response factor uncertainties and the effects of source confusion. Also shown are the data from the HEAO-1 MC (Gursky et al. 1978) obtained from single pass "quick look" observations spanning 1977 September 7 to September 12 (energy band 1 - 13 keV). Because of the possibility of strong spectral evolution of this source (cf. A0620-00, section 4.2), we have made no attempt to convert to absolute units. Instead, all the intensities are shown relative to the Crab Nebula (= 1000 units) Unless the source spectrum is very soft (kT < 2 keV) the extra uncertainty introduced by not correcting for spectral changes should be less than 10%.

The light curve of H1705-25 clearly resembles that of a "classical" x-ray transient. It does however show several novel features, in particular the double-peaked maximum and rather irregular post-maximum decay.

The rise-time to maximum intensity (measured between 0.1 I_{max} and 0.9 I_{max}) is $\sim$1.7 days, somewhat faster than previous transients which have typical rise-times of 3 - 7 days (Pounds, 1976). The short pause (at $\sim$ 0.7 I_{max}) in the rise to maximum intensity (near MJD 43364.2) may be a precursor similar to those seen in A0620-00 (at $\sim$ 0.1 I_{max}; Elvis et al. 1975 and section 4.2) and A1524-61 (at $\sim$ 0.5 I_{max}; Kaluzienski et al. 1975 and section 4.3).

The post-maximum evolution of the light curve is characterised by an initial sharp drop in intensity in $\sim$ 0.7 days, a rise to secondary maximum on the same timescale, a further fast drop to $\sim$ 0.5 I_{max} in 0.8 days, and

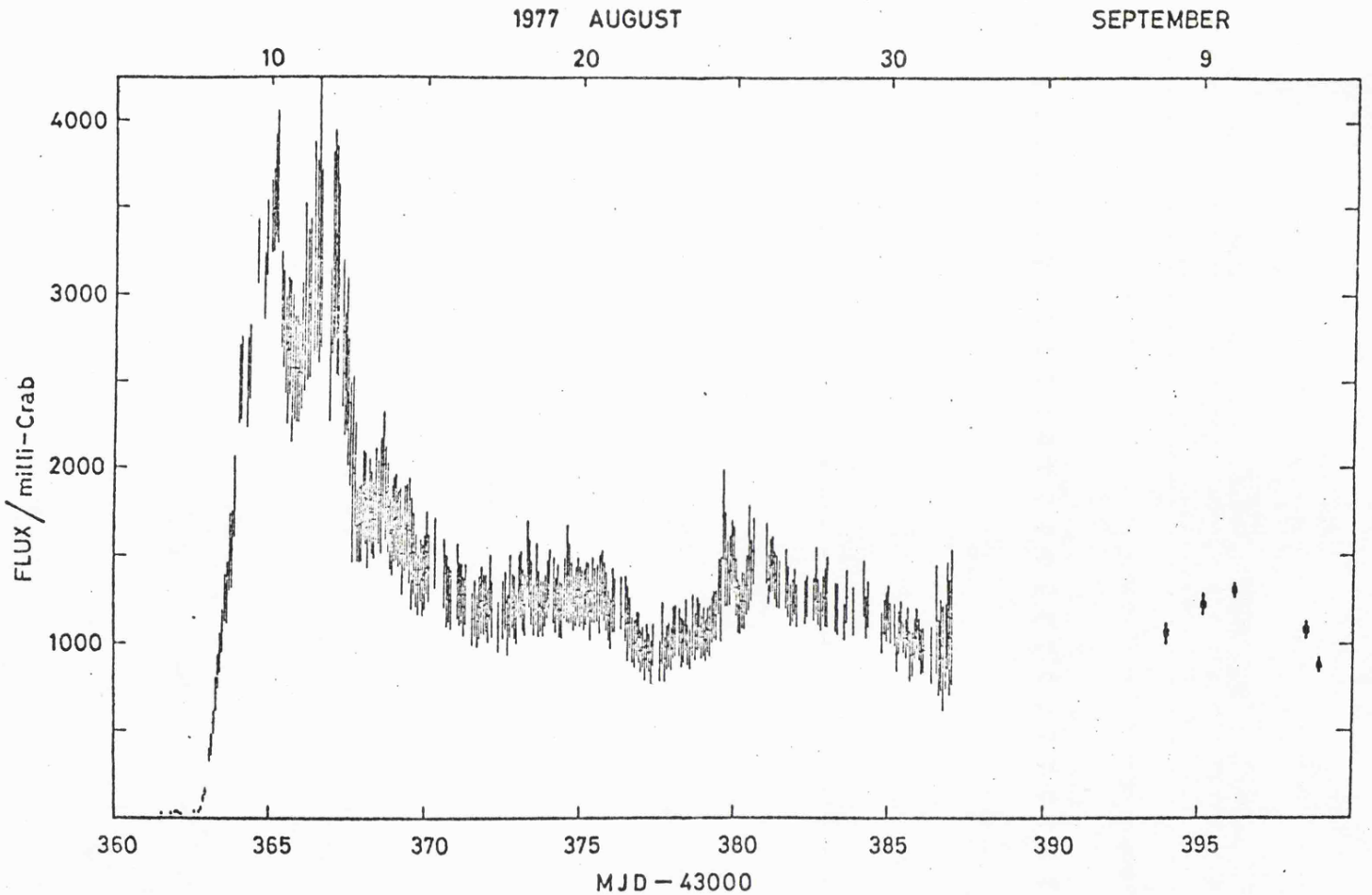

Fig. 4.9 The x-ray light curve of H1705-25 (Nova Ophiuchi 1977). All vertical error bars are $\pm 1\sigma$ where shown. Horizontal bars indicate the length of each observation. Data are from: SSI (~ 2 - 18 keV) ┼
HEAO-1 MC (~ 1.5 - 15 keV) ┼

then a slow irregular decline with intensity reaching $\sim 0.06\ I_{max}$ about $2\frac{1}{2}$ months after the secondary maximum (Kaluzienski, L.J., private communication 1978). The complicated structure of the post-maximum light curve appears to be unique among the x-ray transients which have been extensively observed. The timescale for the slow decay is difficult to determine because of the variability of the source. Immediately after the fast drop to $0.5\ I_{max}$ the decay is very slow and arguably not exponential in form. The data after MJD 43380 show a smoother decay, and when combined with the ASM observations from MJD 43390 - 43455 (Kaluzienski, L.J., private communication 1978) can be fitted with an exponential decay with an e-folding timescale of 30 - 35 days, comparable with that of other well-studied transients.

We have investigated the possibility that the post-maximum variability of H1705-25 might be periodic by folding the SSI data (with a least-squares-fit linear trend subtracted) modulo a range of trial periods between 0.5 and 20 days and examining the behaviour of the χ^2 value with folding period, where the χ^2 value is the χ^2 deviation of the data from the hypothesis that the source is constant. A broad peak appears in the χ^2 vs. period plot centred on a period of 6.7 days. Examination of the light curve does not, however, show a clear modulation at or near this period, particularly when the HEAO-1 MC and ASM observations are taken into account. The power spectrum of the SSI post-maximum data, obtained using the Cooley-Tukey algorithm, shows no significant peaks. We interpret this as implying that there is no regular periodicity in the light curve. No regular modulation is apparent in the ASM data either for periods in the range 1 - 20 days (Kaluzienski, L.J., 1978, private communication). The variability evident in the light curve which gives rise to the apparent modulation at ~ 6.7 days may be similar to the ~ 8 day 'period' reported in both x-ray and optical observations of A0620-00 (see section 4.2.3) and may reflect some characteristic timescale within the

system (for example within the accretion disc) rather than the orbital motion of the x-ray source.

The x-ray spectrum of H1705-25 was measured by the HEAO-1 MC on two quick-look orbits giving a bremsstrahlung temperature kT = 3 ± 0.5 keV, with a column density N_H = (3 ± 1) x 10^{21} H atoms cm^{-2} (Griffiths et al. 1978).

4.4.3 Optical Counterpart

The optical counterpart of H1705-25, Nova Ophiuchi 1977, was identified on plates taken at the AAT and UK Schmidt Telescope on 1977 September 10-11 within one of the small errorboxes determined by the HEAO-1 MC (Griffiths et al. 1978). On the discovery plate the nova had B = $16^m.5$ ± 0.5 compared with an estimated quiescent magnitude of B ~ 21^m on the POSS plates. The spectra of the nova obtained on September 16 and 22 show a continuum with no absorption lines, but clear evidence for λ4686 HeII emission on both nights as is seen in V616 Mon. The colours of the nova, estimated from the continuum, were B-V = 0.64 (Sept.16) and B-V = 0.86 (Sept.22).

On the basis of this preliminary optical work no distance estimate is possible. The x-ray low energy absorption column density, however, implies $A_V \sim 1^m.4 \pm 0.5$ (Griffiths et al. 1978). If the intrinsic colours of Nova Oph 1977 were similar to those of V616 Mon at about the same time after maximum (i.e. a hot black-body) an independent estimate of $E_{B-V} \lesssim 1$ can be made, giving $A_V \lesssim 3^m.3$ (Griffiths et al. 1978). This implies a distance of very approximately 3 Kpc (inherent uncertainties are large). At this distance H1705-25 has a peak x-ray luminosity similar to that of Mon. X-1 (see Table 4.3).

4.4.4 Discussion

Despite some detailed differences in the light curve structure, H1705-25 shows many similarities with both A0620-00 and A1524-61 (see summary in Table

4.3) both in terms of x-ray behaviour and the optical properties of the counterpart. Further optical observations of Nova Oph 1977 will hopefully confirm the similarity with V616 Mon, especially if the emission line spectrum develops as the star fades. It would also be interesting to obtain the photometric light curve in order to obtain the decay timescale, since for both A0620-00 and A1524-61 this is ~ 2 times longer than the corresponding value for the x-ray flux.

By analogy with A0620-00 we expect that at quiescence the optical star will be a late-type dwarf. If the distance and reddening estimates can be relied on, the quiescent apparent magnitude $m_B \sim 21^m$ gives $M_B \gtrsim 4^m.5$ which is certainly consistent with this hypothesis.

4.5 2A0042+323

4.5.1 Introduction

The majority of galactic sources lie at low galactic latitudes as is expected if they lie in the galactic disc with typical distance > 1 Kpc. Conversely those sources at high galactic latitudes show an approximately isotropic distribution (Cooke et al. 1978) and are predominantly identified with extragalactic objects (e.g. clusters of galaxies, active galaxies, etc. - see review by Pounds, 1978). The high latitude population is however significantly contaminated by distant galactic halo sources (e.g. Sco X-1, Her X-1) and by nearby, low-luminosity galactic sources (e.g. AM Her = 2A1815+500, Ex Hya = 2A1251-290). Thus for a few of the weak high latitude sources identification with a galactic object can be expected. Observations of dramatic variability in particular may indicate a galactic nature, although flaring behaviour is also a feature of active galaxy sources (Pounds, 1978 and references therein).

During 1977 February the faint x-ray source 3U0042+32 was observed to flare up over several days to $\sim$ ten times its nominal Uhuru strength

(Ricketts and Cooke, 1977). The new observation, made with the Ariel V Sky Survey Instrument (SSI), stimulated the determination of a more precise location of the source by the rotation modulation collimator on the SAS-3 satellite. This improved 'errorbox' with 90% confidence radius 1 arcmin (Rappaport et al. 1977), lies within the overlap of the Ariel V and Uhuru positions (Cooke, et al. 1978 ; Forman et al. 1978).

Following an optical search of the region near the x-ray source (now 2A0042+323 or 4U0042+32), Charles et al. (1977 , 1978) have proposed its identification with a 19^m G dwarf which shows possible variable λ 4686 HeII emission, a characteristic signature of several x-ray binaries (McClintock et al.1975). Support for this identification, and evidence for the possible binary nature of 2A0042+323 is discussed here on the basis of a more extended study with the SSI.

4.5.2 Ariel V Observations

Figure 4.10 shows the light curve of 2A0042+323 obtained from the SSI observations spanning 1977 Feb.2 - April 1. Each data point is the sum of several satellite orbits, typically $\frac{1}{2}$ day, although longer sums are shown for those periods when the source was weak. The gaps in the light curve are due to spin-axis manoeuvres of the satellite which took the source out of the field of view. Three flaring episodes are evident, with evidence for a fourth (defined by only two points) near the time of the SAS-3 observations. We have investigated the possibility that this behaviour is periodic by folding the data modulo a range of trial periods. The maximum χ^2 deviation from the hypothesis of source constancy occurs for the data folded at period of 11.6 days. The peak in the χ^2 versus period plot is broad and we estimate an error of $\pm$ 0.7 day in the χ^2 max period. Two cycles of the data folded at 11.6 days are shown in Fig. 4.11.

Because of the patchiness and limited extent of the observations, one must be cautious in ascribing a strictly period modulation to the structure

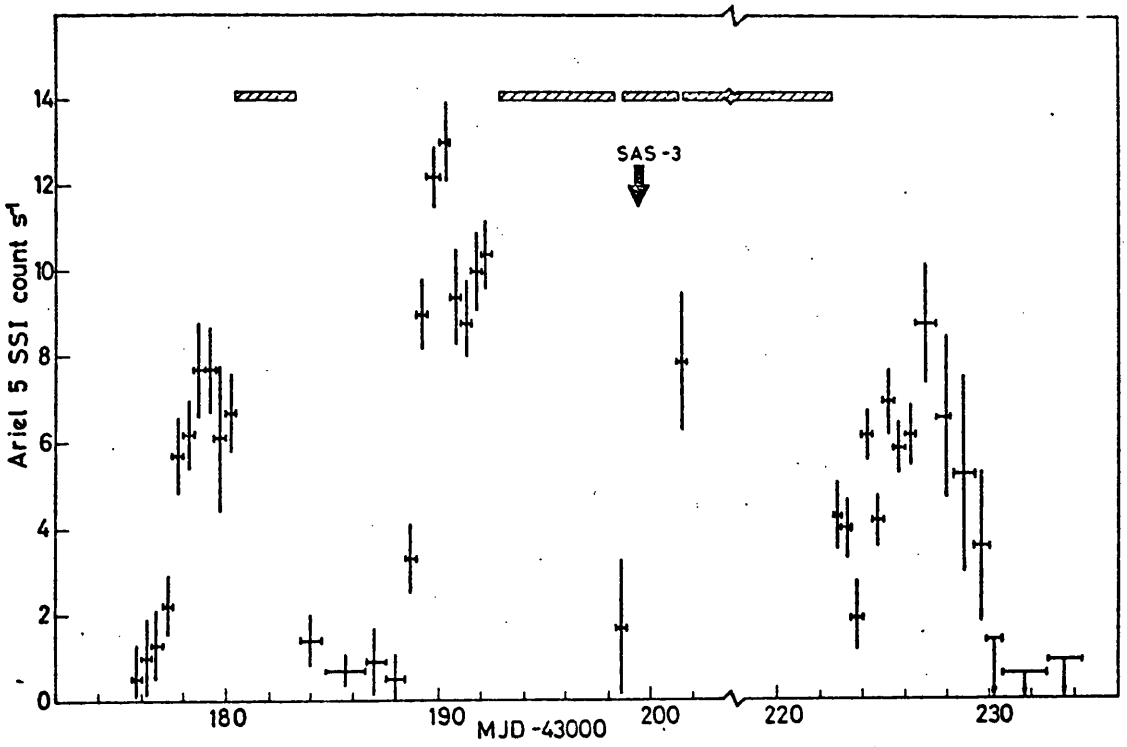

Fig. 4.10 SSI light curve of 2A0042+323 based on observations made between 1977 Feb 2 and Apr 1. Each data point is (typically) a $\frac{1}{2}$ day average (duration shown by horizontal bars) plotted with $\pm 1\sigma$ error bars. Upper limits are 3σ . The shaded bars indicate times when source was out of the field of view and the bold arrow indicates the time only of the SAS-3 observation (intensity was not quoted).

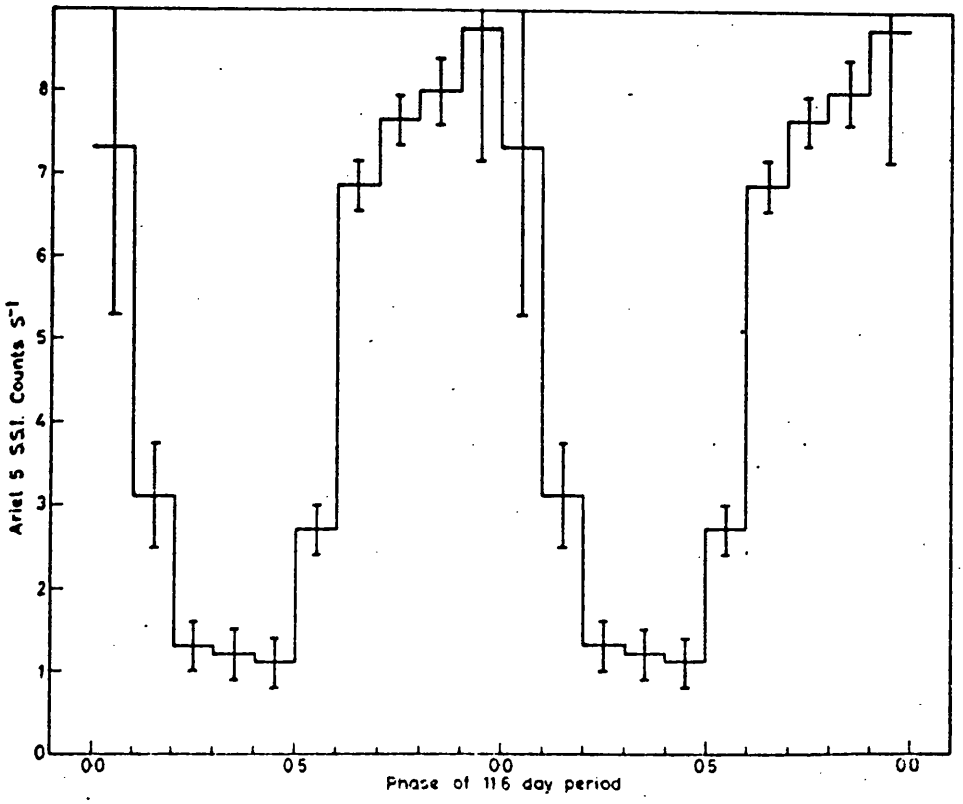

Fig. 4.11 Two cycles of the 2A0042+323 observations folded at a period of 11.6 days with $\pm 1\sigma$ error bars (phase zero is arbitrary).

of the light curve. This must await observational confirmation. Nevertheless, the apparent periodicity does have some interesting consequences.

4.5.3 Discussion

First, we consider the consequences of the strong and apparently periodic x-ray modulation being due to the regular eclipse of the x-ray source by a non-degenerate stellar companion. In this case the eclipse duration, estimated from the folded data shown in Fig. 4.11, would be $\gtrsim 2.3$ days, equivalent to an eclipse semi-angle $\theta_e \gtrsim 36^\circ$. This lower limit must be somewhat uncertain due to the range of possible periods. By analogy with known x-ray binaries such as Vel X-1, which has a similar period and eclipse duration (Watson and Griffiths 1977), we might expect such a long eclipse to involve a supergiant primary in the binary system.

However, the optical field in and near the SAS-3 errorbox contains no early-type stars (Charles et al. 1978), and at this galactic latitude ($b \approx -30^\circ$), with small reddening ($E_{B-V} \lesssim 0.2$), an early-type supergiant would have to be $\gtrsim 50$ Kpc distant if it were the brightest star in the field. Even if the counterpart were a late-type giant its distance would still have to be $\gtrsim 10$ Kpc.

In fact, if we require the source to lie within the galactic halo ($d < 10$ Kpc), then the candidate proposed by Charles et al. must have $M_v \gtrsim 4^m$, consistent with it being a G dwarf as implied by their spectrophotometry (Allen 1973). If this is correct then the modulation cannot, for any reasonable values of the binary system parameters, be due to eclipse. This follows since the Roche-lobe size of the primary (optical) star, which we regard as giving the maximum occulting radius, is far too small to give the length of eclipse observed unless $(\frac{M_p}{M_x}) \gtrsim 7$ (using the Roche-lobe radius approximation given by Paczynski (1971)). For the low-mass primary suggested by the optical observations ($M_p \sim 1\ M_\odot$) this condition can only be satisfied by an extremely low-mass x-ray object ($M_x \lesssim 0.15\ M_\odot$), which is probably below

the lower limit for a neutron star (Weinberg 1972). The presence of a dense, absorbing region near the x-ray object, such as suggested for Cen X-3 (Hatchett and McCray 1977), can of course give an arbitrarily large 'eclipse' even for a low-mass binary.

In summary, whilst the optical and x-ray data point strongly to 2A0042+323 being a low-mass binary system, it appears unlikely that it is eclipsing. If this is so then the observed modulation may still reflect the binary period of the system. One possibility is that the orbit is elliptical, giving rise to strongly varying emission as the binary separation changes. A simple model involving an elliptical orbit and stellar wind powered accretion has been discussed by Avni et al. (1976). Following their analysis we find that the shape of the light curve could be produced with an orbital eccentricity of 0.5 - 0.6. We also note the similarity between 2A0042+323 and Cyg X-2, which is probably a low-mass binary (Crampton and Cowley 1976). Their optical counterparts are both late dwarfs and an, as yet unexplained, 11.2 day periodicity has been reported in the x-ray light curve of Cyg X-2 (Holt et al. 1976b), although the amplitude of this modulation is $\sim$ 10 times smaller than that for 2A0042+323.

Alternatively it might be that the quasi-periodic behaviour of 2A0042+323 is related to recurrent flaring phenomena seen in sources like Aql X-1 (§ 4.6) and 4U1630-47 (Jones et al.1976). In this case the origin of the outbursts might lie in periodic instabilities in the mass transfer rate from the G dwarf to the compact object, possibly similar to the situation in dwarf nova systems.

4.6 4U1908+00 = Aql X-1

4.6.1 Introduction

Aql X-1 displays x-ray behaviour which is intermediate between that of the transient and steady varieties of galactic x-ray source. Although listed in the 3U catalogue (Giacconi et al. 1974) as being variable by a factor of 3,

x-ray observations over the last few years have shown that Aql X-1 has transient-like outbursts lasting ~ months which recur at intervals of 1 - 2 years (Kaluzienski et al. 1977 , Buff et al.1977 , see Fig. 4.12). Between outbursts the source varies between undetectability (< 0.001 I_{Crab}) and a level of ~ 0.02 I_{Crab}. The x-ray spectrum of Aql X-1 is characterised by a low bremsstrahlung temperature (kT < 7 keV, Jones 1977) and to date no evidence has been found for an x-ray pulsation period (Buff et al. 1977).

The optical identification of Aql X-1 has recently been established. The counterpart is a 19^m K dwarf which shows optical flares by 3 - 4 magnitudes at times coincident with the x-ray outbursts (Thorstensen et al. 1978 ; Walter et al. 1978). The optical light curve is shown in Fig. 4.12 including recent observations reported in IAU Circulars. It is interesting to note that an optical outburst occurred in 1974 May, when no x-ray observations were available. The interval between this outburst and the subsequent one is consistent with the mean recurrence period (Thorstensen et al. 1978).

At quiescence the optical counterpart shows the normal spectrum and colours of G7 - K3 dwarf with modest interstellar absorption (E_{B-V} ~ 0.3 - 0.5, Thorstensen et al. 1978). Distance estimates based on the reddening give d = 1.7 - 4 Kpc (Thorstensen et al.1978 , Margon et al. 1978). Note that the maximum x-ray luminosity at this distance is well below the Eddington luminosity for a 1 $M_\odot$ object.

During outburst the counterpart is 3 - 4 magnitudes brighter than in quiescence and significantly bluer (B-V ~ 0.7, as opposed to B-V ~ 1.3, Margon et al. 1978 , Vrba 1978). Optical flickering has also been reported during the 1978 outburst (Vrba 1978). The outburst spectrum shows $\lambda\lambda$4340-50 CIII/NIII and λ4686 HeII emission lines which may be due to x-ray heating (Puetter and Smith 1978, Mook 1978).

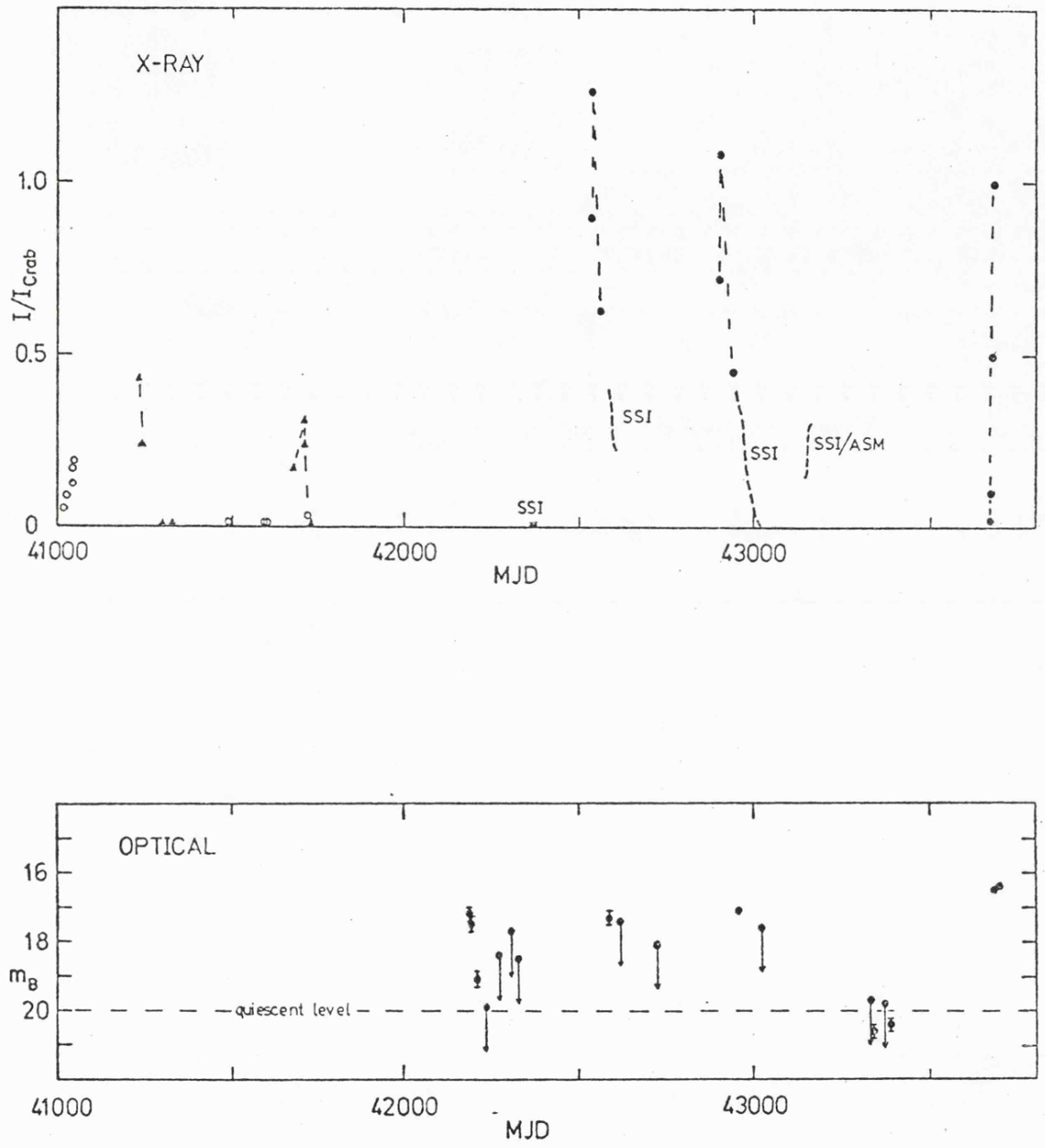

Fig. 4.12 (a) Composite x-ray light curve for Aql X-1 between 1971 and 1978. Data are from:

O - Uhuru (Cominsky et al. 1978)

▲ - OSO-7 (shown in Cominsky et al. 1978)

● - ASM (Kaluzienski et al.1977 and IAU Circ.No.3235)

Dashed lines labelled SSI indicate trend of SSI observations (reported here).

(b) Composite optical light curve for Aql X-1 between 1971 and 1978 based on Thorstensen et al. (1978) with additional points from IAU Circ., No.3243.

4.6.2 SSI Observations

Observations of Aql X-1 were made during the outbursts of 1975 and 1976 (outbursts I and II in what follows - see Fig. 4.12). These are the only unambiguous detections of Aql X-1 by the SSI above a level of $\sim 0.01\ I_{Crab}$ from launch to 1978, except for those made during the rise of the small outburst in 1977 January (reported in IAU Circular 3031). These latter observations are of limited value due to source confusion.

Fig. 4.13 shows the SSI light curve of the observations made between 1975 June 30 and July 9, approximately 25 days after x-ray maximum (the outburst was also monitored by the Ariel V ASM and SAS-3, Kaluzienski et al. 1977, Buff et al. 1977). Superimposed on the quasilinear decline in intensity from ~170 to ~50 count s^{-1} is an obvious modulation. To test for the significance of this modulation and search for possible periodicities, the data were subjected to both χ^2 and power spectrum analysis.

Fig. 4.14 shows the variation of χ^2 with folding period. The χ^2 value plotted is deviation from source constancy for the data folded into 5 phase bins, with the linear trend removed before folding. A prominent peak occurs at a period of 1.3 days with an amplitude far larger than that obtained for simulated data with identical intensity and variance (see Fig. 4.14). Four minima consistent with this period can be seen in the light curve between MJD 42594 and 42599 (Fig. 4.13). Also shown in Fig. 4.14 is the power spectrum of the data calculated using the Maximum Entropy Method. The most significant peak occurs at a frequency corresponding to a period of 1.28 days, consistent with the period obtained from the χ^2 analysis of $P = 1.30 \pm 0.04$ days. The amplitude of the modulation at this period is ~10% of the mean flux.

Kaluzienski et al. (1977) have analysed the ASM observations of Aql X-1 made during the same outburst (their observations do not include the period of SSI monitoring since the ASM and SSI fields of view are mutually exclusive).

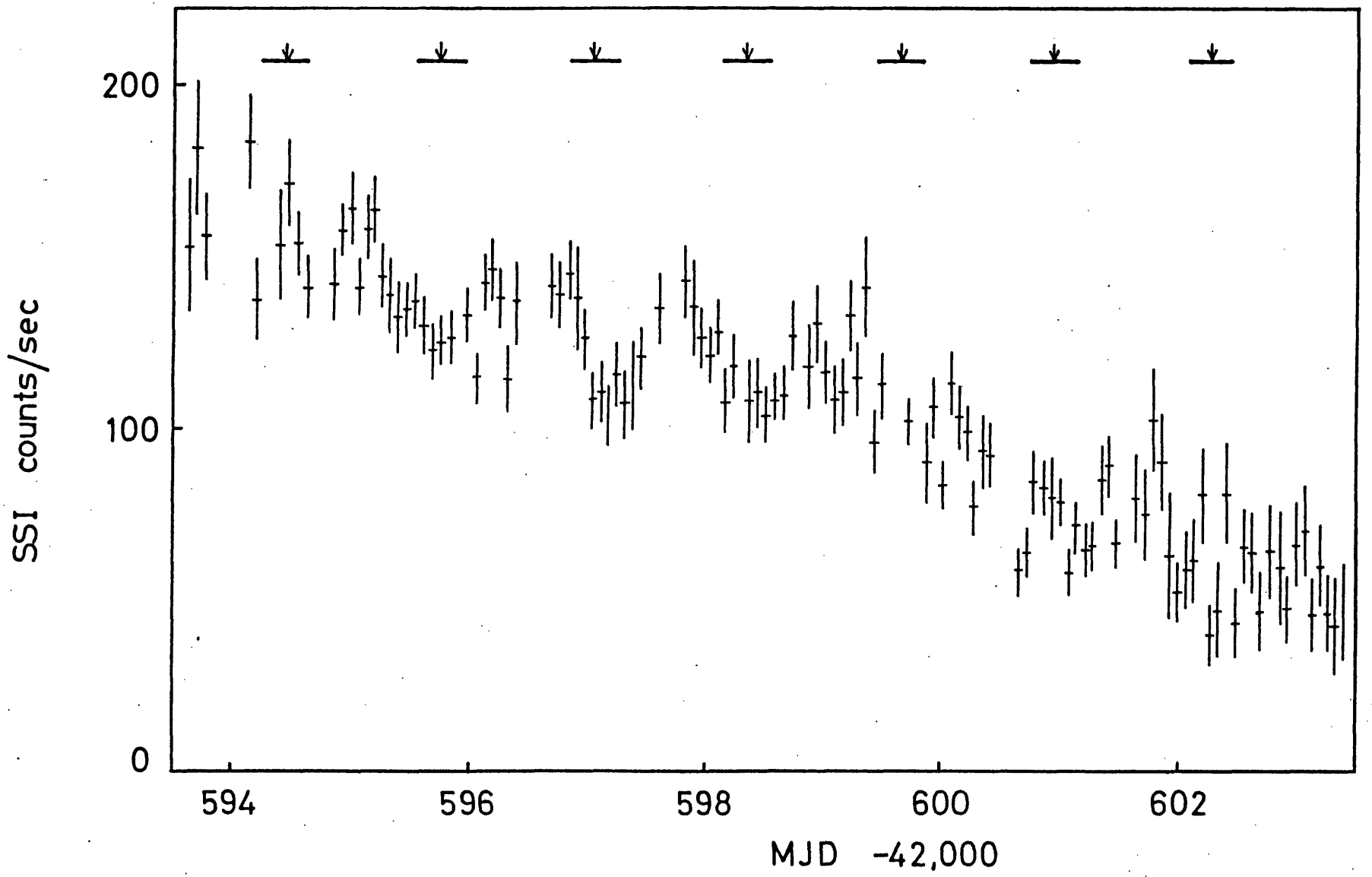

Fig. 4.13 SSI light curve of Aql X-1 between 1975 June 30 and July 9 (outburst I). The arrows indicate the predicted minima of the 1.3 day modulation, error bars are $\pm 1\sigma$.

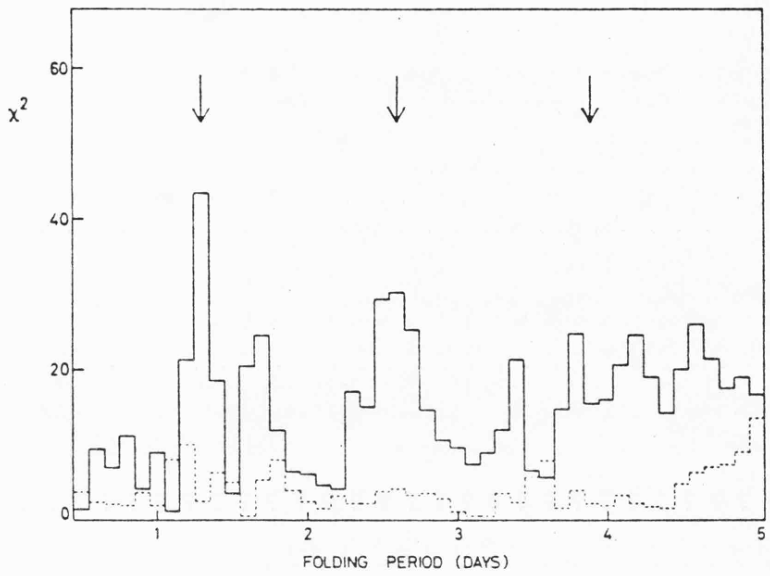

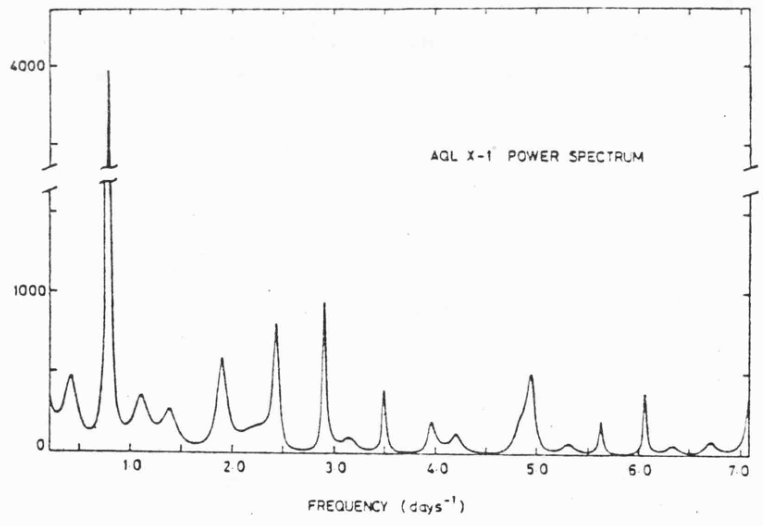

Fig. 4.14 (a) The variation of χ^2 with folding period for the Aql X-1 observations shown in Fig. 4.13 (folded into 5 bins, linear trend removed). The dashed line represents the variation obtained from simulated data with no periodic modulation (see text).
(b) Power spectrum of the Aql X-1 data. Power in arbitrary units.

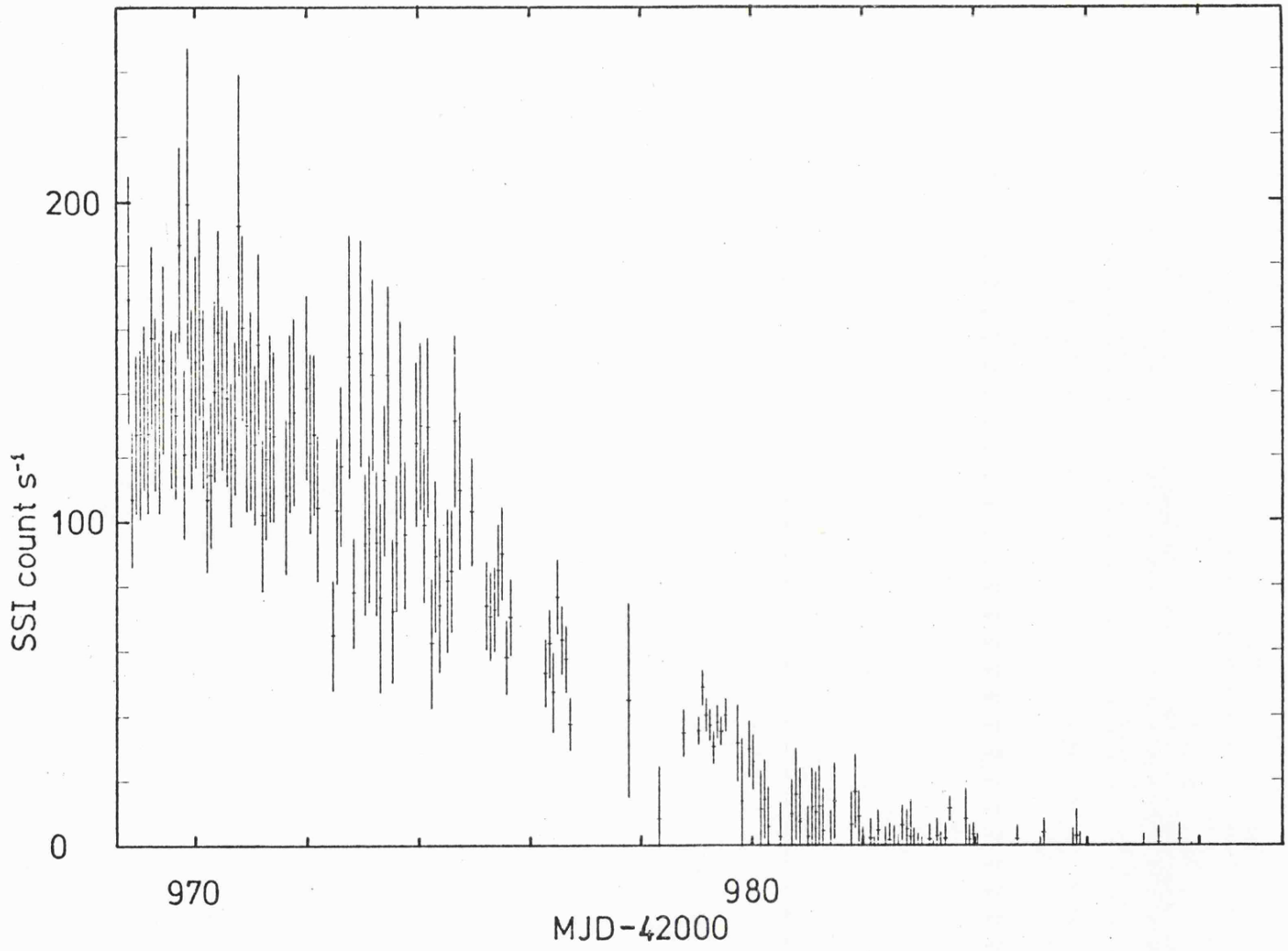

Fig. 4.15 SSI light curve of Aql X-1 between 1976 July 10 and July 30 (outburst II), error bars are $\pm 1\sigma$.

They find marginal evidence for modulation at a period of ~ 1.3 days, with an amplitude of only 3% of the mean flux. The modulation is however in phase with that seen by the SSI, and combining the ASM and SSI data yields a marginally improved period of $P = 1.28 \pm 0.02$ days.

Fig. 4.15 shows the SSI light curve of observations made during outburst II between 1976 Jul 10 and Jul 30, coincidentally at about the same stage of the decay from x-ray maximum (~ 24 days post-maximum). The light curve is much noisier than that obtained for outburst I because the source elevation is greater than 6° for most of the observation. The decay appears to be approximately linear (rather than exponential) with the source intensity falling below detectability around MJD 42982 and staying undetectable until the end of the observation (MJD 42990). Although no obvious modulation is apparent in this observation, the data* have been analysed in an identical manner to that obtained in outburst I. No significant periodicities are found in the data, and the modulation at 1.3 days has an amplitude of $< 5\%$ of the mean intensity. This negative result is perhaps not surprising, since the data is so noisy. A similar analysis of the data summed in 5-orbit bins (~ 0.3 days) to improve the signal-to-noise yielded similar results.

The Ariel V ASM also obtained observations of Aql X-1 during outburst II. The analysis of the ASM data yielded no significant modulation at or near a period of 1.3 days with an upper limit of 2% amplitude (Kaluzienski et al. 1977). Since the amplitude of the modulation at 1.3 days seen by the ASM in outburst I was $\sim 1/3$ of that seen by the SSI, this upper limit is probably consistent with the SSI result.

3.6.3 Discussion

The suggested 1.3 day period persists clearly for three or four cycles in outburst I, but is absent at the same amplitude during outburst II. If it

---

* Excluding data from MJD 42982-990 when source was undetectable.

is real this period is most easily interpreted as being due to modulation of the x-ray flux in a binary system, for example by partial obscuration of the x-ray source by absorbing matter giving the approximately sinusoidal variation. The identification of Aql X-1 with a late-type dwarf implies that a low-mass binary model of the sort discussed in Chapter 1 might be appropriate. A binary period of 1.3 days would certainly be consistent with a semi-detached system of this type (e.g. Avni et al. 1976).

The outburst behaviour is clearly similar to that of the transients discussed earlier, particularly in terms of the outburst profile. The occasional detection of Aql X-1 at a few percent of its peak flux between outbursts is not however a feature of transient sources. On the other hand the repetitive flaring at x-ray and optical wavelengths is reminiscent of the optical behaviour of dwarf novae. The mean recurrence period for outbursts in Aql X-1 is ~ 400 days*, similar to the periods of the dwarf novae EX Hya (465^d) and SW UMa (459^d) (Warner 1976). Note however that the quiescent spectrum of Aql X-1 does not show emission lines, these being found at all times in dwarf novae (Margon et al. 1978).

At maximum the ratio of x-ray to optical luminosity for Aql X-1 is ~ 500 (falling to ~ 20 at quiescence). As pointed out by Margon et al.(1978) it is difficult to reconcile this ratio with a semi-detached, low-mass model for this system comparable with a dwarf nova, since x-ray heating effects in such a close system should give a much larger optical luminosity (and hence smaller ratio). One solution to this problem is to assume that the x-ray emission is highly anisotropic (e.g. due to a large accretion disc), or alternatively to abandon the assumption that the system is semi-detached (thus raising the question of the mode of mass transfer) (see § 4.7).

---

* Kaluzienski (1977) quotes a mean recurrence period of 435 days ($\pm$ 10%). An unbiassed mean of all the outbursts seen in Fig. 4.12 gives however P = 376 $\pm$ 134 days (40%!). However, the intervals between the most intense outbursts seen in Aql X-1 ($I_{max} \gtrsim I_{Crab}$ or $m_v \lesssim 17^m.5$) are ~ 380, 377 and 734 days. An additional outburst near MJD 43310 which would fill the 734^d gap (giving 2 $\sim$370 day intervals) cannot be ruled out from the SSI data. Indeed there is evidence (badly affected by source confusion) that Aql X-1 was brighter than 0.15 I_{Crab} near MJD 43306.

4.7 Models for Transient Sources

A variety of models have been proposed to account for the behaviour of transient and transient-like sources. Here we briefly discuss some of the mechanisms which have been suggested to explain the transient outbursts. In each case it is assumed that the source is in a binary system containing a compact object by analogy with "steady" galactic sources. (Note that models which do not involve a binary system have been proposed, e.g. the "colliding shells" hypothesis, Brecher and Morrison 1976).

(a) Eccentric orbit binary

In this model the transient outbursts are hypothesised to be due to large changes in the accretion rate as a result of the varying stellar separation in an eccentric binary system. A simple model of this kind has been discussed by Avni et al. (1976) for stellar wind powered accretion. To explain the small duty cycle for x-ray emission from transients they find that large eccentricities ($\sim$ 0.9) are required for most transients, and that $\epsilon > 0.99$ is required for A0620-00. Since most x-ray binaries have circular orbits (within the errors, with the exception of 4U0115+63 which has $\epsilon = 0.24$), the implied bimodal distribution or orbital eccentricities makes this model implausible for most transients.

For "recurrent transients" however such as 4U1630-47 and Aql X-1 the eccentricities required are not as extreme and several authors have suggested eccentric orbit models for these sources. For Aql X-1 the lack of a stable period between outbursts makes this explanation unlikely, but for 4U1630-47, for which a regular outburst period of 615 $\pm$ 5 days has been proposed (Forman et al. 1976), this model remains a possibility. Note that the "recurrent transient" 4U0115+63, which does have an appreciable orbital eccentricity, has a recurrence period an order of magnitude longer than its orbital period of 24 days.

(b) Variable companion stars

Variable mass-loss is a feature of several types of relatively normal stellar objects. Some of the best known examples are cataclysmic variables, in particular dwarf novae, which show quasi-regular outbursts in optical light which are probably due to changes in the mass transfer rate; long-period variables (e.g. Mira variables) which have semi-regularly expanding atmospheres, and a variety of early-type stars with variable stellar winds. In the context of type I transients, which are suspected to be low-mass systems, only the dwarf nova variability is likely to be of relevance.

Transient models based on dwarf nova type systems have been proposed by a number of authors (e.g. Avni et al. 1976 ; Endal et al. 1976 for A0620-00). The system envisaged consists of a late-type main sequence (or slightly evolved) star in a close binary with a neutron star (or black hole). The nondegenerate star fills its Roche-lobe and loses mass by lobe overflow resulting in the formation of an accretion disc around the compact object. In such a system large changes in the mass-loss rate will lead directly to corresponding changes in the x-ray and optical emission provided the accretion flow is stable. The causes of the episodic mass-loss rate changes which give the quasi-periodic outbursts in ordinary dwarf novae are not well understood (Bath, 1977), but by analogy it is expected that similar variability might exist in an "x-ray dwarf nova" (i.e. one containing a neutron star instead of a white dwarf).

Although this model is extremely attractive and can be used to construct more detailed scenarios for individual sources, its applicability to at least two sources, A0620-00 and Aql X-1, has been questioned on the basis of arguments concerning x-ray heating. X-ray heating is expected to be important when (Bahcall 1978):

$$L_h \gtrsim L_o \qquad (4.1)$$

where $$L_h \approx \propto (\frac{\Omega}{4\pi})\, L_x \quad ; \quad \Omega \approx (\frac{\pi R_p^2}{a^2}) \qquad (4.2)$$

R_p is the nondegenerate stellar radius, a the orbital separation, L_h, L_o are the heating and intrinsic optical luminosities of the star and L_x is the x-ray luminosity, and α is an albedo factor ($\alpha \sim 0.5$). For an "x-ray dwarf nova" with $M_p \approx M_x \approx 1\ M_\odot$, and the nondegenerate star filling its Roche-lobe, $(\frac{\Omega}{4\pi}) \sim 0.04$ giving $L_h \sim 0.02\ L_x$. Thus for the <u>total</u> optical luminosity L_{opt} ($\geqslant L_h$ by definition) we have:

$$\frac{L_x}{L_{opt}} \lesssim 50 \qquad (4.3)$$

For both A0620-00 and Aql X-1 observations made during outburst give values of L_x/L_{opt} an order of magnitude larger than this, indicating that x-ray heating effects are not significant. Possible solutions to this problem are: (i) the binary separation is rather larger than assumed (making it difficult for a low-mass star to fill its Roche-lobe); (ii) the non-degenerate star does not fill its Roche-lobe; (iii) the nondegenerate star is only partially illuminated by x-rays (e.g. due to obscuration by a thick accretion disc). Note that only the third possibility allows us to retain the "x-ray dwarf nova" model. The first and second suggestions also raise the question of the mode of mass transfer, although the possibility of self-excited winds in low-mass binaries has been discussed (e.g. Oke 1977).

(c) <u>Other possibilities</u>

A variety of other mechanisms have been suggested including both physical and purely geometrical effects. Under the heading of physical mechanisms are included accretion disc instabilities, nuclear burning models and <u>decreases</u> in a supercritical accretion rate. The main geometrical effect which has been considered is a modulation analogous to that which gives the 35 day cycle in Her X-1 (precession of the accretion disc?). The last possibility would of course only be appropriate for sources which had approximately periodic

outbursts. Although some of these other possibilities may be the appropriate mechanisms for some individual sources, the most attractive model for low-mass, type I transients and related sources remains the "x-ray dwarf nova". Further observational and theoretical work will hopefully clarify some of the contradictions apparent with the simple version of this model.

Chapter 5

C O N C L U S I O N

5.1 Introduction

The observational data presented in Chapters 4 and 5 have all been plausibly discussed in terms of models involving accreting compact objects (neutron stars or black holes) within close binary systems, the variety of behaviour being explained by detailed differences in the accretion processes taking place. All the evidence, both direct and indirect, argues that such models are an essentially correct description of these sources, and that by analogy a large proportion of the known galactic sources which show similar observational properties will also turn out to be binary systems of broadly similar type.

Nevertheless it would be surprising if all galactic x-ray emitters were "standard" x-ray binaries, indeed a few examples of rather different classes of x-ray source are already known and have been briefly mentioned in Chapter 1. In this last chapter we briefly discuss two classes of galactic source which are particularly relevant to this theme: the "galactic bulge" sources for which observational evidence of binary membership (or otherwise) has proved singularly elusive, and x-ray emitting dwarf novae which are a good example of a rather different type of accreting binary system.

5.2 The "galactic bulge" Sources

It has been recognised for several years that a large fraction of the total galactic x-ray emission comes from a small number of bright sources at low galactic latitudes with a marked concentration in the direction of the galactic centre. In fact, of the ~ 150 sources in the 4U catalogue (Forman et al.1978) with $|b| \lesssim 15^{\circ}$, 24 of the 33 brightest sources ($I_{max} \gtrsim$ 100 U.F.U.) lie within 40° of the galactic centre (see Fig. 5.1). A subset

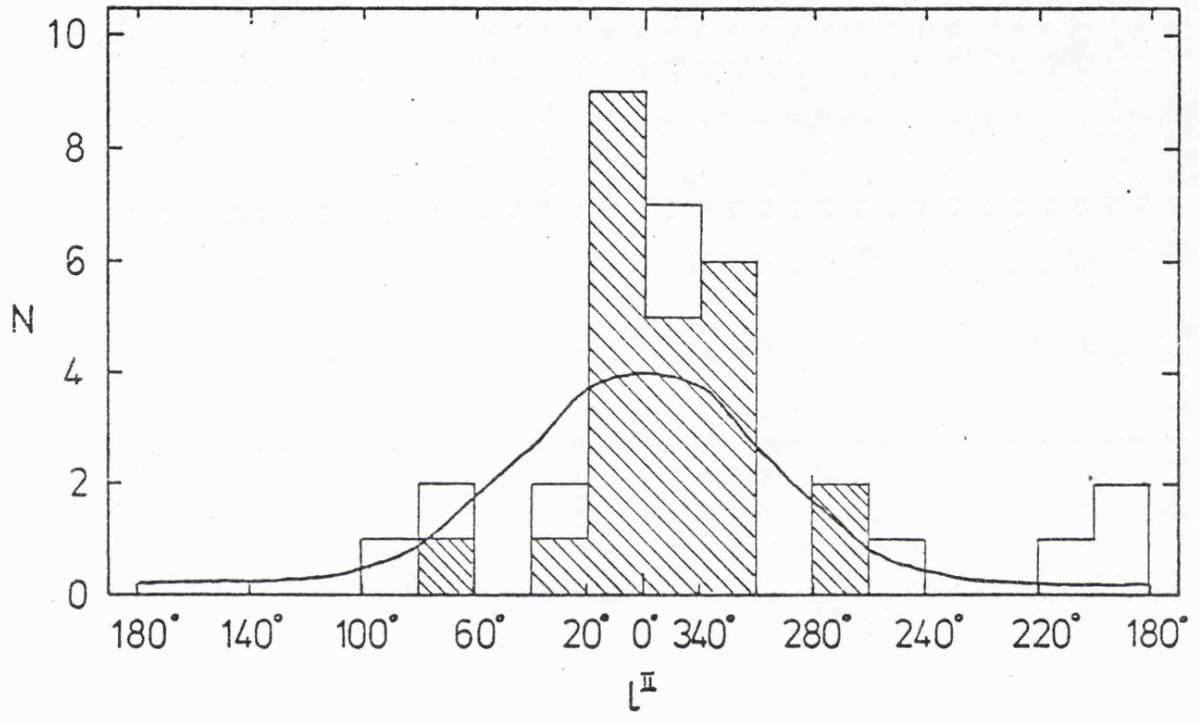

Fig. 5.1 Longitudinal distribution for all 4U catalogue sources with $|b| \lesssim 15^{o}$ and $I_{max} \gtrsim 100$ U.F.U. Unshaded parts of the histogram correspond to identified sources with $d \lesssim 5$ Kpc. The solid curve is the distribution expected for a uniform disc distribution of sources with radius 15 Kpc centred 10 Kpc from the sun.

of these bright sources are commonly known as the "galactic bulge" sources, the full list numbering 10 - 15, depending on the criteria used for selection (e.g. Margon and Ostriker 1973; Watson et al. 1978a; Bradt 1978).

These "galactic bulge" sources show rather similar observational properties including soft x-ray spectra ($kT \lesssim 8$ keV), small long-term variability (by factors of 2 - 5), and no evidence for any periodic modulation In the full list of 15 sources given by Bradt (1978), 7 are optically identified (two rather tentatively), 5 are x-ray bursters, one is in a globular cluster and 3 sources probably have associated weak radio emission (these categories do, of course, overlap). Eight sources however remain unidentified despite extensive optical searches in the small x-ray errorboxes (all with radius $\lesssim 30"$). If some or all of the galactic bulge sources are members of a particular class of x-ray emitter, then their longitude distribution (Fig. 5.1) naturally leads to the conclusion that they have an approximately isotropic distribution about the galactic centre with a mean distance of $d \sim 10$ Kpc, and hence luminosities $> 5 \times 10^{37}$ erg s^{-1}. This conclusion is supported by the substantial low energy cutoffs seen in the spectra of several of these sources implying distances of this order, provided the absorption is not intrinsic.

Extensive observations of eleven of the galactic bulge sources have been made by the SSI, including two long scans made in 1975 July - August (26 days) and 1976 November (20 days) (Watson et al. 1978a). Their light curves show considerable similarities including: (i) total variability by a factor of only 1.5 - 3; (ii) typical timescales for this variability of 0.5 - 5 days with suggestions of quasi-periodic behaviour. None of the light curves however show evidence for true periodic modulation. Eclipse periodicities in the range ~ 0.5 - 20 days are excluded (the lower limit assuming an eclipse duration > 100 minutes), and a conservative upper limit

of 10% can be set to any modulation in the period range 0.5 - 13 days as a result of power spectrum analyses of the data. Searches for periods shorter than 0.5 days have been made using the data obtained from other satellite experiments including Copernicus (White et al. 1976), Uhuru (W.Forman and C.Jones, private communication 1977) and SAS-3 (e.g. Lewin et al. 1976; Buff et al. 1977a) with negative results in every case.

The lack of observed periodicities severely constrains any binary model for these sources, since it would seem that the binary period must be very short ($P \ll 1$ day), very long ($P > 20$ days), or that the binary nature produces rather small modulation of the x-ray flux. The last condition is easily satisfied if, for example, the orbital inclination is low enough, but such solutions become somewhat artificial when 10 - 15 objects are under consideration.

A number of specific models have been suggested for the galactic bulge sources. These include systems with very short periods ($P < 0.1$ day) and correspondingly brief eclipses observable for only a narrow range of inclination angles (Joss and Rappaport 1978) and models involving obscuration by matter in the orbital plane such that the bright sources observed are those which are preferentially near pole-on for which little modulation of the x-ray flux is expected (Jones and Raine 1978 , Milgrom 1978). The detailed model of Jones and Raine, invoking supercritical accretion in low-mass close binary, also explains the positive correlation between spectral temperature and intensity seen in at least seven of these sources (e.g. Watson et al.1978a).

Models not involving binary systems have also been proposed including the suggestion that these sources might be isolated $\sim 10^3$ $M_\odot$ black holes accreting from the interstellar medium (Forman et al. 1976). Other authors,

noting the similarities between galactic bulge sources and those in globular clusters, and those which show x-ray burst activity have pursued the links between these three types of object (e.g. Ostriker 1977). Since satisfactory models are not available for globular cluster or bursting sources either, these similarities do not (at present) advance our understanding to any extent. The nature of these rather special sources in the nuclear bulge of the galaxy remains one of the more intriguing problems in galactic x-ray astronomy.

5.3 Dwarf Novae

Dwarf novae are a class of cataclysmic variable which have repetitive outbursts of $\sim 3^{m}$ recurring on typical timescales of 20 - 100 days. They are generally believed to be close binary systems in which variable mass transfer is occurring between a low mass main sequence star and a solar mass white dwarf. Because of their similarity with known x-ray binaries, dwarf novae have been considered as potential x-ray emitters for some time, but it was generally assumed that accretion onto a white dwarf could not produce a bright, luminous x-ray source. Recent work by Fabian et al.(1976) (based on the pioneering work of Hoshi (1973) and Aizu (1973))has however shown that accretion onto a magnetised white dwarf (ensuring radial accretion even in the case of mass transfer via an accretion disc) can produce a "hard" ($>$ 2 keV) x-ray source with a luminosity up to $\sim 10^{36}$ erg s^{-1}.

Soft x-ray emission has been reported from a number of dwarf novae (see refs. in Ricketts et al. 1978), but it is only recently that observations with the SSI have conclusively demonstrated the existence of a "hard" x-ray flux from the dwarf nova SS Cygni (Ricketts et al. 1978). The x-ray emission from SS Cygni is characterised by variability by a factor of 10 or more; of particular interest, however, is the disappearance of the x-ray source during optical outbursts. This remarkable anti-correlation

establishes without question the association of the x-ray source with SS Cyg. (Further confirmation comes from the precise HEAO-1 A3 position recently published by Fabbiano et al. (1978)).

As a result of the SSI observations of SS Cyg a sensitive search for x-ray emission from other dwarf novae has been carried out using the Point Summation Technique (PST) on the SSI data (Watson et al.1978b). This survey gave clear evidence for x-ray emission from EX Hydrae, a somewhat fainter dwarf nova which had previously been suggested (on positional grounds alone) as the counterpart of the Uhuru source 2U1253-28. EX Hya lies within 3 arcminutes of the centre of the revised SSI errorbox for 2A1251-290 and is thus a good candidate for the x-ray source on a positional basis. Supporting evidence for the identification comes from the SSI x-ray light curve which indicates variability by a factor ~ 3, an expected feature of dwarf nova x-ray emission. (This identification has also been confirmed by a precise HEAO-1 MC position (Schwartz et al. 1978)).

The list of detected dwarf novae has recently been extended to include U Gem which has been seen in both soft and hard x-ray bands by the HEAO-1 A2 experiment (Mason et al.1978 , Swank et al.1978), and also the old nova GK Per which underwent a transient-like x-ray flare in the SSI observations coincident with an optical outburst (King et al. 1978). AM Her, a cataclysimic variable broadly similar to the dwarf novae, has of course been detected over a wide energy range for a couple of years.

The mechanism for the production of x-rays in dwarf novae (and related systems) is now the subject of increased theoretical interest. The accreting magnetic white dwarf model of Fabian et al. (1976), has been developed by Ricketts et al. (1978) and used to satisfactorily explain the anticorrelated x-ray/optical behaviour of SS Cyg, and to provide very reasonable estimates of the range of accretion rates and white dwarf magnetic field in this system.

The less demanding observations of Ex Hya and GK Per can also be explained in terms of the same model.

X-ray emission is expected on the basis of this model from a variety of other cataclysmic variables. A recent survey of x-ray emission from nova-like variables using the PST on the SSI data has already indicated V751 Cyg as an x-ray source candidate (unpublished SSI results). With the increased sensitivity available from observatories such as HEAO-2 we can confidently expect the discovery of many more examples of x-ray emission from cataclysmic variables.

Postscript

Without doubt the study of galactic x-ray sources has already reached a degree of maturity in the sense that the nature of a fair number of sources is no longer the puzzle that it was ten years ago. On the other hand, the results briefly discussed in this chapter indicate two ways in which the subject will no doubt progress - in the understanding of sources such as those in the galactic bulge; and in the study of entirely new classes of x-ray emitter such as cataclysmic variables.

Even with those sources which are now recognised as binary systems, it will be interesting to see if the classification scheme proposed here, into high and low mass binaries, will still have any value in a few years time. Some of the other problems in galactic x-ray astronomy, particularly the explanation of the observed spatial and source count distributions may soon be resolved by studies of external galaxies with observatories such as HEAO-2. Indeed observations with this observatory may produce such a wealth of detail as to provide solutions to many of the current problems. Even if this is the case, we need have no fears for the future of the subject, since we can confidently expect that there will also be no shortage of new mysteries to address.

References

This list has been produced on a computer printer (hence upper case only). References to the same author in the same year are distinguished either by letters (i.e. 77a,77b),or by the chapter no. given in brackets in the left margin.

AIZU,K.,1973. PROG.THEOR.PHYS.,49,1184.

ALLEN,C.W.,1973. "ASTROPHYSICAL QUANTITIES",3RD EDITION (ATHLONE PRESS,LONDON).

ALME,M.L.,AND WILSON,J.R.,1976. AP.J.,210,233.

APPARAO,K.M.V.,ET AL.,1978. NATURE,271,225.

AVNI,Y.,1976. AP.J.,209,574.

AVNI,Y.,AND BAHCALL,J.N.,1975A. AP.J.,197,675.

AVNI,Y.,AND BAHCALL,J.N.,1975B. AP.J.,202,L131.

AVNI,Y.,ET AL.,1976. M.N.R.A.S.,175,297.

BAHCALL,J.,1978. IN "PROC.ENRICO FERMI SCHOOL ON THE PHYS.AND ASTROPHYSICS OF NEUTRON STARS AND BLACK HOLES",EDD.R.GIACCONI,R.RUFFINI (ACADEMIC PRESS, NEW YORK).

BARTOLINI,C.,ET AL.,1978. IAU CIRC.,3167.

BASKO,M.M.,ET AL.,1974. ASTRON.ASTROPHYS.,31,249.

BASKO,M.M.,ET AL.,1977. AP.J.,215,276.

BATH,G.T.,1976. IN "STRUCTURE AND EVOLUTION OF CLOSE BINARY SYSTEMS",IAU SYMP.,73,173

BATH,G.T.,1977. Q.J.R.A.S.,IN PRESS.

BECKER,R.H.,ET AL.,1977A. IAU CIRC.,3039.

BECKER,R.H.,ET AL.,1977B. AP.J.(LETT.),216,L11.

BESSELL,M.S.,ET AL.,1975. AP.J.(LETT.),195,L117.

BIDELMAN,W.P.,AND SANDULEAK,N.,1977. IAU CIRC.,3146.

BLUMENTHAL,G.R.,AND TUCKER,W.H.,1974. IN "X-RAY ASTRONOMY",EDD.R.GIACCONI,H.GURSKY (D.REIDEL,DORDRECHT).

BOK,B.J.,ET AL.,1972. ASTR.J.,77,733.

BOLEY,F.,ET AL.,1976. AP.J.(LETT.),203,L13.

BRADT,H.V.,1978. ADVANCES IN SPACE EXPLORATION,3,IN PRESS.

(1) BRADT,H.V.,ET AL.,1977. NATURE,269,21, AND REFERENCES THEREIN.

(4) BRADT,H.V.,ET AL.,1977. NATURE,269,496.

BRECHER,K.,AND MORRISON,P.,1976. IN "X-RAY BINARIES",NASA SP-389,P.359.

BUFF,J.,ET AL.,1977. AP.J.,212,768.

CANIZARES,C.R.,ET AL.,1974. AP.J.(LETT.),191,L75.

CARPENTER,G.F.,ET AL.,1976. PROC.ROY.SOC.LOND.A,350,521.

CASTOR,J.I.,ET AL.,1975. AP.J,195,157.

CHARLES,P.A.,ET AL.,1976. IN "X-RAY BINARIES",NASA SP-389,P.629.

CHARLES,P.A.,ET AL.,1977. IAU CIRC.,3096.

CHARLES,P.A.,ET AL.,1978. M.N.R.A.S.,183,29P.

CHEVALIER,C.,AND ILOVAISKY,S.A.,1975. IAU CIRC.,2778.

CHEVALIER,C.,AND ILOVAISKY,S.A.,1977. ASTRON.ASTROPHYS.,59,L9.

CHEVALIER,C.,ET AL.,1977. IN "NOVAE AND RELATED STARS",ED. M.FRIEDJUNG,P.145 (D.REIDEL,DORDRECHT).

CLARK,D.H.,ET AL.,1975. NATURE,254,674.

CLARK,G.,ET AL.,1978. AP.J.(LETT.),221,L37.

COMINSKY,L.,ET AL.,1978A. AP.J.,224,46.

COMINSKY,L.,ET AL.,1978B. IAU CIRC.,3163.

COOKE,B.A.,ET AL.,1969. NATURE,224,134.

COOKE,B.A.,ET AL.,1978. M.N.R.A.S.,182,455.

COWLEY,A.P.,ET AL.,1977. AP.J.(LETT.),218,L3.

COWLEY,A.P.,AND CRAMPTON,D.,1975. AP.J.(LETT.),201,L65.

CRAMPTON,D.,AND COWLEY,A.P.,1976. AP.J.(LETT.),207,L171.

CRAMPTON,D.,ET AL.,1978. AP.J.(LETT.),225,L63.

DAVIDSEN,A.,1975. IAU CIRC.,2824.

DAVIDSEN,A.,ET AL.,1974. AP.J.(LETT.),193,L25.

DAVIDSEN,A.,ET AL.,1976. AP.J.,203,448.

DAVIDSEN,A.,ET AL.,1977. AP.J.,211,866.

DAVIDSON,K.,AND OSTRIKER,J.P.,1973. AP.J.,179,585.

DAVISON,P.J.N.,1977A. M.N.R.A.S.,179,35P.

DAVISON,P.J.N.,1977B. IAU CIRC.,3047.

DAVISON,P.J.N.,AND FABIAN,A.C.,1977. M.N.R.A.S.,178,1P.

DAVISON,P.J.N.,AND TUOHY,I.R.,1975. M.N.R.A.S.,173,33P.

DAVISON,P.J.N.,ET AL.,1977. M.N.R.A.S.,181,73P.

DE CUYPER,J.P.,ET AL.,1976. ASTRON.ASTROPHYS.,52,315.

DOWER,R.,ET AL.,1977. B.A.A.S,9,297.

(1) DOWER,R.,ET AL.,1978. NATURE,273,364.

(3) DOWER,R.,ET AL.,1978. IN PREPARATION (QUOTED IN BRADT (1978)).

DOXSEY,R.,ET AL.,1976. AP.J.(LETT.),203,L9.

DUERBECK,H.W.,AND WALTER,K.,1976. ASTRON.ASTROPHYS.,48,141.

EACHUS,L.J.,ET AL.,1976. AP.J.(LETT.),203,L17.

EADIE,G.,ET AL.,1975. M.N.R.A.S.,172,35P.

ELVIS,M.,ET AL.,1975. NATURE,257,656.

ELVIS,M.S.,1978. PH.D. THESIS, UNIVERSITY OF LEICESTER.

ENDAL,A.S.,ET AL.,1976. ASTROPHYS.LETT.,17,131.

EPSTEIN,A.,ET AL.,1977. AP.J.,216,103.

EWART,G.M.,ET AL.,1975. AP.J.,202,238.

FABIAN,A.C.,ET AL.,1976. M.N.R.A.S.,175,43.

FABBIANO,G.,ET AL.,1978. NATURE,IN PRESS.

FAULKNER,J.,1976. IN "STRUCTURE AND EVOLUTION OF CLOSE BINARY SYSTEMS", IAU SYMP.,73,193.

FLANNERY,B.P.,AND ULRICH,R.,1977. AP.J.,212,533.

FORMAN,W.,ET AL.,1973. AP.J.(LETT.),182,L103.

FORMAN,W.,ET AL.,1976. AP.J.,208,849.

FORMAN,W.,ET AL.,1978. AP.J.SUPPL.,IN PRESS.

GALLAGHER,J.,AND STARRFIELD,S.,1976. PREPRINT.

GARMIRE,G.,1978.ADVANCES IN SPACE EXPLORATION,3,IN PRESS.

GIACCONI,R.,AND GURSKY,H.,1974. IN "X-RAY ASTRONOMY",EDD.R.GIACCONI,H.GURSKY (D.REIDEL,DORDRECHT).

GIACCONI,R.,ET AL.,1967. AP.J.(LETT.),148,L119.

GIACCONI,R.,ET AL.,1974. AP.J.SUPPL.,27,37.

GINZBURG,V.,1967. IN "RADIO ASTRONOMY AND THE GALACTIC SYSTEM",IAU SYMP.,31,411.

GLASS,I.S.,1978. M.N.R.A.S.,183,335.

GLASS,I.S.,1976. IAU CIRC.,2974.

GOSS,W.M.,AND MEBOLD,U.,1977. M.N.R.A.S.,181,255.

GOTTLIEB,E.W.,ET AL.,1975. AP.J.(LETT.),195,L33.

GRINDLAY,J.E.,1977A. HIGHLIGHTS OF ASTRONOMY,4,111.

GRINDLAY,J.E.,1977B. IAU CIRC.,3104.

GRINDLAY,J.E.,1978. AP.J.(LETT.),224,L107.

GRINDLAY,J.E.,ET AL.,1978. NATURE,274,567.

GRINDLAY,J.E.,AND LILLER,W.,1978. AP.J.(LETT.),TO APPEAR.

(2) GRIFFITHS,R.E.,ET AL.,1976. M.N.R.A.S.,175,449.

(4) GRIFFITHS,R.E.,ET AL.,1976. M.N.R.A.S.,177,429.

GRIFFITHS,R.E.,ET AL.,1977. IAU CIRC.,3110.

GRIFFITHS,R.E.,ET AL.,1978. AP.J.(LETT.),221,L63.

GUNN,G.E.,AND OSTRIKER,J.P.,1970. AP.J.,160,979.

GURSKY,H.,AND SCHREIER,E.,1975. IN "NEUTRON STARS,BLACK HOLES AND BINARY X-RAY SOURCES",P.175 (D.REIDEL,DORDRECHT)

GURSKY,H.,ET AL.,1978. AP.J.,SUBMITTED.

HAMMERSCLAG-HENSBERGE,G.,ET AL.,1976. ASTRON.ASTROPHYS.,49,321.

HATCHETT,S.,AND MCCRAY,R.,1977. AP.J.,211,552.

HILTNER,W.A.,1973. IAU CIRC.,2502.

HJELLMING,R.M.,1976. IN "X-RAY BINARIES",NASA SP-389,PP.233-40.

HJELLMING,R.M.,AND WADE,C.M.,1971. AP.J.(LETT.),168,L21.

HOFFMAN,J.A.,ET AL.,1977. AP.J.(LETT.),217,L23.

HOLT,S.S.,ET AL.,1976A. AP.J.(LETT.),205,L143.

HOLT,S.S.,ET AL.,1976B. NATURE,260,592.

HOSHI,R.,1973. PROG.THEOR.PHYS.,49,776.

HUTCHINGS,J.B.,ET AL.,1974. AP.J.(LETT.),191,L101.

HUTCHINGS,J.B.,1974A. AP.J.,188,341.

HUTCHINGS,J.B.,1974B. AP.J.,192,685.

IVES,J.C.,ET AL.,1975. NATURE,254,578.

JACKSON,J.C.,1975. M.N.R.A.S.,172,483.

JERNIGAN,G.,1975. IAU CIRC.,2817.

JOHNS,M.,AND KOSKI,A.,1978. IAU CIRC.,3171.

JOHNSON,H.M.,1978. AP.J.,224,381.

JOHNSTON,M.,ET AL.,1978. IAU CIRC.,3163.

JONES,B.C.,AND RAINE,D.J.,1978. ASTRON.ASTROPHYS.,IN PRESS.

JONES,C.,1977. AP.J.,214,856.

JONES,C.,AND LILLER,W.,1973. AP.J.(LETT.),184,L121.

JONES,C.,AND FORMAN,W.,1976. AP.J.,209,L131.

JONES,C.,ET AL.,1974. AP.J.(LETT.),191,L71.

JONES,C.,ET AL.,1976. AP.J.(LETT.),210,L9.

JOSS,P.C.,AND RAPPAPORT,S.,1976. NATURE,264,219.

JOSS,P.C.,AND RAPPAPORT,S.,1978. ASTRON.ASTROPHYS.,IN PRESS.

JOSS,P.C.,ET AL.,1978. AP.J.,221,645.

KALUZIENSKI,L.J.,1977. PH.D THESIS,UNIV. OF MARYLAND.(GSFC PREPRINT X-661-77-107)

KALUZIENSKI,L.J.,ET AL.,1975. AP.J.(LETT.),201,L121.

KALUZIENSKI,L.J.,ET AL.,1976. AP.J.(LETT.),208,L71.

KALUZIENSKI,L.J.,ET AL.,1977. NATURE,265,606.

(4) KALUZIENSKI,L.J.,AND HOLT,S.S.,1977. IAU CIRC.,3104.

(3) KALUZIENSKI,L.J.,AND HOLT,S.S.,1977A. IAU CIRC.,3099.

(3) KALUZIENSKI,L.J.,AND HOLT,S.S.,1977B. IAU CIRC.,3108.

KALUZIENSKI,L.J.,AND HOLT,S.S.,1978. IAU CIRC.,3171.

KATZ,J.I.,1977. AP.J.,215,265.

KING,A.R.,ET AL.,1978. M.N.R.A.S.,IN PRESS.

KONDO,Y.,ET AL.,1976. IN "X-RAY BINARIES",NASA SP-389,P.499.

KRZEMINSKI,W.,1973. IAU CIRC.,2569.

LAMB,F.K.,1975. PROC.INT.CONF.ON X-RAYS IN SPACE,UNIV.OF CALGARY,P.613.

LAMERS,H.J.G.L.M.,ET AL.,1976. ASTRON.ASTROPHYS.,49,327.

LEWIN,W.H.G.,AND JOSS,P.C.,1977. NATURE,270,211.

LEWIN,W.H.G.,1978. ADVANCES IN SPACE EXPLORATION,3,IN PRESS.

LEWIN,W.H.G.,ET AL.,1976. M.N.R.A.S.,177,93P.

LEWIN,W.H.G.,ET AL.,1977. IAU CIRC.,3075.

LIGHTMAN,A.P.,ET AL.,1977. IN "PROC.ENRICO FERMI SCHOOL ON THE PHYS.AND ASTROPHYSICS OF NEUTRON STARS AND BLACK HOLES",EDD. R.GIACCONI AND R.RUFFINI (ACADEMIC PRESS, NEW YORK).

LI,F.K.,ET AL.,1977. M.N.R.A.S.,179,21P.

LLOYD,C.,ET AL.,1977. M.N.R.A.S.,179,675.

LONGMORE,A.,ET AL.,1977. IAU CIRC.,3110.

LUCKE,R.,ET AL.,1976. AP.J.(LETT.),206,L25.

MCCLINTOCK,J.E.,ET AL.,1975. AP.J.,198,641.

MCCLINTOCK,J.E.,ET AL.,1976. AP.J.(LETT.),206,L99.

MCCLINTOCK,J.E.,ET AL.,1977A. AP.J.(LETT.),216,L15.

MCCLINTOCK,J.E.,ET AL.,1977B. NATURE,270,320.

MCCRAY,R.,1976. HIGHLIGHTS OF ASTRONOMY.

MARASCHI,L.,ET AL.,1977. AP.J.,216,819.

MARGON,B.,1978. ADVANCES IN SPACE EXPLORATION,3,IN PRESS.

MARGON,B.,AND BRADT,H.,1977. IAU CIRC.,3144.

MARGON,B.,AND OSTRIKER,J.P.,1973. AP.J.,186,91.

(1) MARGON,B.,ET AL.,1978. AP.J.(LETT.),

(4) MARGON,B.,ET AL.,1978. NATURE,271,633.

MASON,K.O.,1977. M.N.R.A.S.,178,81P.

MASON,K.O.,ET AL.,1978. AP.J.(LETT.),226,L129.

MATILSKY,T.,ET AL.,1973. AP.J.,181,753.

MATILSKY,T.,ET AL.,1976. AP.J.(LETT.),210,L127.

MATILSKY,T.,AND JESSEN,J.,1978. IAU CIRC.,3193.

MAUDER,H.,1976. IAU CIRC.,2946.

MESZAROS,P.,1975. ASTRON.ASTROPHYS.,44,59.

MIDDLEDITCH,J.,AND NELSON,J.,1976. AP.J.,208,567.

MILGROM,M.,1978. ASTRON.ASTROPHYS.,67,L25.

MOOK,D.,ET AL.,1978. IAU CIRC.,3251.

MORTON,D.AND MURDIN,P.,1978. IAU CIRC., NO.3247.

MURDIN,P.,ET AL.,1974. M.N.R.A.S.,169,25.

MURDIN,P.,ET AL.,1977. M.N.R.A.S.,178,27P.

NOVIKOV,I.D.,AND THORNE,K.S.,1973. IN "BLACK HOLES",EDD.C.DE WITT AND B.DE WITT,P.343 (GORDON AND BREACH, NEW YORK).

OKE,J.B.,1977. AP.J.,217,181.

OKE,J.B.,AND GREENSTEIN,J.L.,1977. AP.J.,211,872.

OSMER,P.S.,ET AL.,1975. AP.J.,195,705.

OSTRIKER,J.P.,1977. ANN.N.Y.ACAD.SCI.,302,229.

PACZYNSKI,B.,1971. ANN.REV.ASTRON.ASTROPHYS.,9,183.

PARKES,G.E.,ET AL.,1978. M.N.R.A.S.,184,73P.

POUNDS,K.A.,1974. IAU CIRC.,2729.

POUNDS,K.A.,1976. COMMENTS ON ASTROPHYSICS,6,145.

POUNDS,K.A.,1978. ADVANCES IN SPACE RESEARCH,3,IN PRESS.

POUNDS,K.A.,ET AL.,1975. M.N.R.A.S.,172,473.

PRAVDO,S.H.,1976. PH.D. THESIS,UNIVERSITY OF MARYLAND, NASA X-661-76-280.

PRENDERGAST,K.H.,AND TAAM,R.E.,1974. AP.J.,189,125.

PRINGLE,J.E.,AND REES,M.J.,1972. ASTRON.ASTROPHYS.,21,1.

PRINGLE,J.E.,1973. NAT.PHYS.SCI.,243,90.

PRINGLE,J.E.,1974. M.N.R.A.S.,168,13P.

PUETTER,R.C.,AND SMITH,H.E.,1978. IAU CIRC.,3243.

RAPPAPORT,S.,AND JOSS,P.C.,1977. NATURE,266,683.

RAPPAPORT,S.,ET AL.,1976. AP.J.(LETT.),206,L103.

RAPPAPORT,S.,ET AL.,1977A. NATURE,268,705.

RAPPAPORT,S.,ET AL.,1977B. AP.J.(LETT.),217,L29.

RAPPAPORT,S.,ET AL.,1978. AP.J.(LETT.),224,L1.

REES,M.J.,1976. IN "STRUCTURE AND EVOLUTION OF CLOSE BINARY SYSTEMS",IAU SYMP.,73,225

RICKETTS,M.J.,AND COOKE,B.A.,1977. IAU CIRC.,3039.

RICKETTS,M.J.,ET AL.,1975. NATURE,257,657.

RICKETTS,M.J.,ET AL.,1978. M.N.R.A.S.,IN PRESS.

ROSENBERG,F.D.,ET AL.,1975. NATURE,256,628.

ROTHSCHILD,R.E.,ET AL.,1974. AP.J.(LETT.),189,L13.

ROTHSCHILD,R.E.,ET AL.,1977. AP.J.,213,818.

RUFFINI,R.,1975. IN "NEUTRON STARS,BLACK HOLES AND BINARY X-RAY SOURCES",P.59 (D.REIDEL,DORDRECHT).

SANFORD,P.W.,AND IVES,J.C.,1976. PROC.ROY.SOC.LOND.A,350,491.

SCHREIER,E.,ET AL.,1972. AP.J.(LETT.),172,L79.

SCHREIER,E.,ET AL.,1976. AP.J.,204,539.

(1) SCHWARTZ,D.A.,ET AL.,1978. B.A.A.S.,9,661.

(3) SCHWARTZ,D.A.,ET AL.,1978. NATURE,275,517.

(5) SCHWARTZ,D.A.,1978. TALK PRESENTED AT SAN DIEGO HEAD MEETING.

SHAKURA,N.K.,AND SUNYAEV,R.A.,1973. ASTRON.ASTROPHYS.,24,337.

SHLOVSKY,I.S.,1968. SOV.ASTRON.,11,749.

SHU,F.H.,1976. IN "STRUCTURE AND EVOLUTION OF CLOSE BINARY SYSTEMS",IAU SYMP.,73,253

SILK,R.,1976. PH.D. THESIS, UNIVERSITY OF LEICESTER.

SMITH,J.F.,AND COURTIER,G.M.,1976. PROC.ROY.SOC.LOND.A,350,421.

SPADA,G.,ET AL.,1974. AP.J.(LETT.),190,L113.

STEINER,J.E.,1977. IAU CIRC.,3107.

STIER,M.,AND LILLER,W.,1976. AP.J.,206,257.

SUNTANTYO,W.,1974. ASTRON.ASTROPHYS.,35,251.

SWANK,J.H.,ET AL.,1978. AP.J.(LETT.),226,L133.

TANANBAUM,H.,ET AL.,1976. AP.J.(LETT.),209,L125.

TARENGHI,M.,AND REINA,C.,1972. NAT.PHYS.SCI.,240,53.

THOMAS,R.M.,ET AL.,1978. M.N.R.A.S.,185,29P.

THORSTENSEN,J.,ET AL.,1977. IAU CIRC.,3088.

THORSTENSEN,J.,ET AL.,1978. AP.J.(LETT.),220,L131.

TOOR,A.,1977. AP.J.(LETT.),215,L57.

TSUNEMI,H.,ET AL.,1977. AP.J.(LETT.),211,L15.

TUOHY,I.R.,1976. IN "X-RAY BINARIES",NASA SP-389,P.219.

ULMER,M.P.,ET AL.,1972. AP.J.(LETT.),178,L121.

VAN DEN HEUVEL,E.P.J.,1976. IN "STRUCTURE AND EVOLUTION OF CLOSE BINARY SYSTEMS", IAU SYMP.,73,35.

VAN DEN HEUVEL,E.P.J.,1977. ANN.N.Y.ACAD.SCI.,302,14.

VAN PARADIJS,J.A.,ET AL.,1976. IN "X-RAY BINARIES",NASA SP-389,P.643.

VIDAL,N.V.,ET AL.,1973A. IAU CIRC.,2503.

VIDAL,N.V.,ET AL.,1973B. AP.J.(LETT.),182,L77.

VIDAL,N.V.,1976. IN "X-RAY BINARIES",NASA SP-389,P.575.

VILLA,G.,ET AL.,1976. M.N.R.A.S.,176,609.

VRBA,F.J.,1978. IAU CIRC.,3243.

WALTER,F.,ET AL.,1978. IAU CIRC.,3243.

WARWICK,R.S.,AND PYE,J.P.,1978. M.N.R.A.S.,183,169.

WARNER,B.,1976. IN "STRUCTURE AND EVOLUTION OF CLOSE BINARY SYSTEMS",IAU SYMP.,73.

WATSON,M.G.,1975. IAU CIRC.,2808.

WATSON,M.G.,1976. M.N.R.A.S.,176,19P.

WATSON,M.G., AND GRIFFITHS,R.E.,1977. M.N.R.A.S.,178,513.

WATSON,M.G.,AND RICKETTS,M.J.,1978. M.N.R.A.S.,183,35P.

(1) WATSON,M.G.,ET AL.,1978. AP.J.(LETT.),221,L69.

(5) WATSON,M.G.,ET AL.,1978A. M.N.R.A.S.,SUBMITTED.

(5) WATSON,M.G.,ET AL.,1978B. M.N.R.A.S.,184,79P.

WEINBERG,S.,1972. "GRAVITATION AND COSMOLOGY" (J.WILEY AND SONS INC.,NEWYORK).

WHELAN,J.A.J.,ET AL.,1977A. M.N.R.A.S.,180,657.

WHELAN,J.A.J.,ET AL.,1977B. M.N.R.A.S.,181,259.

WHITE,N.E.,1977. IAU CIRC.,3118.

WHITE,N.E.,1978. NATURE,271,38.

WHITE,N.E.,ET AL.,1976A. M.N.R.A.S.,176,201.

WHITE,N.E.,ET AL.,1976B. AP.J.(LETT.),209,L119.

WHITE,N.E.,ET AL.,1977. NATURE,267,229.

WICKRAMSINGHE,D.T.,1974. M.N.R.A.S.,168,297.

WILSON,A.M.,1977. M.SC. THESIS, UNIVERSITY OF BIRMINGHAM.

WILSON,A.M.,AND CARPENTER,G.F.,1976. NATURE,261,295.

WU,C-C.,ET AL.,1976. ASTRON.ASTROPHYS.,50,445.

ZEL'DOVICH,YA.B.,AND NOVIKOV,I.D.,1966. SUPP.NUOVO.CIMENTO,IV,810.

ZUIDERWIJK,E.J.,ET AL.,1974. ASTRON.ASTROPHYS.,35,363.

ACKNOWLEDGMENTS

Ken Pounds supervised my progress towards this thesis and made many constructive criticisms of the first draft. I would like to thank him for all his help and guidance.

I owe a large debt to all who have played a part in the successful operation of Ariel V for the last four years, both the staff at the Appleton Laboratory Operation Control Centre, and many colleagues at Leicester. The original analysis software for the SSI was principally the work of Gavin Eadie, Martin Turner and Clive Page. Later developments are due to Clive Page, with important contributions by Martin Ricketts and John Pye.

Much of the work reported in this thesis was done in collaboration with Martin Ricketts and Richard Griffiths, and all of it has benefited from advice and discussions with other members of the X-ray Astronomy Group, especially Martin Elvis, John Pye, Clive Page, Brin Cooke, Andy Lawrence, Bob Warwick and Ian McHardy; and Andrew King and Brian Jones of the Astronomy Department. Thanks to them all.

Finally, special thanks to Jose Buckland for her excellent typing, to Lorna Duffin and Martin Elvis for friendship and encouragement, and to Wig Whitehouse for all her help and for being so patient.

M.G.WATSON Ph.D. THESIS 1979

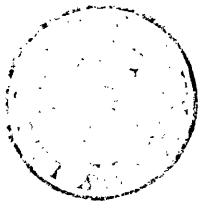

X-ray Binary Systems - Ariel V SSI Observations

M.G.Watson

ABSTRACT

The basis of our current theoretical understanding of galactic x-ray sources is reviewed. Models are outlined involving close binary systems containing a compact object accreting mass which has been lost from the nondegenerate star by a variety of mechanisms. The present status of galactic x-ray astronomy is discussed, with emphasis on the links between established observational categories and the characteristics of the proposed models.

Observational results, consisting primarily of extended x-ray light curves derived from analysis of Ariel V SSI data are presented for two main classes of galactic x-ray source: (i) high-mass x-ray binaries containing an early-type giant or supergiant star; (ii) low-mass x-ray binaries in which the nondegenerate star is a late-type dwarf. For the high-mass binaries emphasis is placed on the determination and improvement of the orbital parameters; for the low-mass binaries, where a less complete picture is available, the discussion centres on the type of system involved, taking into account the optical observations of the source.

Finally, the properties of two further categories - the sources in the galactic bulge and those associated with dwarf novae - are discussed as examples of rather different types of galactic x-ray emitter. In the case of the galactic bulge sources current observations have not lead so far to a clear picture of the nature of the systems involved, indeed their binary membership is not established. X-ray emission from dwarf novae and related objects is a relatively recent discovery and represents the opening up of a new field of galactic x-ray astronomy.